Università degli Studi di Padova

Sede Amministrativa: Università degli Studi di Padova

Dipartimento di Medicina Molecolare

CORSO DI DOTTORATO DI RICERCA IN MEDICINA MOLECOLARE
CURRICOLO BIOMEDICINA
CICLO XXXII

Molecular Pathophysiology of Cholangiopathies: Lessons from Polycystic and Fibropolycystic Liver Disease

Coordinatore: Ch.mo Prof. Stefano Piccolo
Supervisore: Ch.mo Prof. Luca Fabris

Dottoranda: Dott.ssa Valeria Mariotti

INDEX

PART II

ABSTRACT (ITALIANO)

I colangiociti, ossia le cellule epiteliali che rivestono l'albero biliare intra ed extraepatico, svolgono un ruolo essenziale nella regolazione della produzione della bile e delle funzioni digestive. I colangiociti sono anche coinvolti nella riparazione del danno epatico in seguito a patologie dell'albero biliare, o colangiopatie, un ampio gruppo di malattie epatiche croniche acquisite, congenite o genetiche. Le colangiopatie sono una frequente causa di morbidità e mortalità e sono una frequente causa di indicazione a trapianto di fegato. Ad oggi, il trattamento delle colangiopatie risulta insoddisfacente e lo sviluppo di migliori trattamenti rappresenta una delle più sentite necessità dell'epatologia moderna.

I colangiociti oltre ad essere un bersaglio di malattia, contribuiscono anche allo sviluppo della stessa. A seguito di un danno biliare, i colangiociti diventano "reattivi", acquisendo la capacità di produrre una grande quantità di citochine, mediatori infiammatori e fattori di crescita e di promuovere infiammazione e fibrosi portale che esitano nel tempo in cirrosi e insufficienza epatica cronica. Un tratto distintivo di questo processo nosologico è l'attivazione di diverse vie morfogenetiche intracellulari, tra cui quelle di Notch, di Wnt/β-catenina e del VEGF; le quali sono coinvolte nell'embriogenesi fisiologica durante lo sviluppo dell'albero biliare, al termine della quale solitamente vengono disattivate.

La comprensione dei meccanismi alla base della riattivazione di queste vie di segnale è stata aumentata dalla recente disponibilità di modelli animali che fenocopiano le colangiopatie congenite e genetiche. L'utilizzo di tali modelli ha consentito una sempre piú profonda conoscenza della fisiopatologia dei colangiociti e lo sviluppo di nuove strategie terapeutiche.

Le colangiopatie acquisite sono malattie complesse per le quali ad oggi sono disponibili solo modelli animali e cellulari insoddisfacenti. Pertanto, l'approccio adottato dal nostro laboratorio è stato quello di studiare la patogenesi delle colangiopatie genetiche che presentassero un gene causale noto e che potessero essere utilizzate come modelli per lo studio anche di altre malattie biliari ed epatiche. Durante il corso di dottorato, mi sono concentrata principalmente sullo studio del meccanismo molecolare che guida la progressione di malattia di due colangiopatie ereditarie: 1) la malattia del fegato policistico associata alla malattia renale policistica

autosomica dominante **(PLD-ADPKD)**, in cui la proliferazione anormale dei colangiociti cistici è associata sia a cambiamenti nell'omeostasi del Ca^{2+} intracellulare che alla riattivazione dei segnali angiogenetici biliari e, 2) le malattie fibropolicistiche **(malattia di Caroli e fibrosi epatica congenita)**, caratterizzate dal deficit di fibrocistina, una proteina la cui assenza porta all'attivazione della via di segnale della β-Catenina che causa la secrezione di chemochine proifiammatorie ed il reclutamento di macrofagi e di cellule mesenchimali. Tale reclutamento è la causa primaria della deposizione di fibrosi epatica che può esitare in ipertensione portale. La tesi è divisa in due parti:

nella parte I, abbiamo dimostrato come nei colangiociti, la policistina 2 (PC2), la proteina ciliare che risulta deficitaria nella PLD-ADPKD, sia un regolatore dell'omeostasi Ca^{2+} e della via di segnale di cAMP. L'espressione di PC2 è essenziale per la regolazione del calcio intracellulare: poiché le cellule mancanti di PC2 sono caratterizzate da un aumento dell'attività delle via di segnale mediate da cAMP/PKA e della secrezione di VEGF a seguito dell'attivazione della via di Ras/Raf/ERK/mTOR/HIF1-α. Abbiamo voluto comprendere le relazioni che intercorrono tra l'alterata omeostasi di Ca^{2+} e l'aumento della produzione di cAMP. Abbiamo osservato che l'aumento della produzione di cAMP è sostenuta dall'attivazione dell'adenilato ciclasi 5 (AC5), un'isoforma di AC, solitamente inattiva alle normali concentrazioni intracellulari di Ca^{2+}, ma che risulta attivata dalla diminuzione della concentrazione intracellulari di Ca^{2+} tipica del colangiociti con deficit di PC2. Poiché l'attivazione di AC5 risulta essere dipendente anche da STIM1, una proteina che agisce da sensore del calcio dell'ER, responsabile dell'attivazione dell'ingresso Ca^{2+}, abbiamo concluso che l'assenza di PC2 in associazione con una diminuita concentrazione di Ca^{2+} intracellulare degli store endoplasmatici, promuove l'interazione di STIM1 con AC5, che esita in un'aberrante produzione di cAMP, con conseguente stimolazione della proliferazione dei colangiociti che formano le cistici e da una loro espansione causata dall'ipersecrezione di VEGF. Questi risultati indicano che AC5 potrebbe rappresentare un potenziale bersaglio per lo sviluppo di una terapia per tale malattia; a supporto di ciò, abbiamo dimostrato come il trattamento con SQ22,536, un inibitore specifico di AC5, causi il blocco della crescita delle cisti in un modello di topo ortologo della patologia umana (parte di questo lavoro è stato pubblicato in: *Spirli C., et al., Journal of Hepatology, 2017).*

Nella parte II di questa tesi, abbiamo studiato quali siano I meccanismi di sviluppo della fibrosi nella malattia di Caroli e nella Fibrosi Epatica Congenita, due varianti delle malattie fibropolicistiche causate dalla carenza congenita della fibrocistina (FPC); queste sono caratterizzate da dilatazioni dell'albero biliari e da fibroinfiammazione epatica ingravescente. In studi precedenti, abbiamo dimostrato che in questa condizione nosologica, la deposizione di fibrosi non era una conseguenza diretta del danno necro-infiammatorio all'albero biliare, ma piuttosto di un'infiammazione cronica che colpisce i colangiociti FPC-KO che stimolano il reclutamento peribiliare di macrofagi. Poichè tale effetto è dipendente da un'aumentata secrezione di CXCL10 da parte dei colangiociti con deficit di FPC, abbiamo deciso di studiare più approfonditamente quali fossero meccanismi patogenetici che legano il deficit di FPC con l'aumento della secrezione di CXCL10. Abbiamo scoperto che, in assenza di fibrocistina, la secrezione di CXCL10 è stimolata dalla nuclearizzazione della β-catenina causata da una fosforilazione aberrante del residuo di Serina675 della β-catenina e dall'anormale secrezione di IL-1β dovuta all'attivazione del complesso dell'inflammasoma NLRP3. Questi risultati suggeriscono che la fibrosi periportale possa essere generata da un'infiammazione cronica di basso grado originata dai colangiociti con deficit di FPC e apre nuove possibilità terapeutiche volte a colpire la via di segnale della β-catenina e dell'infiammosoma. (Questo lavoro è stato pubblicato in: *Kaffe E. et al., Hepatology, 2018)*

L'identificazione di questi meccanismi patobiologici ha chiarito alcuni aspetti generali della sequenza di eventi che portano dalla disfunzione dei colangiociti all'iperplasia degli stessi fino all'instaurazione della fibrosi biliare. Questo processo è il risultato dell'aumento dei livelli di cAMP, della secrezione di chemochine pro-infiammatorie e di fattori angiogenetici e del reclutamento di macrofagi; questi meccanismi possono rappresentare bersagli terapeutici anche per il trattamento di altre colangiopatie acquisite che condividono tratti patogenetici comuni a quelle studiate in questa tesi.

ABSTRACT (ENGLISH)

Cholangiocytes, the epithelial cells lining the intra- and extrahepatic biliary tree, play an essential role in regulating the production of bile and digestive functions. Cholangiocytes are also involved in the repair from liver damage and are also the target of cholangiopathies a group of acquired, congenital, or genetic complex chronic liver diseases , that represents a substantial cause of morbidity and mortality and a frequent indication for liver transplant. Treatment of cholangiopathies is unsatisfactory and these diseases are among the main unmet needs in modern hepatology. .

Cholangiocytes in addition of being the target of the disease, also contribute to disease development. After biliary damage cholangiocytes, become “reactive”, acquire the ability to produce a number of cytokines and inflammatory mediators and growth factors and to promote further inflammation and portal fibrosis that ultimately may lead to cirrhosis and chronic liver failure. A hallmark of this process is the activation of intracellular morphogenetic signaling, such as the Notch, Wnt/β-catenin and VEGF pathways that are transiently involved in the development of the biliary epithelium during embryogenesis. The understanding of the mechanism underlying the reactivation of these intracellular signaling pathways has been boosted thanks to the availability of animal models that phenocopy the congenital and genetic cholangiopathies. These translational tools improved the knowledge of the pathophysiology of cholangiocytes and provided experimental therapeutic strategies.

Acquired cholangiopathies are complex diseases for which only unsatisfactory animal and cellular models are available. Therefore, the approach taken by our laboratory has been to study the pathogenesis of genetic cholangiopathies with an identified causative gene and derive “lessons” that can be applied to the more general field of biliary and liver diseases.

During the Ph.D. program, I mainly focused on investigating the molecular mechanism that drives the progression of two inherited cholangiopathies: 1) the polycystic liver disease associated with autosomal dominant polycystic kidney disease (**PLD-ADPKD**), in which the abnormal proliferation of cystic cholangiocytes is associated with changes in intracellular Ca^{2+} homeostasis and with the reactivation of biliary angiogenetic signals and, 2) the fibro-polycystic disease (**Caroli Disease and Congenital Hepatic Fibrosis**), where the aberrant lack of fibrocystin leads to

activation of β-Catenin, chemokine secretion and recruitment of macrophages and fibrogenic mesenchymal cells , leading to liver fibrosis and portal hypertension. The thesis is divided in two parts; for both parts, the experimental methodology used is reported in the method section.

In part I, we show that polycystin 2 (PC2), the ciliary protein affected in PLD-ADPKD, is a regulator of Ca^{2+} homeostasis and cAMP signaling in cholangiocytes. Expression of PC2 is essential for cytoplasmic and endoplasmic reticulum (ER) calcium handling. As PC2-deficient cells are also characterized by increased cAMP/PKA signaling and by Ras/Raf/ ERK/mTOR/HIF1α-dependent VEGF secretion, we aimed at understanding the relationships between altered Ca^{2+} homeostasis and increased cAMP production. We found that increased cAMP production is sustained by Adenylyl Cyclase 5 (AC5), an AC that is inactive at the normal intracellular Ca^{2+} concentrations,but it is activated at the decreased intracellular Ca^{2+} concentrations measured in PC2-deficient cystic cholangiocytes. As activation of AC5 was also dependent on STIM1 (a ER calcium sensor protein responsible for activation of the store-operated Ca^{2+} entry) we also concluded that the absence of PC2, intracellular Ca^{2+} store depletion promotes the interaction of STIM1 with AC5, resulting in aberrant cAMP production, stimulation of cystic cholangiocyte proliferation and cyst growth via Ras/Raf/ERK/mTOR/HIF1α-dependent VEGF secretion. These findings indicate that AC5 is an attractive target for therapy, as also demonstrated by inhibition of cyst growth in mice treated with the AC5 inhibitor SQ22,536. (*Part of this work has been published. Spirli C., et al., Journal of Hepatology, 2017*)

In part II, we studied how fibrosis develops in Caroli Disease and Congenital Hepatic Fibrosis, two variants of the fibropolycystic diseases resulting from congenital deficiency of fibrocystin and characterized by biliary cysts and severe liver fibrosis. In prior studies we showed that in this condition, fibrosis was not a consequence of necroinflammatory damage to the biliary tree, but rather of a low grade chronic inflammation originating from the fibrocystin-deficient cholangiocytes and the consequent recruitment of macrophages. As macrophages recruitment depended on increased secretion of CXCL10 by fibrocystin-defective cholangiocytes we aimed to better understand the link between fibrocystin deficiency and increased CXCL10 secretion. We found that in the absence of fibrocystin, CXCL10 secretion is mediated

by β-catenin nuclearization through phosphorylation at the Serine675 and by the abnormal secretion of IL-1β through the activation of NLRP3 inflammasome complex. These findings suggest that periportal fibrosis can be generated by a chronic low level inflammation originating from the fibrocystin deficient cholangiocytes and open new therapeutic avenues aiming at targeting β-catenin signaling and the inflammasome. (*This work has been published. Kaffe E. et al., Hepatology, 2018*)

The identification of these pathobiological mechanisms has clarified some general aspects of the sequence of events leading from cholangiocyte dysfunction to hyperplasia and biliary fibrosis. This process is the result of increased cAMP levels, secretion of pro-inflammatory chemokines and angiogenetic factors, and macrophage recruitment; all these steps which may be targeted also for the treatment of acquired cholangiopathies that share common pathobiological traits.

LIST OF PUBLICATIONS

This thesis is based on the following articles:

• Spirli C, Mariotti V, Villani A, Fabris L, Fiorotto R, Strazzabosco M. In Polycystic Liver Disease (PLD-ADPKD) Adenylyl cyclase 5 links changes in calcium homeostasis to cAMP-dependent cyst growth in polycystic liver disease. J Hepatol. 2017 Mar;66(3):571-580.

• Kaffe, E., Fiorotto, R., Pellegrino, F., Mariotti V., Amenduni, M., Cadamuro, M., Fabris, L., Strazzabosco, M., Spirli, C. β-Catenin and interleukin-1β–dependent chemokine (C-X-C motif) ligand 10 production drives progression of disease in a mouse model of congenital hepatic fibrosis. Hepatology . 2018 May;67(5):1903-1919.

This work was realized under the mentorship of Prof. Luca Fabris and in close collaboration with Dr. Mario Strazzabosco. I will be always grateful for their support and encouragement.

List of other articles:

• Fabris L., Fiorotto R., Spirli C., Cadamuro M., Mariotti V., Perugorria MJ., Banales JM. and Strazzabosco M. Pathobiology of inherited biliary diseases: a roadmap to understand acquired liver diseases. Nature Reviews Gastroenterology & Hepatology. 16, pages497–511 (2019).

• Cadamuro, M., Brivio, S., Mertens, J., Vismara, M., Moncsek, A., Milani, C., Fingas, C., Cristina Malerba, M., Nardo, G., Dall'Olmo, L., Milani, E., Mariotti V., Stecca, T., Massani, M., Spirli, C., Fiorotto, R., Indraccolo, S., Strazzabosco, M., Fabris, L. Platelet-derived growth factor-D enables liver myofibroblasts to promote tumor lymphangiogenesis in cholangiocarcinoma. J Hepatol. 2019 Apr;70(4):700-709.

• Cadamuro, M., Brivio, S., Stecca, T., Kaffe, E., Mariotti V., Milani, C., Fiorotto, R., Spirli, C., Strazzabosco, M., Fabris, L. Animal models of cholangiocarcinoma: What they teach us about the human disease. Clin Res Hepatol Gastroenterol. 2018 Oct;42(5):403-415.

• Strazzabosco, M., Fiorotto, R., Cadamuro, M., Spirli, C., Mariotti V., Kaffe, E., Scirpo, R., Fabris, L. Pathophysiologic implications of innate immunity and autoinflammation in the biliary epithelium Biochim Biophys Acta Mol Basis Dis 2018 Apr;1864(4 Pt B):1374-1379.

• Fiorotto, R.*, Amenduni, M.*, Mariotti V., Fabris, L., Spirli, C., Strazzabosco, M. Src kinase inhibition reduces inflammatory and cytoskeletal changes in ΔF508 human cholangiocytes and improves cystic fibrosis transmembrane conductance regulator correctors efficacy. Hepatology. 2018 Mar;67(3):972-988.

• Fiorotto, R., Amenduni, M., Mariotti V., Fabris, L., Spirli, C., Strazzabosco, M. Liver diseases in the dish: iPSC and organoids as a new approach to modeling liver diseases. Biochim Biophys Acta Mol Basis Dis. 2018 Sep 5. pii: S0925-4439(18)30331-4.

• Mariotti V., Cadamuro, M., Spirli, C., Fiorotto, R., Strazzabosco, M., Fabris, L. Animal models of cholestasis: An update on inflammatory cholangiopathies. Biochim Biophys Acta Mol Basis Dis 2018 Aug 11. pii: S0925-4439(18)30274-6.

• Fiorotto, R., Amenduni, M., Mariotti V., Cadamuro, M., Fabris, L., Spirli, C., Strazzabosco, M. Animal models for cystic fibrosis liver disease (CFLD). Biochim Biophys Acta Mol Basis Dis 2018 Jul 30, pii: S0925-4439(18)30275-8.

• Cadamuro M, Stecca T, Brivio S, Mariotti V., Fiorotto R, Spirli C, Strazzabosco M, Fabris L. The deleterious interplay between tumor epithelia and stroma in cholangiocarcinoma. Biochim Biophys Acta. 2018 Apr;1864(4 Pt B):1435-1443.

• Mariotti V, Strazzabosco M, Fabris L, Calvisi DF. Animal models of biliary injury and altered bile acid metabolism. Biochim Biophys Acta. 2018 Apr;1864(4 Pt B):1254-1261.

INTRODUCTION

Cholangiocytes physiology

The biliary tree is a complex network of interconnected tubular structures within the liver, lined by specialized epithelial cells, also known as cholangiocytes[1]. Originating at the level of the Canals of Hering, described as ductule-canalicular junction lined by hepatocytes and cholangiocytes, these ductular structures progressively merge into a system of interlobular, septal, major ducts that ultimately marge with the duodenum[1, 2]. Although they comprise only for 3% to 5% of the liver population, cholangiocytes have major physiological functions. Cholangiocytes selectively control the transport of ions and molecules from/to bile, and act against pathogens and harmful molecules by function as a physical barrier(through tight junction, bile secretion, production of defensins and IgA, etc.)[3]. Cholangiocytes also favor the contact, via their basolateral plasma membrane, to the immune and vascular systems[4, 5]. Ultimately cholangiocytes contribute to bile production, a critical process for the life-sustaining functions of the liver[6].

The wide network of biliary tree within and outside the liver is mirrored by a considerable morphological and functional heterogeneity of cholangiocytes along the biliary tree[2]. Small cholangiocytes that line the Canal of Hering and the terminal cholangioles are considered less mature, and defined by a cuboidal shape with a basal nucleus, and are involved in controlling inflammation, regeneration and reparative response to liver and/or biliary injury[3]. More differentiated cholangiocytes are those that make up the larger and interlobular ducts (diameter from 20 μm up to 800 μm); these have a columnar shape and are mainly involved in secretory functions such as alkalization, hydration, and modification of bile, due to the presence of numerous carriers and hormone receptors on the cholangiocytes' plasma membrane (**Fig.**1A).

Changes in cholangiocytes' differentiation profile may also occur in part due to differences in vascularization along the biliary ducts. The intrahepatic biliary tree (IHBD) runs parallel to a branch of the portal vein, and with one or two branches of the hepatic artery, forming the portal triad[3, 4]. This allows the establishment of an intimate anatomical and functional association with the arterial vasculature. The IHBD are encircled by a network of capillaries, known as the peribiliary plexus (PBP), which

provides for the metabolic and functional needs of cholangiocytes, which facilitates their differentiated features[4, 5]. Moreover, these anatomical features enable the exchange of signals between biliary epithelial cells and different vascular cell types, such as endothelial and mural cells.

Secretory and absorptive functions of cholangiocytes

Cholangiocytes perform both secretory and absorptive activities. Hepatocytes produce the primary bile and generate the osmotic impetus via secretion of bile acids, lipids, glutathione, organic cations, and anions. Several ion carriers located on both apical (canalicular) and basolateral (sinusoidal) plasma membrane guarantee the transport of solute, which is linked with the passive transport of molecules of water across the cellular junctions. The subsequent modification of primary bile by cholangiocytes occurs during the transit through the biliary tree thanks to absorptive and secretive processes[7]. In fact, in addition to their secretory functions, cholangiocytes re-absorb fluid, electrolytes, amino-acids, bile acids, glucose and secrete water, chloride ion (Cl^-), bicarbonate ($HCO3^-$) and immunoglobulin A (IgA)[7].

The net amount of fluid and bicarbonate secretion is due to the combination of pro-secretory effects, including, but not limited to secretin, glucagon, and vasoactive intestinal polypeptide (VIP), and anti-secretory activities mediated by somatostatin, insulin, and endothelin, etc.. [8, 9]The mechanism of ductal secretion is based on the interaction of the above-mentioned factors with adenyl cyclase (AC). ACs are transmembrane enzymes that are present in the basolateral membrane of cholangiocytes, and are able to regulate intracellular cAMP level by converting ATP to cAMP. Nine different types of AC exist, and the intrahepatic biliary epithelium expresses seven of these AC isoforms (AC4-9), with a heterogeneous pattern of expression among different cholangiocyte sub-populations[10]. Among ACs expressed in cholangiocytes, AC5 and AC6 are inhibited by Ca^{2+}, even at the physiologic cytoplasmic concentrations. In large cholangioles (which line the large bile duct), for example, the interaction between AC8 and AC9 and secretin leads to increased intracellular levels of cAMP, stimulation of protein kinase A (PKA), and phosphorylation of the cystic fibrosis transmembrane conductance regulator (CFTR) channel[11]. This leads to Cl^- secretion into the ductal lumen and bicarbonate efflux through the Cl^-/ $HCO3^-$ exchanger (AE2)[12, 13]. Cholangiocytes express other Cl^-

channels that are also important for bile formation, such as a Cl^- Ca^{2+}-dependent channels, a Ca^{2+} and cAMP-intensive high conductance anion channel, a barium-sensitive K^+ conductance channels that modulates K^+ efflux, maintaining the membrane hyperpolarization needed to provide the driving force for Cl^- exit, and finally, a bumetanide-inhibitable Na^+- K^+-2Cl co-transport, which participates in basolateral Cl^-uptake[14]. Notably, Ca^{2+} can also stimulate $HCO3^-$ secretion; in fact, stimulation of apical Ca^{2+}-activated Cl^- channels (such as transmembrane protein 16F (TMEM16) by increased intracellular Ca^{2+}, promotes efflux of Cl^- that is then exchanged with $HCO3^-$ through AE2-mediated $Cl^-/HCO3^-$ exchange[13]. Notably, several other molecules that constitute the bile can trigger biliary $HCO3^-$ secretion. Indeed, extracellular nucleotides and nucleosides stimulate different subtypes of purinergic receptor (P2Y), localized at the apical membrane of cholangiocytes, and promote efflux of K^+, Cl^- and $HCO3^-$ (**Fig.**1A).

The reabsorption function of the biliary epithelium is guarantee by the expression of transport proteins both on the apical and basolateral membrane of cholangiocytes. For example, cholangiocytes can take up bile acids from bile through the apical Na^+-dependent bile salt transporter (ASBT), and secrete them into the peribiliary vascular plexus (PBP) through p-glycoprotein multidrug resistance protein 3 (MRP3)[11, 15]. It is worth note that the reabsorption of bile salts occurs in the chole-hepatic circulation.

Thus, the bi-directional transport of various molecules, including organic and inorganic anions and cation, as well as proteins, is guaranteed in cholangiocytes by the polarized distribution of a number of transporters, primarily multi-drug resistance proteins, which consequently initiate intracellular signal transduction pathways (such as cAMP and Ca^{2+})[16].

An important organelle with a role in the regulation of bile secretion is the primary cilium, which extend from the apical membrane into the ductal lumen. The primary cilium detects changes in bile flow, composition, and osmolarity, and subsequently regulates intracellular signaling mechanisms[17]. For example, an alteration in luminal flow will be detected by blending of the primary cilia, which in turn will induce an intracellular calcium $[Ca^{2+}]_i$ influx, and activate different signaling pathways involved in the regulation of epithelial cell proliferation, secretion, and apoptosis[16]. On the other hand, when changes to nucleotide or osmolarity are detected, a signal to induce bicarbonate secretion will be generated by the primary

cilia. Thus, primary cilia possess pleiotropic biological functions, and act as mechano, osmo, and chemosensory organelles. The defective function of ciliary proteins may be associated to polycystic diseases in the liver, kidney, and other organs.

Ultimately, when reaching the small intestine, bile contains a variety of components that comprise electrolytes, bile acids, bilirubin, lipids (cholesterol, lecithin), amino-acids (glutamic acid, aspartic acid, glycine), vitamins (folic acid B9, piridossin B6, cobalamin B12), metals, inorganic molecules (Na^+, Cl^-, $HCO3^-$), enzymes, proteins, and endobiotic and xenobiotic compounds[7].

The latter molecules contribute to health by maintaining the enterohepatic circulation, supporting the absorption of digested lipids in the small intestine and by facilitating the elimination of cholesterol and xenobiotic compounds from the body.

Pathobiology of cholangiocytes

Perturbation of normal cholangiocyte functions, in response to several types of damage and inflammatory insults induces cholangiocytes to acquire the phenotype of ‘reactive ductular cells’ (RDC)[3, 14, 18]. Features of activated cholangiocytes include proliferation and secretion of pro-fibrotic and pro-inflammatory agents. Thus, activated cholangiocytes contribute to recruitment as well as the cross-talk with immune, vascular, and mesenchymal cells, trough the expression of specific proteins, and the secretion of an array of molecules such as cytokines, chemokines, growth factors, and angiogenetic elements[19]. Reactive ductular cells become the main actor in the reparative response to biliary injury via pleiotropic autocrine and paracrine inflammatory signals, resulting from the loss of the normal homeostasis in cholangiocytes. Reactive ductular cells are part of the so-called ‘ductular reaction’ (DR), along with mesenchymal, immune and endothelial cells[20, 21]. An increased number of RDCs is found in diseases characterized by a significant increase in inflammation infiltrate and portal fibrosis, such as in viral hepatic disease, metabolic disorders, and in disorders associated with impaired embryogenesis, e.g. Alagille syndrome and biliary atresia. Fine-tuned cross-talk between activated cholangiocytes and mesenchymal cells (due to the complementary expression of an array of agonists and their receptors) mediate cellular events associated with the biliary repair response[22-24]. Furthermore, RDCs secrete pro-inflammatory and pro-fibrotic molecules such as connective tissue growth factor (CTGF), CXC-chemokine ligands

(CXCL), platelet-derived growth factor B homodimer B (PDGFBB), transforming growth factor-β2 (TGF-B2), tumor necrosis factor-α (TNF), interferon-γ (IFNγ), vascular growth factor-A (VEGF-A), and interleukin-6, -8 and -1B (IL-6, IL-8, and IL-1β, respectively)[23], which modifies the periductular microenvironment, and mediates the recruitment of innate and adaptive immune cells to protect against biliary insults, in addition to resident and recruited mesenchymal and endothelial cells in order to repair and remodel the biliary tree (**Fig.**1B).

In most cases, the pro-inflammatory response and injury to the biliary tree resolves. However, an exaggerated cholangiocytes' response, alongside with persistent biliary cell damage, causes a chronic inflammatory reaction that endorses a "pathological" reparative reaction, with excessive deposition of fibrous tissue around the injured ducts (periportal fibrosis), increased proliferation (hyperplasia), biliary cirrhosis, and eventually, chronic liver failure.

Cholangiocyte proliferation

The proliferative response of cholangiocytes during biliary injury/damage is regulated by an intricate interplay of various autocrine and paracrine molecules that are released in the injured microenvironment. Among the different molecules involved in this process, IL-6 has been found to be mitogenic for normal biliary epithelial as well as during biliary disease progression. IL-6 production has been found to significantly increase in response to inflammatory stimuli such as LPS, or by the stimulation of pro-inflammatory cytokines IL-6 and TNF-a[25]. Several *in vitro* studies have demonstrated that cholangiocyte growth through IL-6 stimulation occurs via two different mechanisms. Indeed, IL-6 is able to directly stimulate cholangiocytes' DNA synthesis and inhibit apoptosis, by increasing the Bcl2/bax ratio[26, 27]. On the other hand, cholangiocytes stimulated by other pro-inflammatory cytokines produce and secrete IL-6, which can act as an autocrine factor on reactive cholangiocytes themselves. These findings highlight the role of IL-6 in cholangiocytes' proliferation, and demonstrate that cholangiocytes can both produce and respond to IL-6 to further support the presence of an autocrine growth control loop, which acts via the activation of the p44/p42 MAPK signaling pathway[26]. Similar to IL-6, several other growth factors, such as hepatocyte growth factor (HGF)[28], insulin-growth factor (IGF)-1[29],

and vascular growth factor (VEGF)[30, 31] have been found to be involved in cholangiocytes' proliferation during biliary injury. Increased knowledge related to the mechanism of cholangiocytes' proliferation has been made possible, thanks to the use of animal models that mimic liver human disease conditions[32, 33].

Cholangiocyte' proliferation is further supported by secretin, a known activator of the intracellular cAMP, as well as by the expressed male and female sex hormone receptors (including estrogen, progesterone, testosterone, and follicle-stimulating hormone (FSH)). In cholangiocytes, the progesterone-mediated progesterone receptors stimulation induces an increase in the biliary mass. Likewise, a decrease in the intrahepatic biliary mass and a block in the biliary secretion has been shown upon castration or anti-testosterone therapy in bile-duct-ligated (BDL) animal models, owing the rapid onset of fibrous deposition. Concomitant with proliferative stimuli, in pathological conditions, this effect is counterbalanced by the effect of anti-proliferative peptides such as gastrin, melatonin, somatostatin, and gamma-aminobutyl acid (GABA)[34].

It is worth noting that many of the morphogenetic signals (such as Wnt/β-Catenin, Notch, and Hippo pathways) that regulate biliary development also appear to regulate cholangiocytes' cell-fate decisions in pathological conditions[19].

Biliary fibrosis

Liver fibrosis is a complex and highly integrated physio-pathological process that results from an aberrant reparative response to liver injury. It has been proposed that initiation of fibrous deposition, via direct epithelial-mesenchymal transition (EMT), or indirectly via the activation of other liver cell types, is mediated by the aberrant cholangiocytes proliferation. The role, if any, of epithelial mesenchymal transition in biliary repair remains unclear.

During biliary fibrosis, proliferating cholangiocytes are the main source of the profibrogenic connective tissue growth factor (CTGF), in addition to that produced by hepatic stellate cells (HSC), and activated by cholangiocytes themselves. CTGF modulate the transduction of extracellular signals by interacting with membrane glycoproteins (integrins), growth factor (TGFβ1), and with different components of the

extracellular matrix (ECM)[35]. Furthermore, CTGF stimulates the recruitment of different cell types, including macrophages, and supports their inflammatory response[36].

In addition, cholangiocytes recruits the main immune and mesenchymal cellular component of ductular reaction. Similarly, in the context of biliary injury, apoptosis and/or necrosis of the epithelium stimulates the recruitment of inflammatory and mesenchymal cells. Additionally, necrotic cells release genetic material and debris (danger associated molecular patterns – DAMPs) into the intracellular space; these are recognized by appropriate receptors in HSCs and portal fibroblasts that transdifferentiate into myofibrobalsts and produce ECM proteins[37].

Among all the pro-fibrotic cytokines, transforming growth factor β1 (TGFβ1)is a well-known factor involved in the formation of liver fibrosis. Fibroblasts and macrophages secrete TGFβ1 and activate HSCs, which are responsible for the deposition of ~90% of matrix proteins upon their trandifferentiation in myofibroblasts (MF), the key effectors in the fibrotic process[37]. In fact, these cells acquire the expression of smooth muscle alpha-actin and appear more responsive to fibrogenic, chemoattractant, and mitogenic stimuli[38]. MF actively secrete ECM proteins, particularly laminin and fibrillar collagen, causing an alteration in the normal composition of the matrix. In addition to modifying ECM composition, MFs secrete proteins involved in matrix degradation such as metalloproteases, as well as their inhibitor (TIMP), which regulates ECM composition during chronic hepatic injury[39]. Cholangiocytes also retain the ability to secrete MMPs, and thus actively contribute to the modification of ECM composition. Treatment with a broad range of MMP inhibitors in an animal model of fibropolycystic liver disease resulted decreased liver cysts area and a reduction of the expression of collagen[39].

Although debated, MFs located in the portal spaces may also originate from a specific subset of fibroblasts resident in the portal spaces and distinct from HSC[38]. Furthermore, several studies have shown that bone marrow-derived fibrocytes may contribute to ECM deposition. Bone marrow-derived circulating fibrocytes own an transitional phenotype, being originate from monocytes and act as myofibroblasts, to which they can trans-differentiate[40]. The maintenance of this in-between status suggests a key role of fibrocytes in would healing and during the modulation of the immune response in different tissue and organs.The transdifferentiation of monocytes

into fibrocytes is stimulate by several cytokines, such as interleukine-13, -4 (IL-13 and IL-4, respectively), TGFβ1 and the chemokine stromal cell-derived factor-1 (SDF1) (also known as C-X-C motif chemokine 12,CXCL12), a potent chemoattractant for peripheral blood mononuclear cells (PBMCs)[41, 42]. In models characterized by the rapid establishment of liver fibrosis, such as bile duct ligation (BDL), fibrocytes make only a small contribution to the collagen-producing cell (<5%)[43]. However, in other organs fibrocytes represent an important population among the collagen producing cells and the number varies from 25-30% in lung fibrosis to 20% in renal fibrosis[41, 42].

Cholangiopathies and polycystic liver diseases

Understanding the pathobiological mechanism relevance of the above-mentioned process is of fundamental importance to decipher the pathophysiology of cholangiopathies, an heterogeneous group of human diseases, affecting the biliary epithelium. Independently from their etiology, the common features of cholangiopathies include the simultaneous presence in the biliary epithelium of proliferation, apoptosis, fibrosis, inflammation, and eventually cholestasis, a biochemical, functional, and clinical consequence of bile flow impairment, as well as modification of bile composition, which may initiate or worsen the cholangiopathic process[3, 18, 44].

Cholangiopathies cause significant morbidity and mortality, resulting from a lack of effective medical therapies. Cholangiopathies are rare, but as a group, represent an important indication for liver transplantation, ranging from 10% to 20% of the adult liver transplantation performed, and scaling up to 80% of the indications for pediatric liver transplantation[45, 46]. Cholangiopathies can be classified into three groups: (i) genetic and inherited (i.e. cystic fibrosis, Alagille syndrome, polycystic liver diseases, etc.); (ii) immune-mediated (i.e. primary biliary cholangitis (PBC), primary sclerosing cholangitis (PSC), etc.); (iii) idiopathic, drug-induced, ischemic, and malignant cholangiopathies (Table 1).

Polycystic liver diseases (PLDs)

Among the genetic cholangiopathies, we have focused on polycystic liver diseases (PLDs). Polycystic liver diseases (PLDs) are phenotypically characterized by multiple cysts scattered throughout the liver parenchyma[47, 48]. Genetic analysis of PLD patients revealed mutations in genes involving proteins located in the endoplasmic reticulum (ER), and in the primary cilium of biliary cells (see part I). Thus, PLDs are a member of a group of diseases called 'ciliopathies'[19, 48, 49].

The pathogenesis of PLDs is linked with the embryonic development of the intrahepatic bile ducts (IHBDs)[19]. The development of the IHBDs requires the remodeling of the ductal plate, a structure corresponding to the most immature state of the biliary tree, and involving finely turned epithelia-mesenchyme interactions, in cooperation with several morphogenetic signaling processes, as described above. Interruptions in the remodeling of the ductal plate may result in the persistence of the embryonic ductal plate's epithelial ducts, known as ductal plate malformation (DPM)[50]. DPM may affect all levels of the IHBDs, i.e. segmental, septal, interlobular, and the smaller ducts of the terminal portal tract. The Von Meyenburg complexes (VMCs), or biliary micro-hamartomas, represent the most common form of DPM. VMCs are benign conditions characterized by small cystic dilatation of the IHBD, embedded in abundant fibrous stroma[48].

The immaturity of the bile tracts at different developmental phases leads to different anatomo-clinical features that can be classified into: (i) diseases characterized by different degrees of dilatation of the biliary tree, in association with fibrosis, i.e. Caroli disease (CD) and congenital hepatic fibrosis (CHF), defined as fibropolycystic liver disease; (ii) diseases characterized by the formation of multiple cysts scattered throughout the liver parenchyma (autosomal dominant polycystic liver disease -ADPLD-), either confined to the liver or in association with similar lesions in the kidney (autosomal dominant polycystic kidney disease (ADPKD))[51-53]. The basis for this modern classification is shown in Table 2. Among the DPMs that are not embryonically lethal, PLD linked to autosomal dominant polycystic kidney disease (PLD-ADPKD), and autosomal recessive polycystic kidney disease (PLD-ARPKD),are the focus of the present work.

Symptoms, diagnosis, and clinical management of PLDs

Typically, PLD patients will remain asymptomatic for many years, until the number and volume of cysts cause hepatomegaly[54]. However, symptoms can become evident in an age-dependent fashion, because of the mass-effects of the enlarging cysts, or because of complications related to the cysts, such as infection or hemorrhages[47, 54]. Symptoms may include abdominal distension and pain, early satiety, abdominal discomfort, portal hypertension, ascites, jaundice, and dyspnea. Symptomatic cyst complications include cyst hemorrhage, infection, and rupture. Among fibropolicystic liver diseases, severe portal hypertension dominates the clinical picture of congenital hepatic fibrosis, while recurrent cholangitis is typical of Caroli Disease. Several case reports have been published reporting malignancies such as adenocarcinoma, squamous cell carcinoma, and particularly cholangiocarcinoma complicating fibropolycystic diseases of the liver[51].

Patients with moderate-to-severe PLDs and impaired quality of life can benefits for short-term and modest therapeutic options, which include a chronic treatment with somatostatin analogues, or surgical procedures (aspiration, sclerotherapy, cyst fenestration, or segmental hepatic resection) for symptomatic cysts[55]. However, the only curative options remain liver transplantation[19].

FIGURES INTRODUCTION

Figure 1. Cholangiocytes in Physiology e Pathobiology

(A) Bile produced by hepatocytes (primary bile) is delivered into the bile ducts, where cholangiocytes provide to its final composition by secretion and absorption of electrolytes, fluids and bile acids, among a vast array of biliary components. Enlargement of a large cholangiocytes show the main ion carriers and receptor involved in the secretion of bicarbonate ($HCO3^-$), which is fundamental for bile flow and the elimination of xenobiotics and for protection towards bile acids toxicity. The binding of secretin to the basolateral G protein-coupled secretin receptor induces an increase in intracellular cAMP, which leads to PKA activation and secretion of Cl- upon CFTR-phosphorylation. The secretion of Cl^- also occurs via other Ca^{2+} activated Cl channes. Cl^- then re-enters the cell via he anion exchanger 2 (AE2) in exchange with bicarbonate. This generate an electrolyte-osmotic gradient that favor the passive transport of water to the aquaporins (AQPs), resulting in in alkalization and hydration of bile. (B) Genetically determined cholangiocyte malfunction results in a cholangiocytes' reparative response which is characterized by phenotypic changes in cholangiocytes (activation), and the secretion of chemokines, cytokines and growth factors that, acting in both a paracrine and autocrine way stimulate cholangiocytes proliferation as well as inflammatory cell recruitment. This process ultimately results in fibrosis deposition, the major event that leads to the progression of the disease. *(Modified from Banales J., Nature Review Gastroenterology and Hepatology, 2019)*

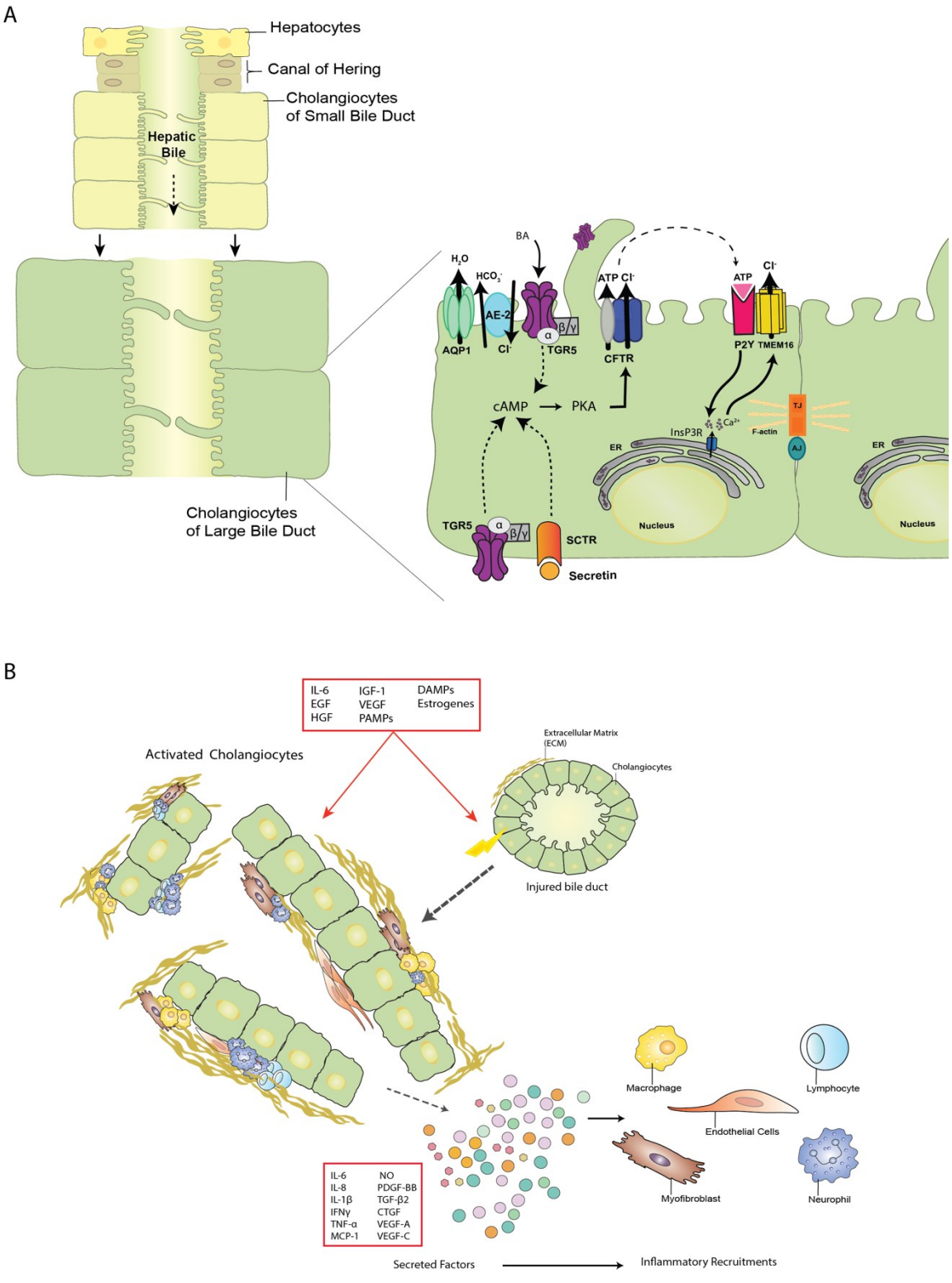
A
Hepatocytes
Canal of Hering
Cholangiocytes of Small Bile Duct
Hepatic Bile
Cholangiocytes of Large Bile Duct
BA
H_2O
HCO_3^-
AE-2
AQP1
Cl^-
TGR5
ATP Cl^-
CFTR
ATP
Cl^-
P2Y
TMEM16
cAMP
PKA
InsP3R
Ca^{2+}
F-actin
TJ
AJ
ER
Nucleus
TGR5
SCTR
Secretin
B
IL-6 IGF-1 DAMPs
EGF VEGF Estrogenes
HGF PAMPs
Activated Cholangiocytes
Extracellular Matrix (ECM)
Cholangiocytes
Injured bile duct
Macrophage
Lymphocyte
Endothelial Cells
Myofibroblast
Neurophil
IL-6 NO
IL-8 PDGF-BB
IL-1β TGF-β2
IFNγ CTGF
TNF-α VEGF-A
MCP-1 VEGF-C
Secreted Factors
Inflammatory Recruitments

FIGURE 1

Table 1| Classification of Cholangiopathies

ADPKD, autosomal dominant polycystic kidney disease; AGS, Alagille syndrome; AMA, Antimitochondrial antibody; ARPKD, autosomal recessive polycystic kidney disease; CD, Caroli's Disease; CF, cystic fibrosis; CHF, congenital hepatic fibrosis; GVHD, graft versus host disease; PBC, primary biliary cholangitis; PSC, primary sclerosing cholangitis.

Groups	Example
Genetic and inherited	- CF - AGS - Polycystic diseases (i.e CD, CHF, ADPKD, ARPKD)
Immuno-mediated	- PBC - PSC - Autoimmune cholangitis (AMA-negative PBC) - Acute/Cronic allograft rejection - GVHD
Idiopathic, drug-induced, ischemic and malignant cholangiopathies	- Biliary atresia (extra or intrahepatic) - Floxuridine-induced cholangiopathy - Postliver transplantation hepatic artery stenosis - Cholangiocarcinoma

Table 2| Classification of PLDs

ADPKD, autosomal dominant polycystic kidney disease; ADPLD, autosomal dominant polycystic liver disease; ARPKD, autosomal recessive polycystic kidney disease; CD, Caroli Disease; CHF, congenital hepatic fibrosis; DPM, ductal plate malformation; PLCDs, polycystic liver disease.

PCLD	Incidence	Genetic Defect	Pathology	Clinical Features and Outcome
ADPKD	*1:1,000*	PKD1 and PKD2 (Polycystin 1 and 2)	DPM, biliary microhamartmas and liver cysts	Renal failure, cyst complication (mass effect, hemorrhage, infection, rupture), preserved liver function; severe hepatic cysts disease
ADPLD	*Nearly 50% of PLDs cases*	PRKCSH (hepatocystin), SEC63 (ER translocator) and LRP5 (PM coreceptor)	DPM, biliary microhamartmas and liver cysts	Similar to ADPKD except for renal involvement
CD	*Rare*	PKHD1 (Fibrocystin)	DPM and cystic dilatation of the intrahepatic bile ducts	Recurrent cholangitis, cyst complications, cholangiocarcinoma (7%)
CHF	*Rare*	PKHD1(Fibrocystin)	DPM and biliary microhamartmas, surrounded by a dense fibrous stroma	Portal hypertension, recurrent cholangitis, cholangiocarcinoma (rare)
ARPKD	*1:20-40,000*	PKHD1(Fibrocystin)	DPM, biliary microhamartmas and cysts	Renal failure, recurrent cholangitis, portal hypertension

PART I

Adenylyl cyclase 5 links changes in calcium homeostasis to cAMP-dependent cyst growth in polycystic liver disease

BACKGROUND

Autosomal dominant polycystic kidney disease (ADPKD) is the most common monogenic hereditary disorder and is predicted to affect more the 10 million people worldwide in all the ethnic groups, representing a substantial economic burden on healthcare systems, mainly for dnd-stage renal failure (ERSD) costs[52, 56]. The prevalence of ADPKD is reported to be between 1 in 400 and 1 in 1000 newborns[57] and ESRD occurs as a result of ADPKD in up to 75% of patients by 70 years of age[58]. Furthermore, based on the ERSD rate, the progression of ADPKD is more marked in men rather than in women (1.2-1.3 men to women). Interestingly, hepatic cysts, which represent the most common extra-renal manifestation in ADPKD, are more prevalent in women, and the average volume of hepatic cysts is higher in women (5.27 mL) versus men (1.94 mL)[58]. These differences in volume seem to be age-dependent and can be explained by the fact that women undergo pregnancies and are exposed to oral contraceptive pills or estrogen-replacement therapy that leads to worse disease.

This multisystem disorder is characterized by progressive enlarge of fluid-filled cysts in the kidney, liver, and pancreas and is associated with kidney failure, hypertension, and brain aneurysm[59].

The genetic basis of ADPKD and the identity of the mutated genes is relatively well known. Patients carrying mutations in PKD1 (chromosome 16p13.3), encoding for polycystin-1, account for ~80% of cases of ADPKD, whereas ~ 10-15% of cases are due to mutation in PKD2 gene (chromosome 4p21), encoding for polycystin 2. The remaining ~ 5-10% cases are genetically indeterminate or due to rare mutations in other gene loci[60]. Rare mutations that generate an ADPKD-like phenotype occurs in genes encoding for the hepatocyte nuclear factor 1 homeobox B (HNF1B, owing the ability to regulate the expression of different PKD-associate genes, including PKHD1 and PKD2), the neutral a-glucosidase AB (GANAB; involved in the folding of the proteins) and in the DNAJB11 gene (which encode for a chaperone protein associated to the Binding Immunoglobulin Protein or BiP)[60-63].

Mutations in genes that are primarily associated with autosomal dominant polycystic liver disease (ADPLD) (i.e. a polycystic disease identical to that associated with ADPKD, but limited to the liver, without kidney involvement) include PRKCSH

(which encode for the regulatory b-subunit of glycosidase 2 that is involved in protein folding) and SEC65 (encode for a protein required for the translocation of proteins across the endoplasmic reticulum (ER) membrane) that account for the ~ 35% of clinically diagnosed cases[64-67]. Patients carrying mutation in GANAB can manifest either ADPKD or ADPLD phenotype. Moreover, genes such as LRP5 (econding for a WNT co-receptor), SEC61B (the b-subunit of SEC61 which role is to transfer glycoproteins) and ALG8 (encoding for a-1.3-glucosyltransferase) formally contribute to the progress of ADPLD[68, 69]. In this sense, mutations taking place in PKD1 and PKD2 genes become the original cause of ADPKD development, even though any mutation involved in the biogenesis process (i.e. transportation, protein folding or glycosylation) or associated with decrease of polycystin-1 and -2 manifestations might imitate ADPKD phenotypically[67]. Importantly to note, hereditary cancer disease tuberous sclerosis and von Hippel-Lindau disease might also imitate ADPKD if extra-renal exhibition is missing or in moderate form[63].

Germline mutation in one allele of either PKD1 and PKD2 genes mainly occurs in ADPKD patients[70]. However, a second event such as a somatic inactivation of the other wild-type allele of PLD-related genes or loss heterozygosity may be required to initiate cysts formation. In has been postulate that also environmental factors can modulate cyst initiation and disease progression[67].

Polycystin-1 (PC1) and polycystin-2 (PC2) are mostly localized in the primary cilia of renal tubular and cholangiocytes where they act to control several signaling pathways associate with ductal morphogenesis, proliferation, and differentiation[71, 72].

PC1 is a large, integral membrane protein of ~450 kDa with eleven-transmembrane domains and a short ~200-amino acid C-terminal cytoplasmic tail. It interacts with PC2 through the coiled-coil domain in the C-terminal region forming a Ca^{2+}-permeable mechanosensitive ion channel. The 3074 amino-acids of the extracellular portion of PC1 contain a G-protein receptor proteolytic site, which when cleaved produced a large N-terminal and a smaller C-terminal fragment[52, 73, 74]. The latter is reported to modulate STAT6 and P100 activity or canonical Wnt signaling. Similarly, regulated intracellular C-terminal tail cleavage releases PC1 fragments that modulate various signaling pathways upon interaction to transcriptional activator, repressor or co-activator[68]. Even if the PC1 has been described in the tight junctions,

adherens junctions, desmosomes, apical vesicles and in the primary cilia, its subcellular localization seems to be dependent on the developmental stage and cells polarization[52, 68, 72].

PC2 is generally described as a 968-amino acid protein with six transmembrane regions that are homologs for PC1 and to the voltage-activated and transient receptors potential channel (TRPC) subunit[75]. TRP channels have been implicated in various cellular functions; depending on the protein it interacts with, such as osmosensing, mechanotransduction, regulation of Mg^{2+} homeostasis, and vasoregulation[76]. At cellular level, TRPC function as a multimodal sensor for a large number of intracellular and extracellular stimuli, and is regulated downstream of phospholipase C (PLC). All the isoforms of the TRP superfamily are localized at the plasma membrane and are non-selective cation channel, with regard for the isoforms TRPV5 and TRPV6, which are highly Ca^{2+} selective, and TRPM4 which is impermeable to Ca^{2+} [77].

PC2/TRPC2 can function as a mechano-chemo-osmo-sensor, or as a non-selective cation channel for the Ca^{2+}, depending on its interaction with other proteins, such as PC1, TRPV4 or ryanodine receptors (RyRs)[78]. Although a portion of PC2 co-localizes with PC1 in the cilium, the major amount of cellular pool of PC2 resides in the basolateral membranes, in the mitotic spindles in dividing cells and in endoplasmic reticulum (ER) where its known to interact with inositol 1,4,5-trisphosphate receptor (InsP3R) and as shown to controls ER-Ca^{2+} homeostasis[79, 80].

Liver complications affect ~90% of ADPKD patients and, besides the complication that occur in kidney, polycystic liver disease (PLD-ADPKD) is one of the leading causes of liver transplantation among genetic cholangiopathies[19, 64]. In accordance with the expression of polycystins in the cholangiocytes, PLD-ADPKD manifests as a chronic and progressive cholangiopathy, due to the maintenance of an immature phenotype incline to proliferative and secretory activities, that are responsible for the formation of multiple, large cysts spanning the liver parenchyma without connection with the biliary tree[71, 81].

The signals linking PC deficiency to cystogenesis and disease progression have been the object of intensive research. Earlier observations showed that in polycystic liver disease associated to ADPKD, the dysmorphic bile ducts are

surrounded by hyperplastic vascular structures with an abnormal ramification resembling a “pollard willow pattern”[14, 19, 53]. Similar to ductal plate cells during development, the cystic biliary epithelium of patients with PLD-ADPKD, shows a strong up-regulation of VEGF and Ang-1 expression, together with their receptors VEGFR2 and Tie2. Furthermore, the increased levels of expression of VEGF and Ang-1 positively correlated with the microvascular density around the growing biliary cysts in ADPKD, suggesting that angiogenesis is crucial for the cysts growth, as the vasculature provides nutrients and metabolic support[82, 83].

Expansion of hepatic cysts is further supported by several factors including functional ciliary abnormalities, cell-cycle dysregulation, enhanced cholangiocytes fluid secretion. Indeed, studies have shown that secretin-stimulated activation of intracellular cAMP increases cystic fluid secretion and enlargement in hepatic cysts associated with ADPDK[10, 84-86]. It has been proposed that increased fluid secretion into hepatic cysts would promote stretching of the cystic cholangiocytes that results in cytokines-dependent cysts growth. Interestingly, IL-8 is released from stretched cholangiocytes and induces a strong proliferative effect and is also present at physiological levels in hepatic cysts of patients with ADPDK[87].

Previous research in our laboratory has revealed several changes in intracellular signaling that are relevant for the pathobiology of PLD-ADPDK and will be discussed in the next chapter.

SUMMARY OF PREVIOUS DATA AND AIM

The study of VEGF-A signaling in ADPKD-related polycystic liver disease has provided important information on the pathobiological mechanism that drive cholangiocyte proliferation.

Our group and others reported a marked upregulation of VEGF together with its receptors VEGFR-1 and VEGFR-2, and of Ang-1 in conjunction with its cognate receptor Tie-2 in cholangiocytes isolated from ADPKD patients, as well as in the cystic epithelium cultured from mice with liver-specific PC2 deletion (*Pkd2-KO*) (**Fig.**2A)[30, 31, 82].

The enhanced expression of angiogenic factors correlated with the microvascular density around the biliary cysts, as shown by increased CD31 expression (marker of ECs) in ADPKD compared with normal liver[82]. On one side, angiogenic factors produced by cholangiocytes are responsible for generating the vascular supply to the growing cysts; on the other hand, they stimulate the proliferation of the biliary epithelium in an autocrine fashion. Indeed, the administration of recombinant VEGF-A induces a dose-dependent stimulatory effect on cholangiocyte proliferation. Furthermore, the co-administration of Ang-1 together with VEGF resulted in a further, intense stimulation of PCNA expression (a marker of proliferation), suggesting that the effect of Ang-1 was synergic to VEGF[83].

Increased production of VEGF was also demonstrated in cultured isolated cystic cholangiocytes, indicating this effect as the direct loss of PC1 or PC2 function without association with hypoxia-induced pathway. The production of VEGF is regulated by the hypoxia-inducible factor 1 (HIF-1α) transcription factor, one of the critical modulators of the tissue response to changes in oxygen levels[31].

HIF-1α can also signal in response to non-hypoxic stimuli such as growth factors, cytokines, and a multiplicity of extracellular soluble mediators (IL-1, IL-6, EGF, HGF, TGFα , 17-β-estradiol, IGF-1) which can stabilize or phosphorylate HIF-1α via PI3K/AKT/tuberin/mTOR or Raf/MEK/ERK or STAT3 signaling pathway[88].

In particular, in mice defective for PC2 (*Pkd2-KO*), our group showed that the proliferation rate of the cystic epithelium is higher and correlates with the upregulation of VEGF, its receptor VEGFR2 and an increased HIF-1α-dependent activation of ERK1/2. Furthermore, we found that the administration of VEGF-A in PC2 defective

cholangiocytes increased VEGFR2 expression and VEGFR2 phosphorylation levels, confirming the functionality of the receptor and the autocrine effects of VEGF in stimulating the growth of the liver cysts[31, 32].

Further studies addressed the importance of the ERK pathway, which is known to be the main signaling pathways regulating cholangiocyte proliferation. The administration of VEGF resulted in dose-dependent phosphorylation of ERK in the cyst epithelium of *Pkd2-KO* mice. Interestingly, this was inhibited by the PKA antagonism PKI, resulting in a decrease in VEGF secretion [31](**Fig.**2B-C). These data support the idea that, in physiological condition, the Raf/MEK/ERK cascade is inhibited by PC2. As a consequence, the lack of PC2 function leads to the inappropriate activation of the Raf/MEK/ERK pathway and an increase in cellular proliferation.

Numerous growth factors able to stimulate cholangiocytes proliferation appear to act through the Ras/Raf/MEK/ERK pathway. HIF-1α-regulated a wide variety of genes, especially the one that encode for proteins related to angiogenesis, energy metabolism, erythropoiesis, cell proliferation and viability, vascular remodeling, and vasomotor responses[89, 90]. Furthermore, histological studies on ADPKD liver specimens described an elevated expression of estrogen receptor (ER), insulin-like growth factor (IGF), IGF receptor, growth hormone receptor, and phosphorylated AKT (pAKT) in cholangiocytes lining the biliary cysts. In line with these studies, a marked overexpression of IGF1, its cognate receptor IGF1-R, together with pAKT, was found in both the human ADPKD and mouse model[30]. Indeed, we reported that the stimulation of mTOR trough AKT by IGF1 ligand binding to its receptor stimulates the PI3K/AKT/mTOR pathway in PC2-defective cholangiocytes. In turn, the increased phosphorylation of AKT and activation of mTOR is responsible for increased HIF-1α-dependent VEGF production and increased VEGFR2-mediated autocrine stimulation of cyst growth in PC2 defective cells[30]. The pathological importance of these pathway relay on the ability of specific inhibitor of VEGFR2 (SU5416) and mTOR (Rapamycin) to decrease VEGF secretion that ultimately results in a reduction of cysts volume in PLD-ADPKD mouse model[30, 31].

Signaling via the MEK/ERK1/2 cascade is usually initiated by the activation of the small G protein Ras. The signal is further transmitted by the recruiting of Raf kinases to the plasma membrane, where they are activated. In epithelial cells, including cholangiocytes, activated Ras promotes Raf kinases activation by Raf-1/B-Raf heterodimerization. In PC2-defective cholangiocytes, cAMP/PKA-dependent

activation of the Ras/Raf/ERK1/2 pathway stimulates the growth of liver cysts, the secretion of VEGF, as well as increased VEGF-dependent fluid secretion[91].

Calcium homeostasis and increased cAMP production

Cyclic adenosine 3',5'- monophosphate (cAMP) acts as a second messenger that couples extracellular signals to intracellular responses and has a role in multiple cellular processes including cell growth and differentiation, glucose, and lipid metabolism. In cholangiocytes, cAMP signaling stimulates both bile secretion and cell proliferation[10, 85, 91, 92].

The hypothesis that, in PLDs of, cAMP plays an essential role in the growth of the cysts by stimulating both cholangiocytes cell proliferation and trans-epithelial fluid secretion, was suggested by studies showing that in kidney epithelial cells isolated from ADPKD patients had an increased fluid secretion upon treatment with cAMP analogues[84, 93]. It has been hypothesized that cAMP-induced fluid secretion is associated with increased activity of the cystic fibrosis transmembrane conductance regulator (CFTR), with subsequent activation of the $Cl^-/HCO3^-$ anion exchanger 2 (AE2) and secretion of bicarbonate ($HCO3^-$) into bile[13, 85]. Data from our laboratory, showing that signaling through the PKA/Ras/Raf/MEK/ERK1/2/VEGF cascade, a downstream pathway activated by cAMP, is overactive in cystic cholangiocytes, further confirmed the central role played by cAMP in cyst growth[30, 31, 91]. In this context, cAMP drive both trans-epithelial fluid secretion and epithelial cell proliferation. Studies in vivo, describing the proliferative effect of forskolin, the direct activator of the adenylate cyclase (AC), via the PKA/ERK1/2 cascade, further highlight the relevance of cAMP in promoting cholangiocyte proliferation. It is also of noteworthy that treatment with somatostatin analogues,(that inhibits cAMP production) reduce cysts growth both in kidney and liver and decrease the proliferation rate of cystic epithelial in PLCs rats[94]. Somatostatin analogues appear to be effective also in patients with ADPKD and ADPLD[54].

Also Ca^{2+} the other main second messenger in cholangiocytes that has been reported altered in cells with defective PC2[95, 96]. For example, PC2-defective cardiomyocytes shown altered Ca^{2+} signaling characterized by a reduced cytoplasmic [Ca^{2+}] and reduced Ca^{2+} release from the sarcoplasmic reticulum (SR) stores compared with wild-type cardiomyocytes[97]. Altered Ca^{2+} homeostasis and reduced

cytoplasmic [Ca^{2+}] has been observed in PC2-defective kidney cells[98]. Previous data from our group showed that the absence of PC2 in cholangiocytes resulted in the inhibition of the store-operated Ca^{2+} entry (SOCE), a mechanism that uses extracellular Ca^{2+} to replenish ER- Ca^{2+} store (**Fig.**2D) [99].

Significant advances have been made concerning the identity of the molecular components of the SOCE machinery. Stromal Interacting Molecule (STIM) has been identified as the molecular sensor protein that links the reduction in ER [Ca^{2+}] with the activation of Store Operated Ca^{2+} entry Channels (SOC) belonging to the ORAI and transient receptor protein channel (TRPC) families in the plasma membrane (PM)[100]. STIM proteins are type 1A single membrane proteins that are largely conserved across the species. Mammalian has two homologous proteins, STIM1 and STIM2, that are expressed ubiquitously in all the cell types. STIM1 proteins have been described as glycosylated phosphoprotein, which resides mainly in ER membrane[101]. The ability of STIM1 in sense small changes of Ca^{2+} levels in the luminal store and thus, trigger the intermolecular interactions, is due the presence of a tightly clustered assembly of short α helices comprising two EF-hand domains and a sterile α-motif (SAM) domain in its N-terminal domain. Indeed, the EF-hands binds Ca^{2+} with low affinity (200-600 nM), therefore when the ER is full (~ 1 mM) Ca^{2+} is bounded to STIM1 and the protein is in inactive state. ER-Calcium store depletion lead the dissociation of Ca^{2+} from EF-hand-SAM domains and activation and oligomerization of cluster of STIM1, also due the presence of contains a serine/proline rich-domain, possibly involved in the cytoskeleton interaction, and a lysine-rich domain in the cytoplasmic C-terminus of STIM1 that mediate its anchoring to the PM. Moreover, the C-terminal region includes an ~100 amino acid segment named the STIM–Orai activating region (SOAR), inside the ER/PM domain, which mediates direct coupling with Orai1 channels (**Fig.** 3), that are ultimately responsible for Calcium influx after intracellular store depletion[100-106].

The channels belonging to the ORAI family, have four transmembrane domains proteins, which are located at the PM. The most important structural domains for Orai1 function is characterized by two glutamate residues that are involved in Ca^{2+} selectivity of the channel. The C-terminus of Orai1 is important for recruitment into the plasma membrane microdomains assembly. The physical interaction between STIM1 and Orai1 at the ER/PM microdomains leads the Ca^{2+} influx to replenish the [Ca^{2+}]ER to maintain the Ca^{2+} homeostasis[100, 106, 107].

Studies from Lefkimmiatis et al. described a mechanism whereby ER Ca^{2+} store-depletion facilitates the recruitment and activation of adenylyl cyclases (ACs), via STIM1-dependent process, which leads to the activation of the cAMP production and was therefore called SOcAMP (store operated cAMP production)[108-110]. In fact, knockdown of STIM1 using a short hairpin RNA (shRNA) produced a marked decrease in the cAMP production as well as the $[Ca^{2+}]$ER[109]. On the other hand, the inhibition of STIM1 translocation thought the ER/PM junctions, by using a non- specific inhibitor of SOCE (2-APB), reversibly blocked SOcAMP. Taken together, these observations suggest that the STIM1 transmembrane protein can serve as a sensor linking $[Ca^{2+}]_i$ to $[cAMP]_i$ production.

Having shown that absence of PC2 induces both an inappropriate production of cAMP and a decreased cytosolic $[Ca^{2+}]$, the **aim of part I** of the present thesis was to understand the which of the Ca^{2+}-inhibited ACs (AC5 or AC6) expressed in cholangiocytes is involved in the STIM1-dependent activation of the PKA/ERK/VEGF-mediated cysts growth in PLD-ADPKD. The reader is referred to the “Introduction” for a discussion about adenylyl cyclases in cholangiocytes.

RESULTS

Blockage of AC5, rather than AC6, reduces the cAMP/pERK/VEGF pathway in PC2-defective cholangiocytes and liver cystic area in Pkd2-KO mice.

We initiated this project observing that depletion of endogenous AC6 by siRNA in PC2-defective cells, triggered a robust reduction of cAMP production after TPEN-induced depletion of intracellular Ca^{2+} store. This finding let us speculate that Ca^{2+} inhibited AC6 was responsible for increased levels of cAMP production and stimulation of cyst growth in *Pkd2-KO* mice. To validate our findings *in vivo* conditions, we generated a conditional double *Pkd2/AC6-KO* mouse line by crossing *Pkd2-KO* mice, in which deletion of PC2 is Cre recombinase-mediated, with AC6-KO mice. Induction of Cre-recombinase can be achieved in the liver and other organs by intraperitoneal injection of the Tamoxifen (0.2mg/g) once every 24 hours for a total of 5 consecutive days.

We confirmed the deletion of AC6 by analyzing its gene expression in cholangiocytes isolated from *Pkd2/AC6-KO* mice as well as in whole livers. As expected, expression of AC6 was absent in liver samples from *Pkd2/AC6-KO*, while there was no significant difference in liver samples obtained from WT and *Pkd2-KO* mice (**Fig.**4A). Similar results were also obtained in isolated cholangiocytes (**Fig.**4B). Eight weeks after induction of Cre-mediated PC2 excision, we evaluated the extension of the liver cystic area of *Pkd2/AC6-KO* mice with respect to *Pkd2-KO* mice. Liver tissues were harvested, immunostained for cytokeratin 19 (K19), as marker of mature cholangiocytes, to allow a correct discrimination of biliary cysts from vascular structures. The histological sample underwent to computer-assisted morphometric analysis using a motorized stage system able to scan, at 4X magnification, the whole liver lobes. Contrary to our expectation, we found that the liver cysts area measured in *Pkd2/AC6-KO* mice was not reduced with respect to *Pkd2-KO* mice. Furthermore, the liver/body weight ratio (g) in *Pkd2/AC6-KO* mice was not significantly different from *Pkd2-KO* mice (**Fig.**4C-D). Genetic deletion of the ADCY6 (AC6) gene had no significant effect on cysts growth in *Pkd2-KO* mice. To understand if knocking down of AC6 induces a reduction of the intracellular cAMP levels, we isolated primary cysts cholangiocytes from WT, *Pkd2-KO* and *Pkd2/AC6-KO* and cultured into collagen-

coated plates and grown as monolayer. To induce intracellular Ca^{2+} store depletion, cultured cholangiocytes were exposed to TPEN (1mM). Consistent with the *in vivo* data, we observed that cAMP level was still clearly increased in *Pkd2/AC6-KO* cells with respect to WT cells, being reduced only by 12% with respect to *Pkd2-KO* cells. These data suggest that an additional Ca^{2+}-inhibitable ACs isoform is involved in liver cysts growth and that, in spite of AC6 deletion, the cAMP increase generated by this second AC is enough to stimulate cyst growth in vivo. (**Fig.**4E, Table 3).

By repeating our previously published AC6 silencing experiment, we found that the siRNA used to silence AC6, actually decreased also the gene expression of AC5 (**Fig.**5A), which, in hindsight was not surprising, given the high molecular homology between the two Ca^{2+}-sensitive AC5 and AC6 isoform. These findings indicate that the cAMP reduction observed in our previous study was likely AC5-dependent

To direct address the role of AC5 as Ca^{2+}-sensitive determinant in our model of PLD-ADPKD, we knocked down endogenous AC5 by specific siRNA in *Pkd2-KO* and *Pkd2/AC6-KO* cells. AC5 knockdown significantly reduced the cAMP levels in *Pkd2-KO* and *Pkd2/AC6-KO* cholangiocytes both at baseline and after treatment with TPEN, to levels similar to those measured in WT cells. To exclude possible off-targets effects of our RNA interference approach and to confirm the role of AC5 in the aberrant cAMP production, we first measured the gene expression of AC6 in cholangiocytes knockdown for AC5. We found that silencing of AC5 did not affected the expression of AC6 (**Fig.**5B). Secondly, we repeated the experiments with two knowns specific AC5 inhibitors, SQ22,536 and NKY80. Monolayer WT, *Pkd2-KO* and *Pkd2/AC6-KO* cholangiocytes were treated with SQ22,536 (1uM) or with NKY80 (1uM) alone for 24h or in combination of SQ22,536 or NKY80 (1mM) for 24 h following 5 minutes of TPEN (1mM) treatment. We found that both AC5 inhibitors SQ22,536(1uM) (**Fig.**5C) and NKY80 (1uM) (**Fig.**5D) were able to reduce the production of cAMP in *Pkd2-KO* and *Pkd2/AC6-KO* cholangiocytes at baseline with respect to WT cells, as well as upon treatment with TPEN.

To investigate whether the decreased cAMP production induced by inhibition of AC5 is associated to attenuation of downstream mediators of liver cysts growth we analyzed ERK1/2 phosphorylation, VEGF secretion and cell proliferation through Western Blot, ELISA and MTS assays, respectively. For all the three assays we cultured WT, *Pkd2-KO* and *Pkd2/AC6-KO* primary cysts cholangiocytes as monolayer and we treated with SQ22,536 alone or in combination of SQ22,536 with the SERCA

inhibitor, Thapsigargin (2uM) to induce the ER- Ca^{2+}store depletion. Cysts proliferation in *Pkd2-KO* is sustained by PKA-dependent ERK1/2-VEGF pathway. ERK1/2 phosphorylation (pERK) and VEGF secretion are downstream of cAMP and therefore should be reduced by SQ22,536. Indeed, pERK/ERK levels assessed by western blot were significantly reduced in *Pkd2-KO* and *Pkd2/AC6-KO* cells co-treated with SQ22,536 and Thapsigargin with respect to treatment with Thapsigargin alone (**Fig.**6A). Similarly, treatment with SQ22,535 significantly reduced the secretion of VEGF upon ER-Calcium store depletion in *Pkd2-KO* and *Pkd2/AC6-KO* (**Fig.**6B). Being cholangiocytes proliferation the ultimate outcome of the cAMP/PKA-mediate activation of ERK1/2/VEGF pathway, we studied the effects of SQ22,536 on cell proliferation using an MTS assay. **Fig.** 6C show that the treatment with SQ22,536 (1uM) significantly reduced cell proliferation induced by Thapsigargin (2uM) in *Pkd2-KO* and *Pkd2/AC6-KO* cells but not in WT cells, when compared with Thapsigargin treatment alone. Of note, SQ22,536 treatment alone was able to significantly reduce cell proliferation in *Pkd2-KO* and *Pkd2/AC6-KO* cells with respect to untreated cells. This findings further indicate that AC5 is responsible for the cAMP production that activates the ERK1/2-VEGF pathway.

Inhibition of AC5 reduces cyst growth in vitro and in vivo.

We recently established conditions allowing long-term expansion of epithelial organoids from cholangiocytes (herein biliary organoids), currently representing the most advanced cellular model to study biliary physiology and pathophysiology.

Taking advantage of this technology we generated biliary organoids from WT, *Pkd2-KO*, and *Pkd2/AC6-KO* mice and we used this model system to investigate PLD-ADPKD pathogenesis. Cholangiocytes were cultured in Matrigel with medium supplemented with growth factors such as ligand Wnt3a, endothelial growth factor (EGF), fibroblast growth factor (FGF4) and hepatocyte growth factor (HGF). Further details are described in the methods section. In these conditions, biliary organoids accurately recapitulate mature cholangiocytes as well as their physiology. To confirm the maturity of cholangiocytes, we evaluate by immunohistochemistry the expression of biliary markers such as K19 and SOX9, the presence of primary cilia by using acetylated-α-tubulin antibody and the presence of the tight junction using ZO-1

antibody (**Fig.**7A). Furthermore, by using transmission electron microscopy (TEM) we observed the presence of numerous microvilli at the luminal surface of cysts and the presence of the primary cilia on the apical surface of the biliary organoids (**Fig.**7B). To study the effects of cAMP on organoids' volume, we used live-cell confocal microscopy and an imaging software that calculates the relative increase in the diameter at different time points upon the addition of a mix of agents able to increase cellular cAMP concentrations (Forskolin, IBMX and db-cAMP). We found that the majority of the organoids respond to the "mix-cAMP" stimulation, as shown in **Fig.** 7C. Together these results show that volume of biliary organoids derived from cultured cysts cholangiocytes increased more than in organoid derived from control cholangiocytes, both in the presence and in the absence of cAMP stimulation.

In order to study the effect of SQ22,536 or NKY80 on biliary organoids growth, we first measured the size of the three different cell lines over time, at basal condition. As shown in **Fig.**7D and Table 3 the size of the *Pkd2-KO* organoids was significantly higher with respect to WT, *Pkd2/AC6-KO* being intermediate between the two. When organoids were grown in the presence of SQ22,536 or NKY80 their size, measured at day 5 was significantly lower with respect to that organoids cultured in the absence of AC5 inhibitors (**Fig.**7E). These data are consistent with a major role for AC5 in mediating liver cyst growth. Contrary to what found *in vivo*, cultured *Pkd2/AC6-KO* organoids showed a growth rate that was intermediate between WT and *Pkd2-KO* (**Fig.**7F). This difference in growth rate is in line with the small decrease in intracellular cAMP levels shown in Figure 5C-D, and suggest that there is a small role for AC6 in cyst growth in vitro.

Finally, to firmly establish the pathophysiological relevance of these mechanisms, we studied the effects of AC5 inhibition in vivo. To this aim, we treated *Pkd2-KO* and *Pkd2/AC6-KO* mice with SQ22,536 (300 µg/Kg/day for 8 weeks, i.p.). The dosage was well tolerated, without mortality or toxicity. At the end of the treatment, mice were sacrificed, liver tissue was harvested, and histological analysis was performed. We found that the cystic area, measured by computer-assisted morphometric analysis of K19 positive areas, was significantly reduced in both *Pkd2-KO* and *Pkd2/AC6-KO* mice treated with SQ22,536 as compared to untreated mice (**Fig.** 8A-B). Furthermore, treatment with SQ22,536 decreased also the liver weight/body weight ratio (**Fig.**8C) in *Pkd2-KO* and *Pkd2/AC6-KO* mice. These observations suggest that targeting AC5 activity significantly reduced liver cysts size

by reducing the levels of intracellular cAMP. To exclude that the effect of SQ22,536 on liver cysts growth was due to secondary event, we decided to analyze the level of of pERK and of the proliferating cell nuclear antigen (PCNA), as marker of cell proliferation, by immunohistochemistry. **Fig.**8D-E shows significant reduction in the pERK positive area upon AC5 inhibition in *Pkd2-KO* and *Pkd2/AC6-KO* mice respect to untreated mice. PCNA staining revealed that treatment with SQ22,536 significantly reduced the number of cysts cholangiocytes entering the cell cycle in *Pkd2-KO* and *Pkd2/AC6-KO* mice (**Fig.**8F-G).

These results suggest that targeting AC5 activity significantly reduces intracellular levels of cAMP and the activation of the pERK1/2-VEGF pathway and consequently liver cysts growth. It is worth noting that the effects of AC5 inhibition in PC2-defective mice were similar irrespective of the expression of AC6, further suggesting that AC6 has a negligible role in cyst growth in vivo.

STIM1 and AC5 co-localize in Pkd2/AC6-KO cholangiocytes after ER-Ca^{2+} depletion

We recently showed that inhibition of STIM1 reduced [Ca^{2+}]ER-stimulated cAMP production in PC2-defective cholangiocytes. To address if AC5 isoform interacts with STIM1 in *Pkd2-KO* and *Pkd2/AC6-KO* and thus mediates the SOcAMP mechanism, confocal microscopy analysis and proximity ligation assay (PLA) were conducted. For all the experiments, WT, *Pkd2-KO* and *Pkd2/AC6-KO* cells were grown on transwell inserts as polarized monolayers and, when confluent, treated with Thapsigargin (2uM) in Ca^{2+}-free Hepes with EGTA(25uM) to induce [Ca^{2+}]ER depletion.

First, the co-localization of STIM1, Orai1, and AC5 or AC6 was analyzed using confocal microscopy and specific antibodies. Serial optical sections (0.5 μm thick) were collected for orthogonal views. We found that in WT cells STIM1 and Orai1 colocalize as expected at the plasma membrane after intracellular calcium store depletion, whereas, in *Pkd2-KO* and *Pkd2/AC6-KO* cells the co-localization of STIM1 and Orai1 was missing (**Fig.**9A). On the contrary, in *Pkd2-KO* and *Pkd2/AC6-KO* cholangiocytes, under the same conditions, we clearly observed the co-localization of AC5 but not of AC6 with STIM1 (**Fig.**9B-C).

To further demonstrate the physical interaction between STIM1 and Orai1 channels or between STIM1 and AC5 or AC6, we used an *in situ* proximity ligation assay (PLA), based on the formation of fluorescent spots when two proteins of interest in their native status are located within a distance of 40 nm. As shown in **Fig.**10A, signals indicating STIM1/Orai1 was induced by thapsigargin in WT cholangiocytes, but not in *Pkd2-KO* and *Pkd2/AC6-KO* cells. On the other hand, also in this case, in *Pkd2-KO* and *Pkd2/AC6-KO* cells but not in WT cells, STIM1 was interacting with AC5 (**Fig.**10B) while there was no interaction between STIM1 and AC6 (**Fig.**10C). As a negative control, we performed similar experiments omitting one of the two antibodies and no signal was detected as expected (data not shown).

Future studies planed and preliminary results

The latter results indicate AC5 as the Ca^{2+}-inhibitable isoform involved in the increased production of cAMP in response to intracellular store depletion in absence of PC2. We next sought to gain further insight into the role of the PC2 in regulating ER- Ca^{2+} homeostasis. We reported that the loss of PC2 results in a decreased cytoplasmic [Ca^{2+}] and a reduction in the mechanism that mediates the replenishment of Ca^{2+} stores (SOCE). These events cannot be explained by an increased [Ca2+] extrusion capacity of the *Pkd2-KO* cells. In fact, the rate of calcium extrusion in absence of PC2 was unaffected compared to WT cells. Furthermore, *Pkd2-KO* cells showed an overall reduction of cytoplasmic [Ca^{2+}], either at baseline and upon stimulation of ATP agonist.

Altered ER- Ca^{2+} homeostasis in Pkd2-KO cholangiocytes

To direct investigate the role of PC2 in ER- Ca^{2+}homeostasis, we measured the [Ca^{2+}]ER taking advantage of the recombinant aequorin (AEQ) approach. Briefly, aequorin is a photoprotein originally isolated from luminescent jellyfish *Aequorea Victoria*. The aequorin complex comprises the apoaequorin protein and the luminophore coelenterazine. calcium binding to aequorin causes slight conformational changes which leads to intramolecular oxidation of the coelenterazine, with a concomitant release of carbon dioxide and active probe with the emission of light at 486nm[111]. Further details are described in the methods section.

For our experiments, we used the *erAEQmut* chimera photoprotein, owing the ability to be retained in the lumen of the ER by the presence of a specific target domain in the N-terminal of the recombinant protein.

Cells transfected with *erAEQmut* were used to determinate the steady of [Ca^{2+}]ER obtained by incubating the cells in medium with EGTA and ionomycin, leading to the removal of extracellular and intraluminal Ca^{2+}, respectively.

Upon reconstitution step, cells were washed with 2% BSA to remove excess ionomycin and transferred them to the perfusion chamber for signal recording. Upon recording the first 60s of luminescence signal, cells were exposed to 1 mM $CaCl_2$ to monitor the refill capacity of Ca^{2+}in the ER (See Box1). Where indicated, cells were then exposed to agonist stimulation with ATP (100uM) causing the generation of IP3 and the consequent release of calcium from the ER (**Fig.**11A). This event occurs upon binding of IP3 to the IP3 receptor (IP3R) on the ER membrane, opening the receptor through which Ca^{2+} is transiently released from ER into the cytosol.

Trace analysis of the different ER-[Ca^{2+}] phases reveals differences between WT and *Pkd2-KO* cells (**Fig.**11B-E). Indeed, the steady-state reached by *Pkd2-KO* cells was significantly lower than that in wild-type cells (**Fig.**11C). *Pkd2-KO* cells also showed a tendency to a reduced velocity in the uptake of Ca^{2+}, compared to WT cells (**Fig.**11D). The steady-state of the ER is regulated by the Sarcoplasmic/endoplasmic reticulum calcium ATPase (SERCA) pumps activity that pumps Ca2+back into the ER after Ca^{2+} release. The second phase of the trace shows the emptying of the ER-[Ca^{2+}] upon ATP-stimulation. It is worth reminding that ATP agonist acts on the plasma membrane receptors and subsequently trigger phospholipase C (PLC) catalytic activity. Indeed, PLC catalyzes the cleavage of phosphoinositol-4,5-bisphosphate into diacylglycerol and IP3. The latter diffuses in the cytoplasm and binds IP3R in the ER, allowing the release of calcium from the intracellular store. **Fig.**11F-G shows no differences in the emptying phase between WT and *Pkd2-KO* cells. Analysis of the Ca^{2+} traces generated on the second phase of the experiment was conducted to compare the rates of Ca^{2+} release from the ER in WT vs PC2-defective cholangiocytes The fast calcium release rate of is the slope of the the initial curve monitoring the decrease in Ca^{2+} ER upon agonist stimulation. On the other hand, the subsequent slow release phase is the one during which the cytosolic portion of the IP3R binds calcium and induce the transient channel closing. During this phase calcium enters and exits from the ER, generating a Ca^{2+} oscillation that, using the aequorin-probe, is

measured as the average of the calcium oscillation, since the cells are not synchronized (a population, rather than a single cell study is performed). In our experiments we did not detect significant differences in these two release rates of between WT and *Pkd2-KO* cells, possibly indicating that IP3R-mediated calcium efflux is not affected by lack of PC2. On the other hand, this preliminary finding suggests that SERCA activity is dysregulated in *Pkd2-KO* cells since the uptake of calcium in the ER was delayed compared to WT cholangiocytes. Because the $[Ca^{2+}]$ER depend on the balance between influx and efflux of intracellular calcium, and the steady-state Ca^{2+} levels are decreased, it is possible that also an IP3-independent leak is increased.

Impaired mitochondrial respiratory capacity and ATP production in Pkd2-KO cholangiocytes

Since transformed ER calcium homeostasis might impact mitochondrial function, we developed the following hypothesis: the lack of PC2 leads to a distinctively impaired respiratory performance. To prove it, we have gauged the oxygen consumption rates (OCR) in defective PC2 cholangiocytes in contrast to wild-type cells.

Certain alterations in cell energy metabolism have been discussed in the description of ADPKD before. Kidney tubular cells that missed PC1 were monitored for any changes in their energy production regime, specifically from oxidative phosphorylation mode to aerobic glycolysis, what could imply mitochondrial dysfunction. Alterations in mitochondrial morphology, in addition to decrease in OCR have also been explored. Relying on the Seahorse XF96 Analyzer, we managed to measure the OCR parameters throughout timescale in cell cultures of WT and *Pkd2-KO* cholangiocytes (**Fig.**12A). Notably, *Pkd2-KO* cholangiocytes showed considerably lower basal mitochondrial respiration parameters (OCR-BASAL) (160.73+/-18.51 pMoles/min) in contrast to WT cholangiocytes (272.68+/-36.78), thus reinforcing lower ATP turnover and consumption. The addition of Oligomycin A [1uM] leads to inhibition of ATP synthase (complex V within the respiratory chain), provoking a reduction in OCR that aligns with the quantity of oxygen consumption rates associated with mitochondrial ATP produced (OCR-ATP). ATP-associated respiration was considerably reduced in *Pkd2-KO* cells (129.83+/-14.26 pMoles/min) in contrast to WT

cells (174.94+/-20.66 pMoles/min). The best possible ATP production of mitochondria could be identified by the inclusion of FCCP [1.5uM], a special uncoupling reagent that breaks the proton gradient and undermines the potential of mitochondrial membrane. This leads to production of maximal oxygen consumption as well as substrate oxidation by complex IV (OCR-MMR, accounted for maximal mitochondrial respiration). In comparison, OCR-MMR was essentially lower in *Pkd2-KO* cells (285.12+/-26.25 pMoles/min) against WT cells (466.66+/-59.38 pMoles/min). We also relied on the spare respiratory capacity (OCR-SRC) to assess the quantity of additional ATP produced by oxidative phosphorylation if energy consumption was unexpectedly high. OCR-SRC was thus identified by deriving OCR-BASAL from FCCP-produced OCR-MMR. Hence, OCR-SRC quantitatively exemplifies the cells' capacity to react to intensified energy consumption signs. It was also found considerably lower in *Pkd2-KO* cells (135.37+/-25.94 pMoles/min) in contrast to WT cells (255.67+/-45.07 pMoles/min) (**Fig.** 12B). All things considered, we have identified a general decrease of all OCR parameters relating to mitochondrial respiration in *Pkd2-KO* cholangiocytes cell cultures. The original source of such mitochondrial dysfunction is yet to be known. According to our hypothesis, the changed Ca^{2+} associated with the mitochondria of defective PC2 cells can be a potential cause.

Altered mitochondrial calcium uptake in Pkd2-KO cholangiocytes

The fine regulation of mitochondria Ca^{2+} is important for many functions, from the modulation of dehydrogenases of the Krebs cycle to the regulation of apoptosis and autophagy to the activation of the NLRP3 inflammasome. To assess the ability of WT and *Pkd2-KO* mitochondria to uptake Ca^{2+}, we measure the [Ca^{2+}] using the previously described aequorin technology (See Box2). Preliminary experiments indicate no changes in calcium levels upon ATP-agonist stimulation in WT and *Pkd2-KO* cells (**Fig.**12C-D), however, the absence of external Ca^{2+}, i.e. in a condition in which mitochondrial calcium depends only on intracellular store, we detected a reduction in the mitochondrial calcium uptake in *Pkd2-KO* cells but not in wild-type cells (**Fig.**12E-F). This experiment was conducted by perfusing cells in absence of $CaCl_2$ and by adding EGTA to buffer solution. Analysis of the trace reveals a significantly lower uptake of calcium in *Pkd2-KO* mitochondria as compared to wild-type. The lower calcium uptake from *Pkd2-KO* mitochondria, upon ATP-agonist

stimuli, may suggest that maintenance of normal levels of mitochondrial calcium uptake in PC2-defective cells derives from an extracellular compartment.

These preliminary observations indicate that, as respect to WT cholangiocytes, the mitochondria of PC2 defective cells have reduced respiratory rates and an impaired Ca^{2+} uptake in response to purinergic stimulation. However, because ATP stimuli can either activate plasma membrane channels independently from IP3 production, we have planned series of experiment in which we will confirm the role of PC2 in the ER by permeabilizing and treating the cells with stabilized concentration of IP3 and measure the calcium uptake in the ER and mitochondria. This will provide additional information of the role of IP3-dependent calcium mobilization in our model. By comparing ER Ca^{2+} in permeabilized WT and PC2-defective cells we will also acquire information on the existence of IP-3 independent leaks and the role of PC2 in their regulation.

In future studies will also investigate the link between calcium signaling and apoptosis, as it bears relevance for PLD-ADPKD pathogenesis. These studies will provide a better understanding of the role of polycystins and InsP3 receptors in mitochondrial functions and the changes that occur when PC2 is genetically absent.

DISCUSSION

Recent data generated by our group demonstrate that, in association with the genetic defect, morphogenic pathways are reactivated determining the progression of the liver phenotype. We established that in mice lacking polycystin-2, cyst growth and disease progression depend on the enhanced secretion of VEGF. Examining this more closely, we observed that cyst growth is due to an aberrant increase in cAMP production, leading to a PKA-dependent activation of the Ras/ERK1/2/mTOR/HIF-1a-dependent production of VEGF-A[30, 31]. The importance of this pathway is further highlighted by the reduction of cyst volume achieved in orthologous rodent models and human PLD-ADPKD patients by VEGFR2 inhibitor, rapamycin, Sorafenib, and somatostatin analogues. For instance, positive results for PLD-ADPKD have been obtained in the conditional *Pkd2-KO* mice model by using a specific and competitive inhibitor of VEGFR-2 (SU5416), or by administrating rapamycin, a specific mTOR inhibitor[30, 31]. The treatment of cystic mice with SU5416 and rapamycin resulted in a significant decrease in the proliferative activity of the cystic epithelium. In particular, the administration of rapamycin significantly reduced the cystic liver area by decreasing proliferation and increasing apoptosis of the biliary epithelium. Furthermore, inhibition of mTOR signaling induced a reduction of IGF1-dependent HIF-1α accumulation and consequently decreased VEGF-A secretion. However, targeting VEGF-A secretion by inhibiting VEGFR2 (SU5416) decreased liver cyst proliferation due to the reduced activation of the ERK1/2 pathway in *Pkd2-KO* mice[30, 31].

Altered calcium and cAMP signaling are the most recognized features of cystic cells in ADPKD. Notably, they are characterized by lower cytoplasmic Ca^{2+} levels and impaired intracellular Ca^{2+} homeostasis. In cholangiocytes deficient in PC2, the endoplasmic reticulum (ER)–Ca^{2+} store is reduced, and the mechanism of store-operated calcium entry (SOCE) is significantly inhibited[99]. In this study we have sought to thoroughly investigate the link between altered Ca^{2+} homeostasis and increased cAMP signaling, as $[Ca^{2+}]$ER depletion stimulates cAMP signaling. In physiological conditions, changes in $[Ca^{2+}]_i$ are known to either enhance or depress cAMP production through the activity of adenylyl cyclase (AC). It has been reported

that SOCE may increase cAMP production by recruitment and activation of AC8 in the SOCE microdomains, defined as lipid raft domains at the plasma membrane, but that it inhibits Ca^{2+}-inhibited AC5/6[108]. Thus, we hypothesize that in cells lacking PC2, STIM1 interacts with Ca^{2+}-inhibited AC, rather than with ORAI1 leading to aberrant cAMP production.

In cholangiocytes, seven AC isoforms are expressed. Among them, Ca^{2+}–calmodulin (CaM)-stimulated AC8 is activated by SOCE and by secretin receptor stimulation, and is linked to $Cl^-/HCO3^-$ secretion[108]. AC6 and AC5 are Ca^{2+}-inhibited isoforms that inactive in normal resting $[Ca^{2+}]_i$ and can become activated at the low $[Ca^{2+}]_i$, reported in PC2-defective cholangiocytes[99]. AC6 is also localized in the cilia of cholangiocytes, and is involved in shear stress-induced signaling and the formation of gap junctions and $[Ca^{2+}]_i$ regulation in endothelial cells[112]. It is also important to mention the presence of a cAMP microdomain where the main components of the cAMP cascade (AC, PKA, and protein phosphatase 2A) are fully assembled into the raft domain and are linked with different A-kinase anchoring proteins (AKAP)[113]. Indeed, Masyuk et al. observed that the primary cilium of renal and cholangiocyte cells contains a protein complex comprising AKAP 150, which tether AC5/6 to synthesize cAMP with downstream effectors PKA and the second messenger cAMP-activated Epac2 (exchange protein directly activated by cAMP 2)[112]. Furthermore, Choi and colleagues showed that the same protein complex is also present in the primary cilia of renal epithelial cells and includes PDE4C and PC2[114].

It was hypothesized that, under normal conditions, PC2 functions as a Ca^{2+} entry channel and may also mediate the levels of $[Ca^{2+}]$i to inhibit the activity of Ca^{2+}-sensitive AC5/6. However, in these previous studies, the authors did not differentiate between the two isoforms. Most of the studies do not discriminate between the two Ca^{2+}-sensitive isoforms, thus referred to as AC5/6, since they share molecular identity and functions.

Our previous data showed a reduction in cAMP production in *Pkd2-KO* cholangiocytes silenced for AC6, after chronic TPEN-dependent $[Ca^{2+}]$ER depletion[99]. Thus, we generated *Pkd2/AC6-KO* mice and expected that in double-KO mice liver cysts would be less-developed. On the contrary, AC6 in *Pkd2/AC6-KO* mice did not result in reduced liver cysts in relation to *Pkd2-KO* mice, suggesting that AC6 was not involved in liver cyst growth. In line with these results, we additionally did not observe a reduction in [cAMP]i. Due to the higher homology between the two Ca^{2+}-

sensitive AC, AC6 and AC5, we analyzed the expression of AC5 in *Pkd2-KO* cholangiocytes silenced for AC6 and found that silencing AC6 with siRNA also resulted in a significant reduction in AC5 expression. Thus, these results prompted us to investigate whether AC5 was the Ca^{2+}-sensitive AC involved in liver cyst growth. Because cross-linking conditional AC5-KO mice with *Pkd2-KO* mice was not feasible, we silenced AC5 using specific AC5 siRNA and tested the effects of SQ22,536 and NKY80[115, 116], two known AC5 inhibitors on cAMP production, upon ER store depletion.

Consistently, an overall reduction of cAMP production at baseline and upon TPEN treatment, to levels similar to WT cholangiocytes, has been observed in either *Pkd2-KO* or in *Pkd2/AC6-KO* cholangiocytes upon AC5 silencing or inhibition with SQ22,536 and NKY80. Phosphorylation ERK1/2 and VEGF secretion downstream (outcomes of cAMP activation) were further reduced, as well as cell proliferation in *Pkd2-KO* and *Pkd2/AC6-KO*-isolated cholangiocytes.

We also conducted studies in cholangiocytes organoids. The limitations of monolayer cell cultures, due to the lack of polarized conditions that recapitulate cellular physiology, have boosted efforts in the last decade to develop three-dimensional (3D) cell cultures. During my Ph.D. program, I established a protocol for the generation of organoids derived from isolated primary cholangiocytes. Briefly, embedding cholangiocytes into an extracellular matrix (Matrigel), along with a short period of stimulation with Wnt3a, allows the formation of organoids that progressively enlarge[117, 118]. We found that *Pkd2-KO*-derived organoids enlarged significantly faster than those deriving from WT mice. Those deriving from the double *Pkd2/AC6-KO* grew at an intermediate rate. In this setting, we found that inhibition of AC5 significantly reduced the size of the organoids in single and double mutants, confirming that AC5 has a central role in signaling mechanisms leading to cyst enlargement. No *AC5-KO* mouse was available to generate a triple PC2/AC6/AC5 mutant and it is most likely that, even if available, it would not have been viable given the functions of these two isoforms in the heart, brain, and kidney[119, 120]. Thus, to further investigate the role of AC5 in liver cyst growth, we treated mice *in vivo* with a dose that had been reported to inhibit only AC5 (300 mg/kg/day)[121]. Our results clearly show a significant decrease in liver cyst area in both *Pkd2/AC6-KO* mice and *Pkd2-KO* mice, suggesting a pivotal role of AC5 in cyst growth.

In our study, we clearly show that cAMP dysregulation and, consequently, cyst hyperproliferation in ADPKD, are associated with the Ca^{2+}-sensitive AC5. Furthermore, we put AC5 in the context of the overall generation of Ca^{2+} and cAMP homeostasis in the cell. Based on our results showing a role for SOcAMP in the aberrant production of cAMP in PC2-defective cholangiocytes, and on the results obtained in vivo in this study, we decided to thoroughly investigate whether AC5 is involved in the activation of SOcAMP. We know that STIM1 binds ORAI1 to maintain Ca^{2+} homeostasis during store operated calcium entry.

Using confocal imaging and PLA we were able to show the colocalization of STIM1 and ORAI1, after intracellular store depletion in WT cholangiocytes, and that mechanism that is absent in *Pkd2-KO* and *Pkd2/AC6-KO* cholangiocytes. On the other hand, our data shows that AC5 interacts with the ER protein STIM1 after Ca^{2+} store depletion in *Pkd2-KO* and *Pkd2/AC6-KO* cells, but not in WT cells.

In summary, in this study, we have provided strong evidence that AC5 activation, and consequently cAMP production, play a pathogenic role in ADPKD. Our study describes a signaling pathway that directly links STIM1 with the production of cAMP, with consequential increased activity of the ERK pathway, which mediates both the increased secretion of VEGF and the increased response to VEGF in the cyst epithelium of PC2-defective cholangiocytes (**Fig.**13). These studies have improved our understanding of the mechanism leading to the progressive growth of cysts in ADPKD, indicating the pharmacologic modulation of AC5 as a more specific target in order to reduce cyst growth in PLD-ADKPD diseases.

An unresolved issue in this scenario is the role of PC2 in ER–calcium handling. PC2 is a member of the TRP ion channel family, also known as TRPP2, acting as a non-selective cation channel. In addition of being localized in the primary cilia of cholangiocytes, PC2 expression has been found in the ER membrane of both renal and biliary epithelial cells[79, 96]. This subcellular localization is due to the presence of an ER retention signal in a C-terminal region of the PC2 protein. The net role of PC2 in ER calcium signaling and on IP3 receptors function remains unclear to these days. This is in part also due to the fact the PC2 can partner with multiple proteins and assume different functions, depending on the role of the protein it is associated to. It has been reported that PC2 can act as a calcium-releasing channel activated by

cytosolic calcium at the ER membrane and participate to intracellular calcium signaling through its interaction with InsP3R[79].

Conversely, it has been proposed that PC2 can lower the [Ca^{2+}]ER, resulting in reduced IP3-dependent responses. Thus, the IP3-dependent responses could be influenced by PC2's differential gating mode (calcium-gated or leak). Our data show that the lack of PC2 in cholangiocytes is associated with a decreased cytoplasmic [Ca^{2+}] and reduced SOCE. SOCE is activated when ER Ca^{2+} levels are acutely decreased[99]. Thus, we suggest that *Pkd2-KO* cells have a long-term reduction on steady state ER [Ca^{2+}], and this somehow results in the reduction of SOCE.

We directly investigated the role of PC2 in ER– Ca^{2+} homeostasis by selectively measuring [Ca^{2+}]ER, using targeted aequorin chimeras developed by our collaborator, Dr. Paolo Pinton at the University of Ferrara. These experiments are still ongoing, however, preliminary data show that in cells lacking PC2, steady state ER [Ca^{2+}] is lower compared to WT cells. Given that the steady state [Ca^{2+}] in the ER depends on the equilibrium between progressive accumulation and passive leak, PC2 could have an effect on either process. The kinetics of calcium accumulation and release revealed that the absence of PC2 had a direct effect on the uptake, suggesting the activity of the SERCA pump, as a reduction in the uptake of calcium had been detected without affecting the IP3-mediated calcium release. The simplest explanation for these results could be that the decrease in the influx of calcium in the ER is an "adaptive" effect to the prolonged reduction in the steady state of [Ca^{2+}]ER. There is a need for in-depth studies on the expression of the different SERCA isoforms and their activity. Recent studies reported that in addition to ORAI1 and STIM1, SERCA co-assembles into ER/PM puncta induced by ER store depletion, in order to facilitate the quick shuttling of Ca^{2+} entering the ER[122, 123]. These findings could further link the decreased SOCE machinery activity with the decreased ER calcium influx, as well as the sustained reduction in [Ca^{2+}] in the ER observed in the absence of PC2.

Perturbation in ER– Ca^{2+} homeostasis is linked to the overall reduction in the cytoplasmic calcium that is known to characterize PLD-ADPDK disease. As well as modulating [Ca^{2+}]c, the calcium released from the ER can directly impact the bioenergetics of the cells, and therefore an altered ER homeostasis can reduce mitochondrial oxidative phosphorylation (OXPHOS)[124]. Cellular bioenergetics

studies, having as outcome oxygen consumption rates, show that a lack of PC2 in cholangiocytes leads to reduced mitochondrial respiration activity, which reflects preliminary data showing that the uptake of calcium into the mitochondria is reduced[125, 126]. Mitochondria is a vital element of metabolism in all cells, as long as the oxygen consumption levels through the electron transport chain is heavily linked to adenosine triphosphate (ATP) production. Moreover, mitochondrial respiration is directly managed by metabolic stimuli and urges[127]. Assuming that reduced mitochondrial respiration reflects overall ATP production, we can hypothesize that impaired ATP production in the mitochondria may result in defective SERCA pump activity in the ER. These routes can generate a loop of Ca^{2+}-dependent events at multiple intracellular sites that could contribute to the pathogenesis of PLD-ADPKD. However, in-depth studies are required to explain whether and how PC2 is involved in the modulation of Ca^{2+} homeostasis in PLD-ADPDK.

FIGURES

Figure 2. Summary of previously published observation generated in PC2-defective rodent cholangiocytes.

(A) Immunohistochemistry (IHC) showing overexpression of VEGF, VEGFR-2, and HIF-1α in PC2-defective mice. WT (top) and Pkd2KO (bottom) mice were stained with H&E or with specific antibodies against VEGF, VEGFR-2, and HIF-1α. (B-C) ERK phosphorylation and VEGF secretion are PKA-dependent in WT, Pkd1-KO and *Pkd2-KO* cells. (D) In PC2-defective cholangiocytes SOCE is significantly inhibited. Ionomycin-induced changes in cytoplasmic $[Ca^{2+}]_i$ were smaller in PC2-decetive cholangiocytes. To measure changes in $[Ca^{2+}]_i$ cells were loaded with the fluorescent Ca^{2+}-dye, fura-2, AM. Representative traces on the top. Summary of experiments as peak increase with respect to baseline or as AUC. Differences between WT and Pkd2KO cholangiocytes were statistically highly significant. *(Modified from Spirli C., et Al., Hepatology 2010 and Gastroenterology 2010).*

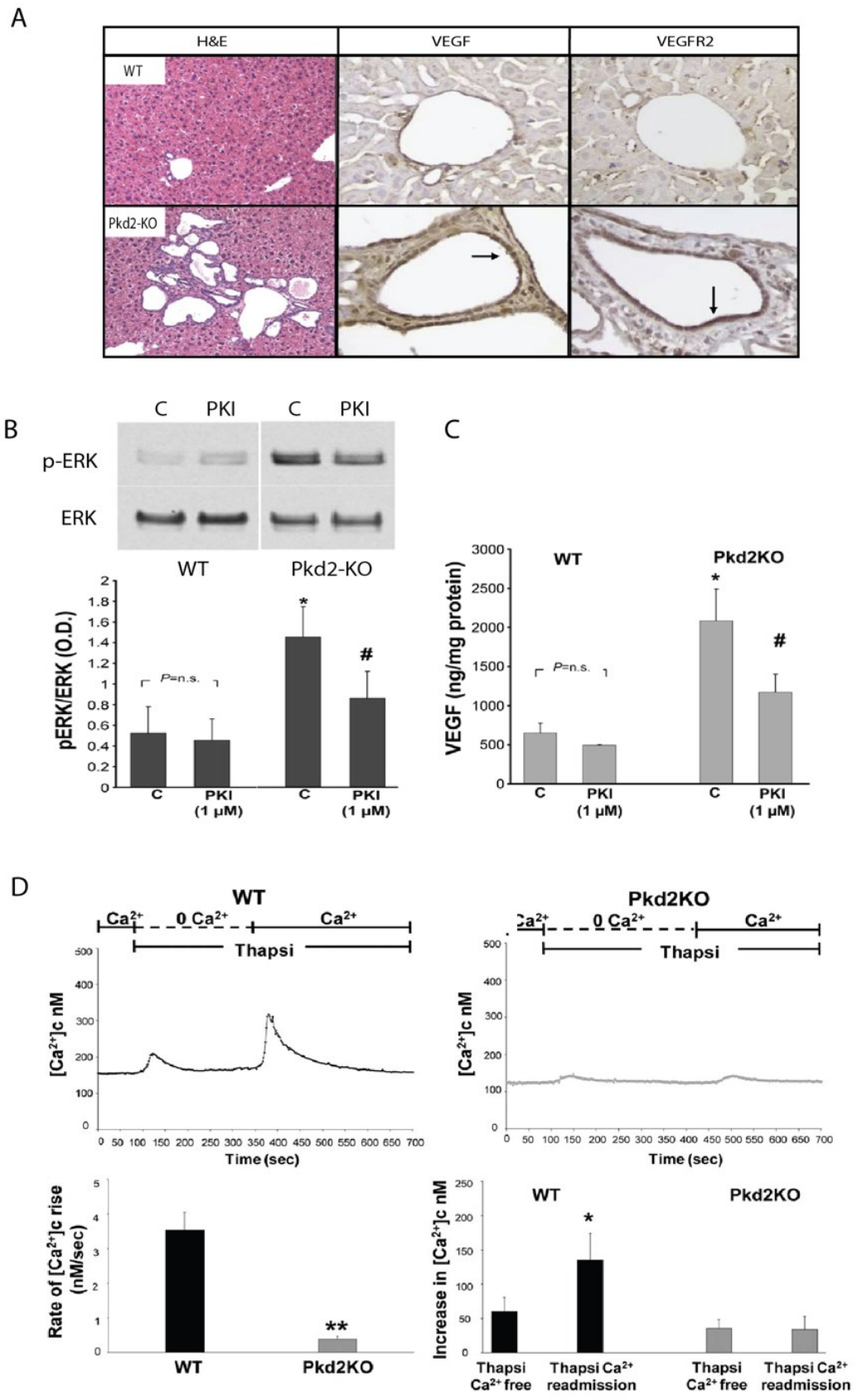
A
H&E
VEGF
VEGFR2
WT
Pkd2-KO
B
C
PKI
C
PKI
p-ERK
ERK
WT
Pkd2-KO
pERK/ERK (O.D.)
P=n.s.
*
#
C
PKI (1 μM)
C
PKI (1 μM)
C
VEGF (ng/mg protein)
WT
Pkd2KO
P=n.s.
*
#
C
PKI (1 μM)
C
PKI (1 μM)
D
WT
Ca2+
0 Ca2+
Ca2+
Thapsi
[Ca2+]c nM
Time (sec)
Pkd2KO
Ca2+
0 Ca2+
Ca2+
Thapsi
[Ca2+]c nM
Time (sec)
Rate of [Ca2+]c rise (nM/sec)
**
WT
Pkd2KO
Increase in [Ca2+]c nM
WT
Pkd2KO
*
Thapsi Ca2+ free
Thapsi Ca2+ readmission
Thapsi Ca2+ free
Thapsi Ca2+ readmission

FIGURE 2

Figure 3. STIM1 mediated the Store Operator Calcium Entry (SOCE)

Representative model of stromal interaction molecule 1 (STIM1) activation and interaction with Orai1. The activation of the STIM1 dimer is initiated by Ca^{2+} dissociation from the STIM1 dimer. STIM1 oligomerize and migrates into ER–plasma membrane junctions. Large aggregates of anchored STIM1 within ER–plasma membrane junctions are able to bind and activate Orai1 Ca^{2+}channel. *(Modified from Soboloff J., et al. Nature Review Molecular Cell Biology, 2012)*

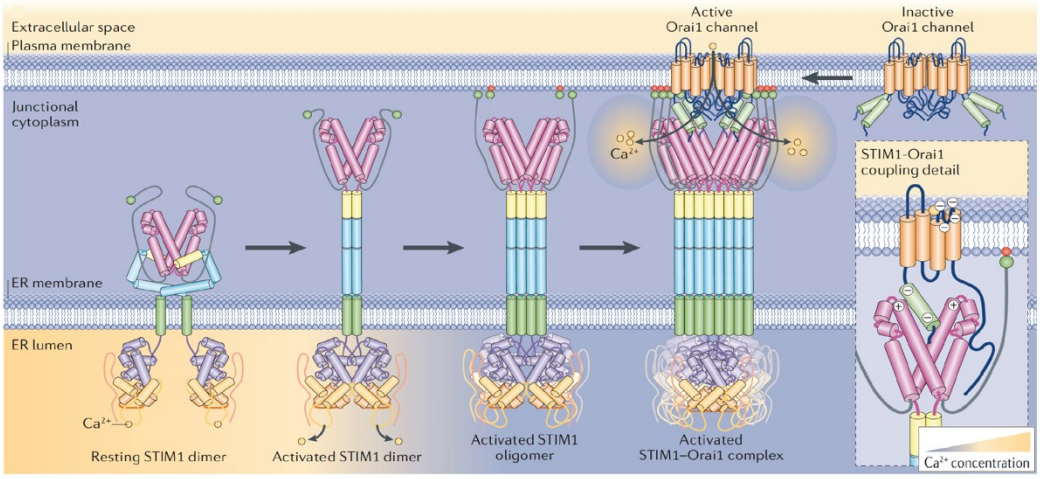
Extracellular space
Plasma membrane
Junctional cytoplasm
ER membrane
ER lumen
Active Orai1 channel
Inactive Orai1 channel
Ca2+
STIM1-Orai1 coupling detail
Ca2+
Resting STIM1 dimer
Activated STIM1 dimer
Activated STIM1 oligomer
Activated STIM1–Orai1 complex
Ca2+ concentration

FIGURE 3

Figure 4. Cystic area and [cAMP]i levels are not reduced in Pkd2/AC6-KO mice.

(A) Analysis of AC6 gene expression by RT-qPCR in WT, *Pkd2-KO* and *Pkd2/AC6-KO* total liver (n=3) and (B) in isolated WT, *Pkd2-KO* and *Pkd2/AC6-KO* cholangiocytes (n=3) confirmed the depletion of AC6 in double-KO mice.

(C) Representative micrographs of *Pkd2-KO* and *Pkd2/AC6-KO* liver specimens stained with the cholangiocyte-specific marker K19. Bar scale, 100um.

(D) Computer-assisted morphometric analysis of K19-positive areas were expressed as percentage with respect to the whole area analyzed. No reduction in cystic area and liver body weight ratio was observed in *Pkd2/AC6-KO* mice, compared with *Pkd2-KO* mice. (*Pkd2-KO* mice, n=9 and *Pkd2/AC6-KO* mice, n=5).

(E) The cAMP levels induced by TPEN (1mM) were not reduced in *Pkd2-KO* and *Pkd2/AC6-KO* cholangiocytes, compared with unstimulated cells (n=5; **p< .01 vs unstimulated cells). Similar results were also obtained in *Pkd2-KO* and *Pkd2/AC6-KO* cells transfected with scramble RNA (50 nM), a negative control of the AC5 siRNA (n=5; **p< .01 vs unstimulated cells). In *Pkd2-KO* and *Pkd2/AC6-KO* cells transfected with AC5 siRNA (50 nM) the production of cAMP induced by TPEN was significantly inhibited (● p<.05 versus unstimulated cells; ° p < .01 versus TPEN-treated cells; n=5).

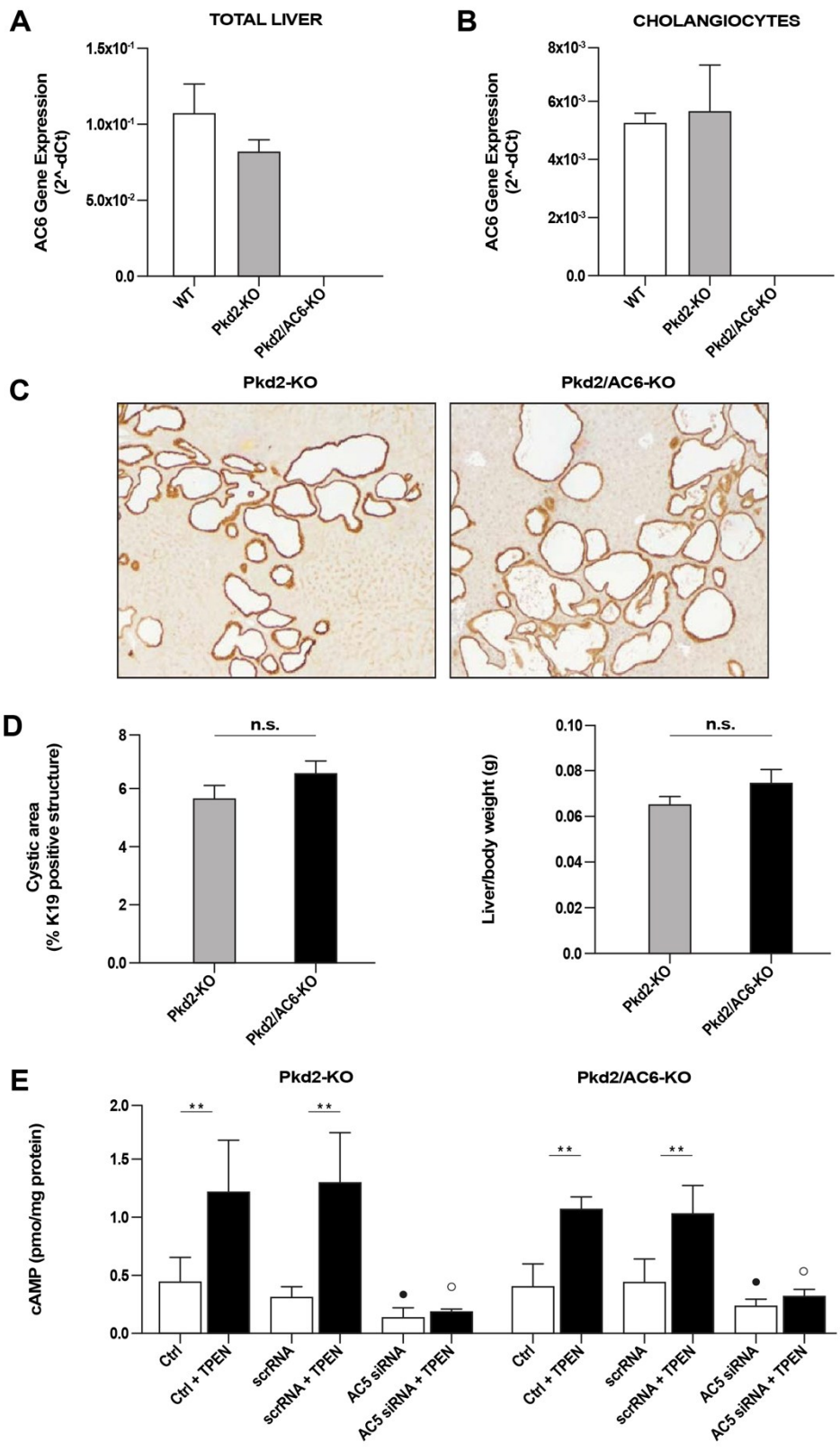
A
TOTAL LIVER
AC6 Gene Expression (2^-dCt)
1.5x10-1
1.0x10-1
5.0x10-2
0.0
WT
Pkd2-KO
Pkd2/AC6-KO
B
CHOLANGIOCYTES
AC6 Gene Expression (2^-dCt)
8x10-3
6x10-3
4x10-3
2x10-3
0.0
WT
Pkd2-KO
Pkd2/AC6-KO
C
Pkd2-KO
Pkd2/AC6-KO
D
Cystic area (% K19 positive structure)
n.s.
8
6
4
2
0.0
Pkd2-KO
Pkd2/AC6-KO
Liver/body weight (g)
n.s.
0.10
0.08
0.06
0.04
0.02
0.0
Pkd2-KO
Pkd2/AC6-KO
E
Pkd2-KO
Pkd2/AC6-KO
cAMP (pmo/mg protein)
2.0
1.5
1.0
0.5
0.0
**
**
**
**
Ctrl
Ctrl + TPEN
scrRNA
scrRNA + TPEN
AC5 siRNA
AC5 siRNA + TPEN
Ctrl
Ctrl + TPEN
scrRNA
scrRNA + TPEN
AC5 siRNA
AC5 siRNA + TPEN

FIGURE 4

Figure 5. AC5 silencing does not affect AC6 gene expression and inhibition of AC5 decreases [cAMP]i induced by ER- Ca^{2+} depletion in PC2-defective cholangiocytes.

WT, Pkd2-KO and Pkd2/AC6-KO cells were transfected with AC5 or AC6 siRNA (50 nM) or scramble RNA (scrRNA) (50 nM). (A) Relative AC6 gene expression was significantly reduced after silencing for AC6 in WT and *Pkd2-KO* cells (n=4, *p<.01 siRNA AC6 vs. CTRL). (B) Relative AC5 gene expression was significantly reduced after both AC5 and AC6 silencing in WT, *Pkd2-KO* and Pkd2/AC6-KO cells (n=4, **p<.001 siRNA AC5 vs CTRL; **p<.001 siRNA AC6 vs CTRL). (C) The cAMP levels induced by TPEN (1mM) were significantly reduced when cells were co-stimulated with the specific AC5 inhibitors, SQ22,536 (1uM). (n=3, *p<.05 TPEN + SQ22,536-treated cells vs TPEN-treated cells, *** p<.0001 TPEN + SQ22,536-treated cells vs TPEN-treated cells, *p<.05 TPEN-treated Pkd2/AC6-KO vs TPEN-treated *Pkd2-KO* cells). (D) Similar reduction in the cAMP production was observed when cells were treated with NKY80(1uM) upon TPEN-induced cAMP levels. (n=3, *p<.05 TPEN + SQ22,536-treated WT cells vs TPEN-treated WT cells, *** p<.0001 TPEN + SQ22,536-treated *Pkd2-KO* cells vs TPEN-treated *Pkd2-KO* cells, **p<.001 TPEN + SQ22,536-treated Pkd2/AC6-KO cells vs TPEN-treated Pkd2/AC6-KO cells *p<.05 TPEN-treated Pkd2/AC6-KO vs TPEN-treated *Pkd2-KO* cell).

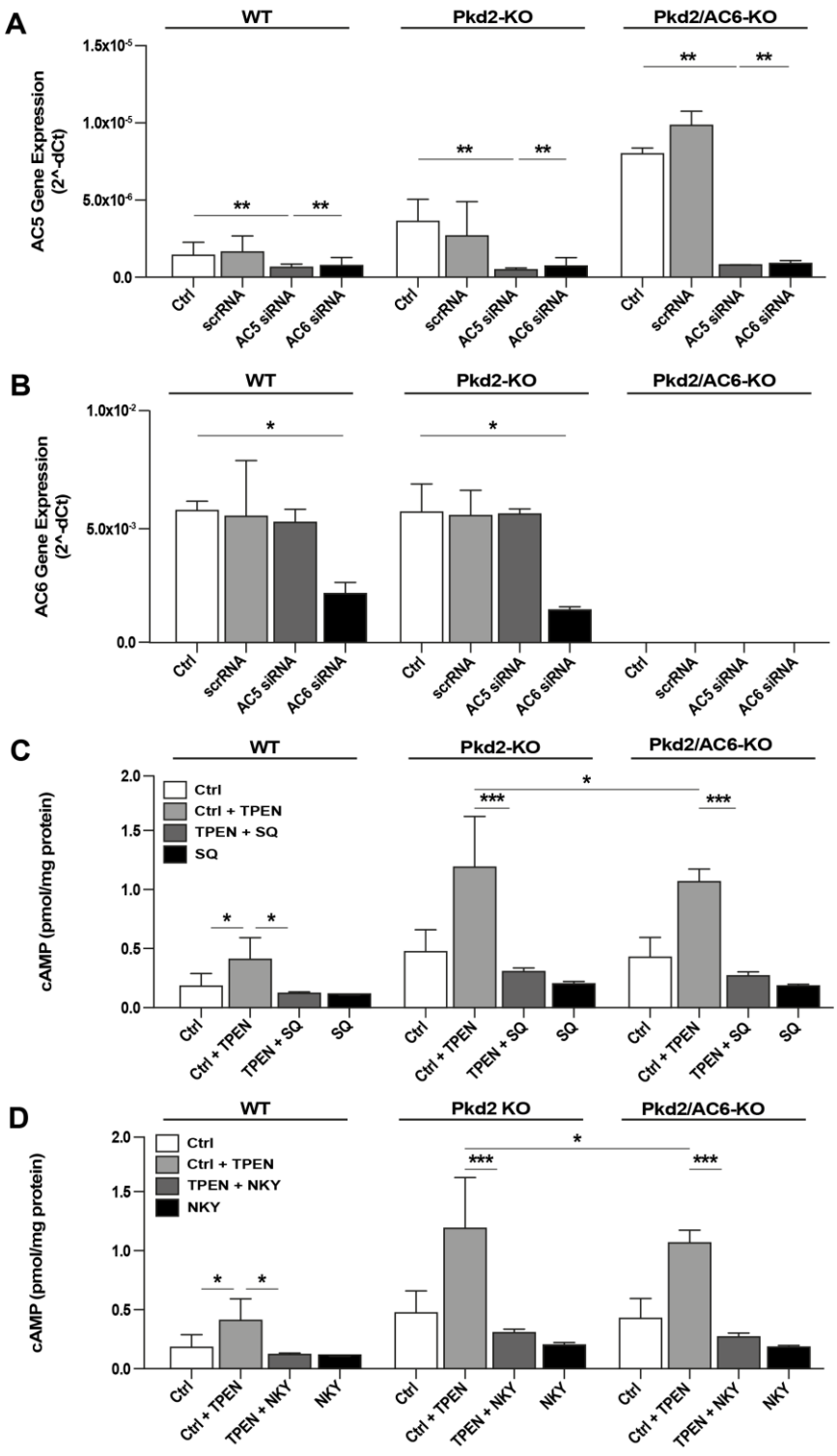
A
WT
Pkd2-KO
Pkd2/AC6-KO
AC5 Gene Expression (2^-dCt)
1.5x10-5
1.0x10-5
5.0x10-6
0.0
**
Ctrl
scrRNA
AC5 siRNA
AC6 siRNA
B
AC6 Gene Expression (2^-dCt)
1.0x10-2
5.0x10-3
*
C
cAMP (pmol/mg protein)
Ctrl
Ctrl + TPEN
TPEN + SQ
SQ
***
D
Pkd2 KO
TPEN + NKY
NKY

FIGURE 5

Figure 6. Inhibition of AC5 decreases pERK expression, VEGF secretion and cell proliferation induced by ER- Ca^{2+} depletion in PC2-defective cholangiocytes.
(A) Treatment with the AC5 inhibitor SQ22,536 (1uM) reduced ERK phosphorylation levels induced by Thapsigargin (2uM) in *Pkd2-KO* and *Pkd2/AC6-KO* cystic cholangiocytes. (*p<.01 Thapsigargin vs Ctrl, ●● p<.01 vs Thapsigargin vs Ctrl, ° p<.05 Thapsigargin + SQ vs Thapsigargin). (B) VEGF secretion induced by Thapsigargin (2uM) was significantly reduced when cells were co-stimulated with the specific AC5 inhibitor SQ22,536 (1uM) in *Pkd2-KO* and Pkd2/AC6-KO (n=3; ** p< .01, ***p<.001 vs CTRL, SQ=SQ22,536 and NKY=NKY80). (C) Thapsigargin (2uM) significantly enhanced cell proliferation in WT, *Pkd2-KO* and Pkd2/AC6-KO cholangiocytes, but this effect was significantly reduced by treatment with the AC5 inhibitor (SQ22536, 1uM) in Pkd2-KO and Pkd2/AC6-KO cells. (*p<.01 in *Pkd2-KO* + Thapsigargin + SQ22,536 vs Pkd2-KO + Thapsigargin, *p<.01 in Pkd2/AC6-KO + Thapsigargin + SQ22,536 vs Pkd2/AC6-KO + Thapsigargin).

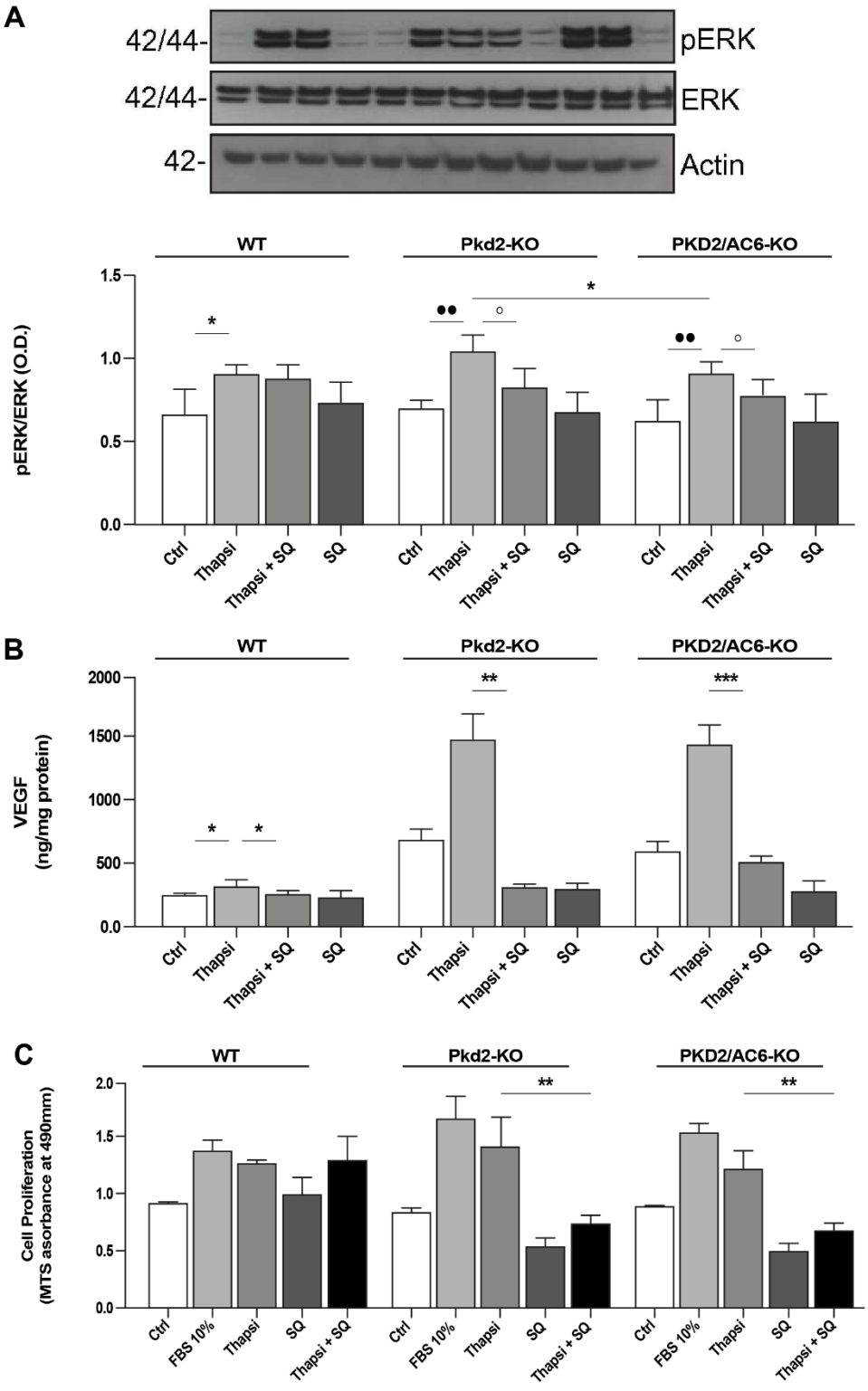
A
42/44-
pERK
42/44-
ERK
42-
Actin
WT
Pkd2-KO
PKD2/AC6-KO
pERK/ERK (O.D.)
1.5
1.0
0.5
0.0
Ctrl
Thapsi
Thapsi + SQ
SQ
B
VEGF
(ng/mg protein)
2000
1500
1000
500
0.0
C
Cell Proliferation
(MTS asorbance at 490mm)
2.0
1.5
1.0
0.5
0.0
FBS 10%

FIGURE 6

Figure 7. Inhibition of AC5 (SQ,22536) reduces the size of organoids derived from *Pkd2-KO* and *Pkd2/AC6-KO* cholangiocytes.

(A) Immunofluoresce stainings of biliary organoids stained for the cholangiocyte markers K19 (green), Sox9 (red), ZO-1 (green) and primary cilium (green). Bar scale, 100um. (B) Representative electron micrographs. The luminal surface of cysts appeared with numerous microvilli and the presence of primary cilia on the apical surface. Bar scale, 10 μm. (C) Representative images of biliary organoids grown in Matrigel and treated with cAMP-mix (Forskolin, IBMX and db-cAMP) to induce spheroids swelling. Images were taken at 4x magnification at 0, 20 and 40 minutes. Bar scale, 100 μm. White lines are representative of spheroid diameter measurements. Graph shows the quantification of biliary organoids swelling in response to cAMP-mix induced cAMP production over time (n=3, p<.05 cAMP-mix treated organoids vs untreated organoids). (D) Representative micrographs of organoids derived from WT, *Pkd2-KO* and *Pkd2/AC6-KO* mouse cholangiocytes untreated (Control), treated with SQ22,536 (1uM) or with NKY80 (1uM) for 5 days. Bar scale,100 μm. Bar graphs show that the volume is significantly reduced in *Pkd2-KO* and *Pkd2/AC6-KO* organoids treated with SQ22,536 (1uM) and NKY80 (1uM). (E) Organoids were cultured for 10 days and pictures were taken every day and volume was measured as described in materials and methods. (F) Graph shows growth rate of WT, *Pkd2-KO* and *Pkd2/AC6-KO* organoids measured every day for 10 days (n=4, *p<.05 *Pkd2-KO* vs WT and •p<.05 *Pkd2-KO* vs *Pkd2/AC6-KO*).

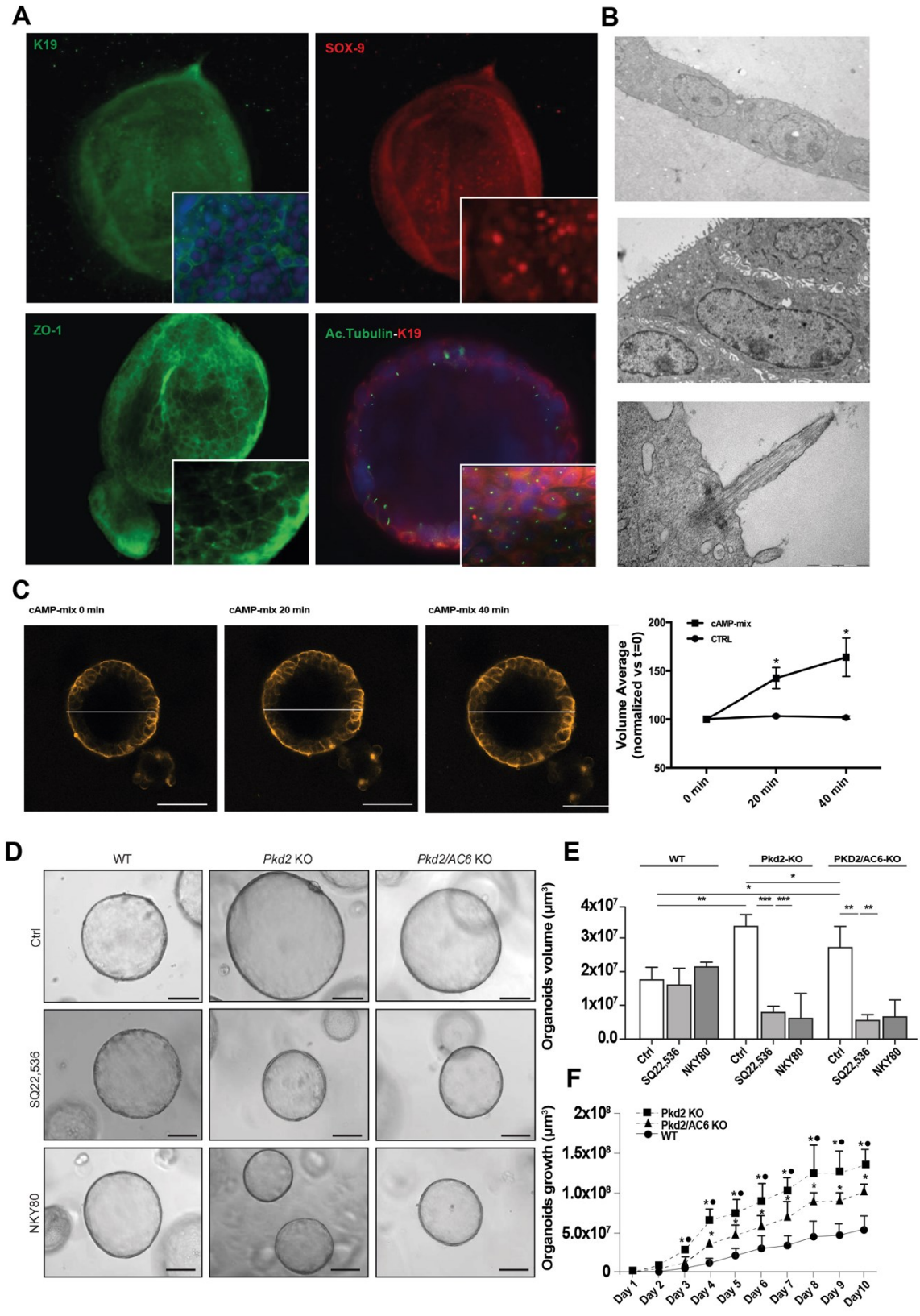
A
K19
SOX-9
ZO-1
Ac.Tubulin-K19
B
C
cAMP-mix 0 min
cAMP-mix 20 min
cAMP-mix 40 min
cAMP-mix
CTRL
Volume Average (normalized vs t=0)
200
150
100
50
0 min
20 min
40 min
D
WT
Pkd2 KO
Pkd2/AC6 KO
Ctrl
SQ22.536
NKY80
E
WT
Pkd2-KO
PKD2/AC6-KO
Organoids volume (µm³)
4x10⁷
3x10⁷
2x10⁷
1x10⁷
0.0
Ctrl
SQ22.536
NKY80
F
Pkd2 KO
Pkd2/AC6 KO
WT
Organoids growth (µm³)
2x10⁸
1.5x10⁸
1.0x10⁸
5.0x10⁷
0
Day 1
Day 2
Day 3
Day 4
Day 5
Day 6
Day 7
Day 8
Day 9
Day10

FIGURE 7

Figure 8. Inhibition of AC5 (SQ,22536) reduces cystic area, liver body weight ratio, pERK and PCNA in *Pkd2-KO* and *Pkd2/AC6-KO* mice.

Pkd2-KO and *Pkd2/AC6-KO* mice received SQ22,536 (300 ug/Kg/day i.p.) or vehicle as described in material and methods section. (A) Liver tissue was stained with the cholangiocyte-specific marker K19. Computer-assisted morphometric analysis of K19-positive areas, expressed as percentage with respect to the whole area analyzed. Bar scale, 100 μm. (B) Liver cysts area was significantly decreased in *Pkd2-KO* and *Pkd2/AC6-KO* mice treated with SQ22,536 (*Pkd2-KO* vehicle, n=9; *Pkd2/AC6-KO* vehicle, n=5; *Pkd2-KO* + SQ, n=6; *Pkd2/AC6-KO*, n=4. **p<.01 in *Pkd2-KO*+SQ22,536 vs. CTRL; ***p<.001 in *Pkd2/AC6-KO*+SQ22,536 vs. CTRL). (C) The decrease in cyst area is reflected also in the significant reduction in liver/body weight ratio (g) in *Pkd2-KO* and *Pkd2/AC6-KO* mice treated with SQ22,536 (**p<.01 in *Pkd2-KO*+SQ22,536 vs. CTRL; *p<.05 in *Pkd2/AC6-KO*+SQ22,536 vs. CTRL). (D) Representative micrographs showing that treatment with SQ22,536 (300 ug/Kg/day for 8 weeks, i.p.) reduces pERK1/2 in *Pkd2-KO* and in *Pkd2/AC6-KO* cystic cholangiocytes. Bar scale, 100 μm. (E) Bar graphs showing a computer-assisted morphometric analysis of pERK1/2 positive area (***p<.001 in Pkd2KO SQ22,536 vs. CTRL; *p<.05 in *Pkd2/AC6-KO* SQ22,536 vs. CTRL). Bar scale, 50 μm. (F) Representative micrographs showing that treatment with SQ22,536 (300 ug/Kg/day for 8 weeks, i.p.) reduces PCNA proliferation marker in *Pkd2-KO* and *Pkd2/AC6-KO* cystic cholangiocytes (***p<.001 in *Pkd2-KO* SQ22,536 vs. CTRL; ***p<.001 in *Pkd2/AC6-KO* SQ22,536 vs. CTRL). (G) Bar graphs showing a computer-assisted morphometric analysis of PCNA expression.(***p <0.001 in *Pkd2-KO* SQ22,536 vs. Ctrl; *** p <0.001 in *Pkd2/AC6-KO* SQ22,536 vs. Ctrl).

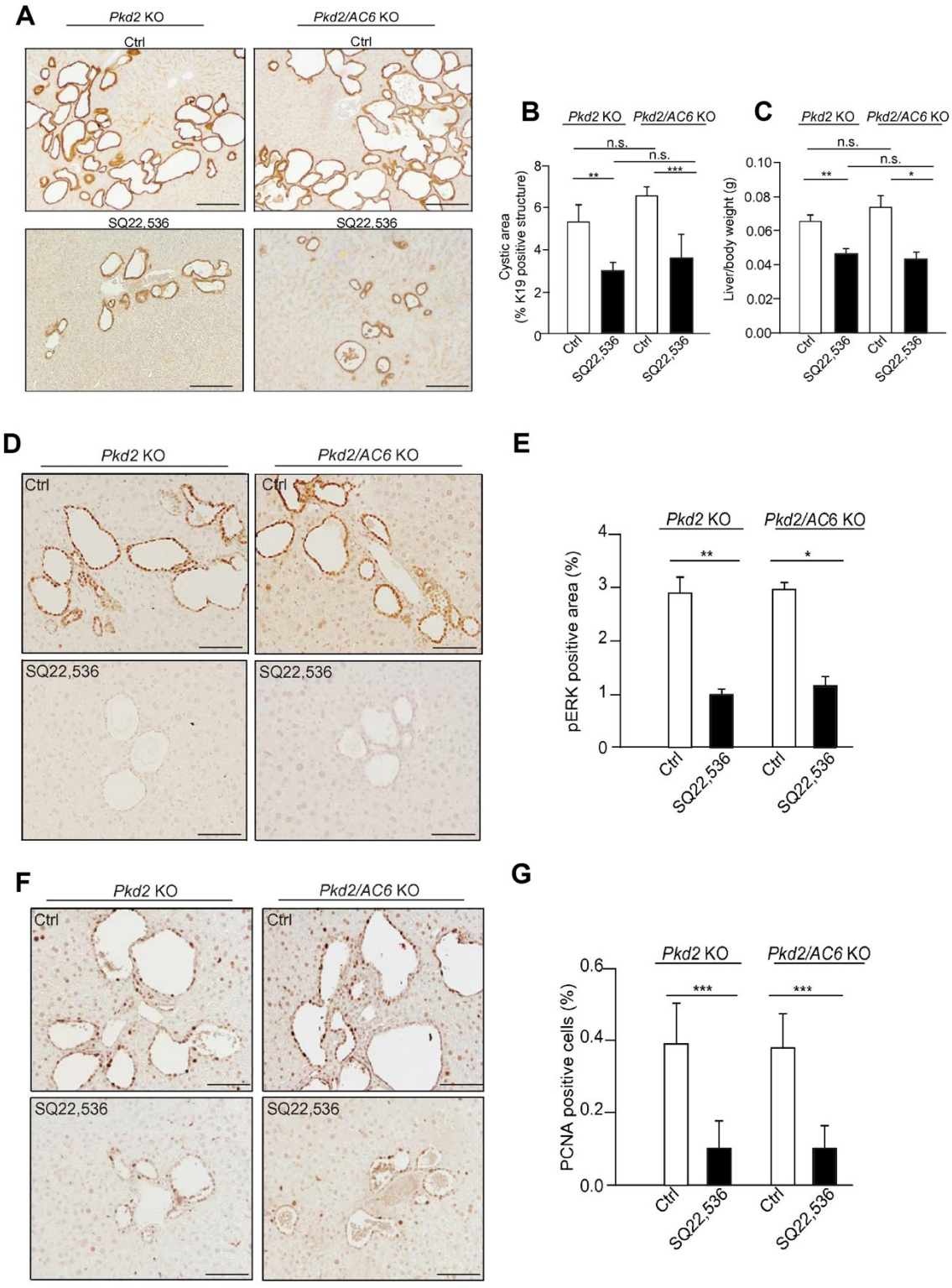
A
Pkd2 KO
Pkd2/AC6 KO
Ctrl
Ctrl
SQ22,536
SQ22,536
B
Pkd2 KO
Pkd2/AC6 KO
n.s.
n.s.
**
***
Cystic area (% K19 positive structure)
0
2
4
6
8
Ctrl
SQ22,536
Ctrl
SQ22,536
C
Pkd2 KO
Pkd2/AC6 KO
n.s.
n.s.
**
*
Liver/body weight (g)
0.00
0.02
0.04
0.06
0.08
0.10
Ctrl
SQ22,536
Ctrl
SQ22,536
D
Pkd2 KO
Pkd2/AC6 KO
Ctrl
Ctrl
SQ22,536
SQ22,536
E
Pkd2 KO
Pkd2/AC6 KO
**
*
pERK positive area (%)
0
1
2
3
4
Ctrl
SQ22,536
Ctrl
SQ22,536
F
Pkd2 KO
Pkd2/AC6 KO
Ctrl
Ctrl
SQ22,536
SQ22,536
G
Pkd2 KO
Pkd2/AC6 KO
***
***
PCNA positive cells (%)
0.0
0.2
0.4
0.6
Ctrl
SQ22,536
Ctrl
SQ22,536

FIGURE 8

Figure 9. STIM1 and AC5 co-localize in membrane of *Pkd2-KO* and *Pkd2/AC6-KO* but not in WT cholangiocytes.

Confocal images of polarized WT, Pkd2KO and Pkd2/AC6KO cholangiocytes co-stained for STIM1-Orai1 (A) or STIM1-AC5 (B) or STIM1-AC6 (C). Serial optical sections (0.5 μm thick) were collected for orthorgonal view (x,y,z). (A) STIM1 and Orai1 co-localized in WT cholangiocytes after treatment with Thapsigargin (2uM) but not in *Pkd2-KO* and *Pkd2/AC6-KO*, while (B) STIM1 co-localized with AC5 but not with Orai1 in *Pkd2-KO* and *Pkd2/AC6-KO* cells. (C) STIM1 and AC6 did not co-localize in WT and *Pkd2-KO* cholangiocytes after treatment with Thapsigargin (2uM).

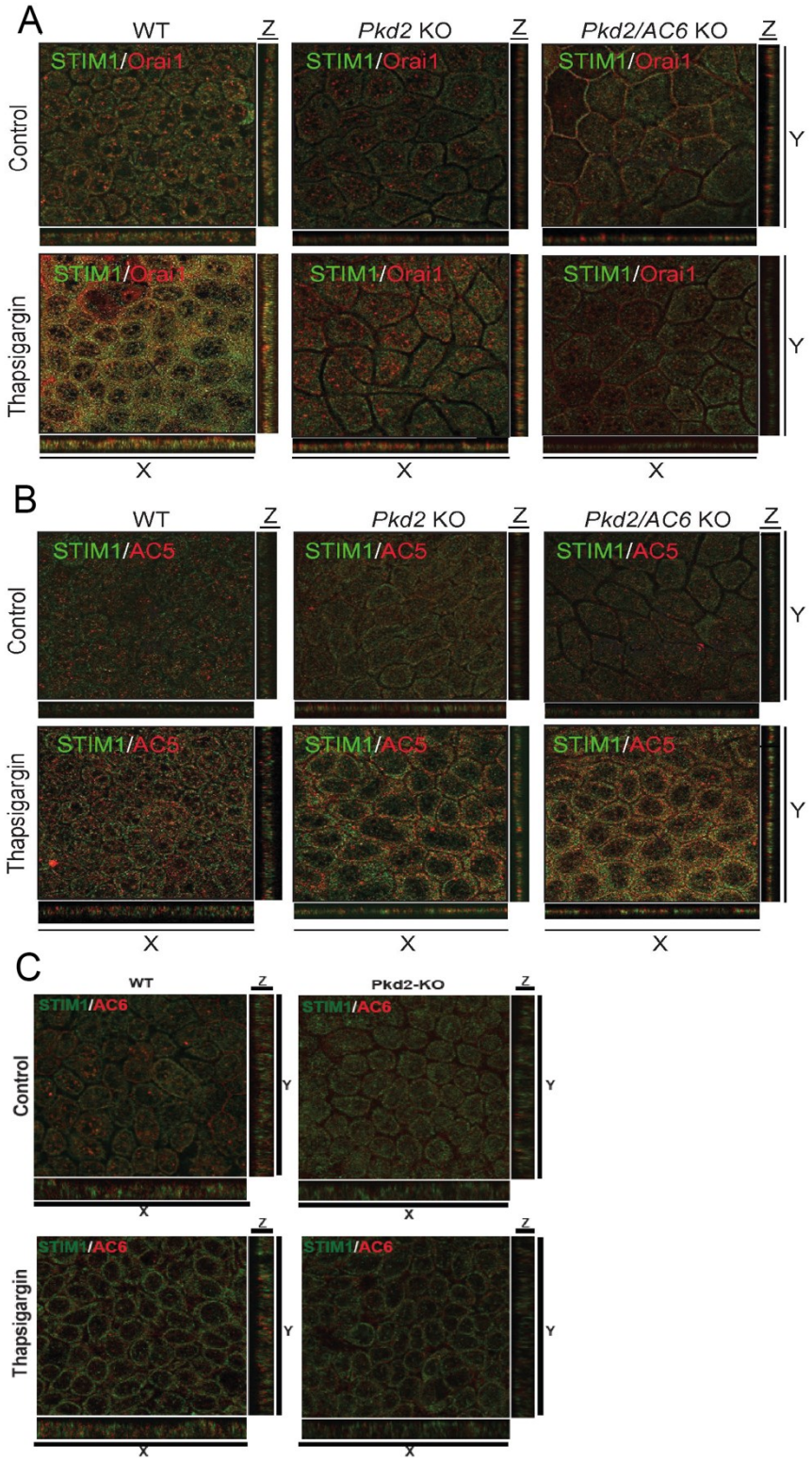
A
WT
Pkd2 KO
Pkd2/AC6 KO
Z
STIM1/Orai1
Control
Thapsigargin
Y
X
B
STIM1/AC5
C
WT
Pkd2-KO
STIM1/AC6

FIGURE 9

Figure 10. STIM-1 co-localizes with AC5 in *Pkd2-KO* and *Pkd2/AC6-KO* cells but not in WT cells.

(A) Fluorescence imaging of in-situ proximity ligation assay (PLA), showed interaction of STIM1 and Orai1 (green dots) in WT cells but not in *Pkd2-KO* and *Pkd2/AC6-KO* cells after Thapsigargin (2uM). (B) STIM1 interacts with AC5 (green dots) in *Pkd2-KO* and *Pkd2/AC6-KO* cells but not in WT cholangiocytes. (C) Fluorescence imaging of in-situ proximity ligation assay (PLA), did not show interaction of STIM1 and AC6 in WT and *Pkd2-KO* cells after Thapsigargin (2uM). Original magnification 10x; inset: 40x.

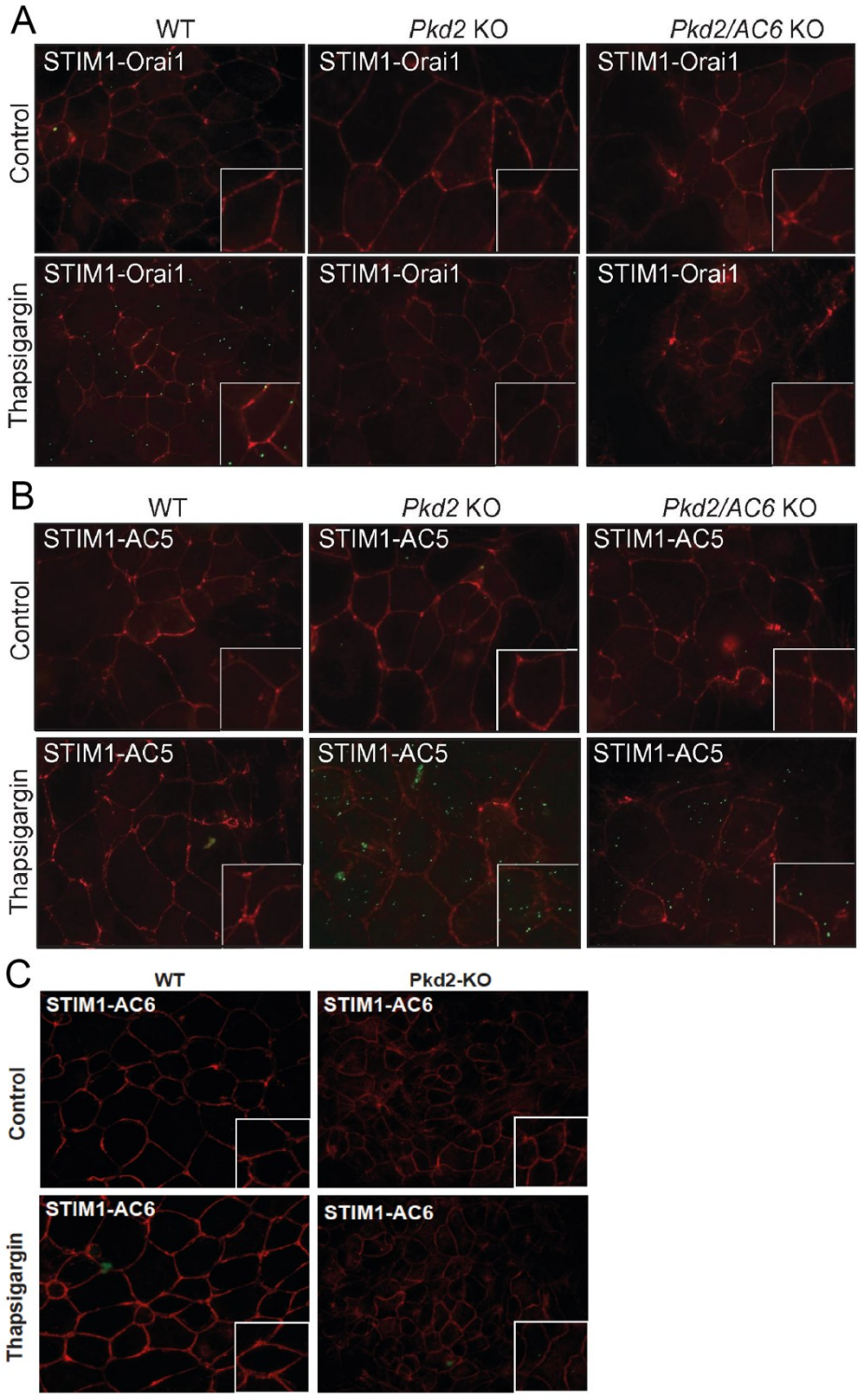
A
WT
Pkd2 KO
Pkd2/AC6 KO
Control
Thapsigargin
STIM1-Orai1
B
STIM1-AC5
C
Pkd2-KO
STIM1-AC6

FIGURE 10

Figure 11. Refill rate of calcium and ER-[Ca^{2+}] are decreased in *Pkd2-KO* cholangiocytes.

(A) [Ca^{2+}] ER dynamics measured with ER-2mutAEQ-i in Ca^{2+}-depleted cells. WT (black trace) and *Pkd2-KO* cells (red trace) expressing ER-2mutAEQ and reconstituted with coelenterazine native were refilled with Ca^{2+} by addition of 1 mM Ca^{2+}-containing medium when indicated. Then, either 100 µM ATP was perfused as indicated. (B) Representative trace of the refilling phase of the ER-calcium content. PC2-deficiency (red traces) causes a decreased refill of the ER compared to WT cells (black trace). (C) Averaged ER-Ca^{2+} uptake response after 1mM of $CaCl_2$ stimulus measured with aequorin-based probe. *Pkd2-KO* cholangiocytes show a significant decrease of calcium uptake ($p<0.05$ vs WT, n=9) and a trend to a decreased rate of calcium compared to WT cells (D)($p=0.07$ vs WT, n=9) (E) Representative trace of the release phase of the ER-calcium content. PC2-deficiency (red traces) does not alter the IP3R-dependent release of calcium from the ER compared to WT cells (black trace). (F-G) Averaged ER-Ca^{2+} release response after 100uM of ATP stimulus measured with aequorin-based probe. Differences were determined not significant by unpaired t test.

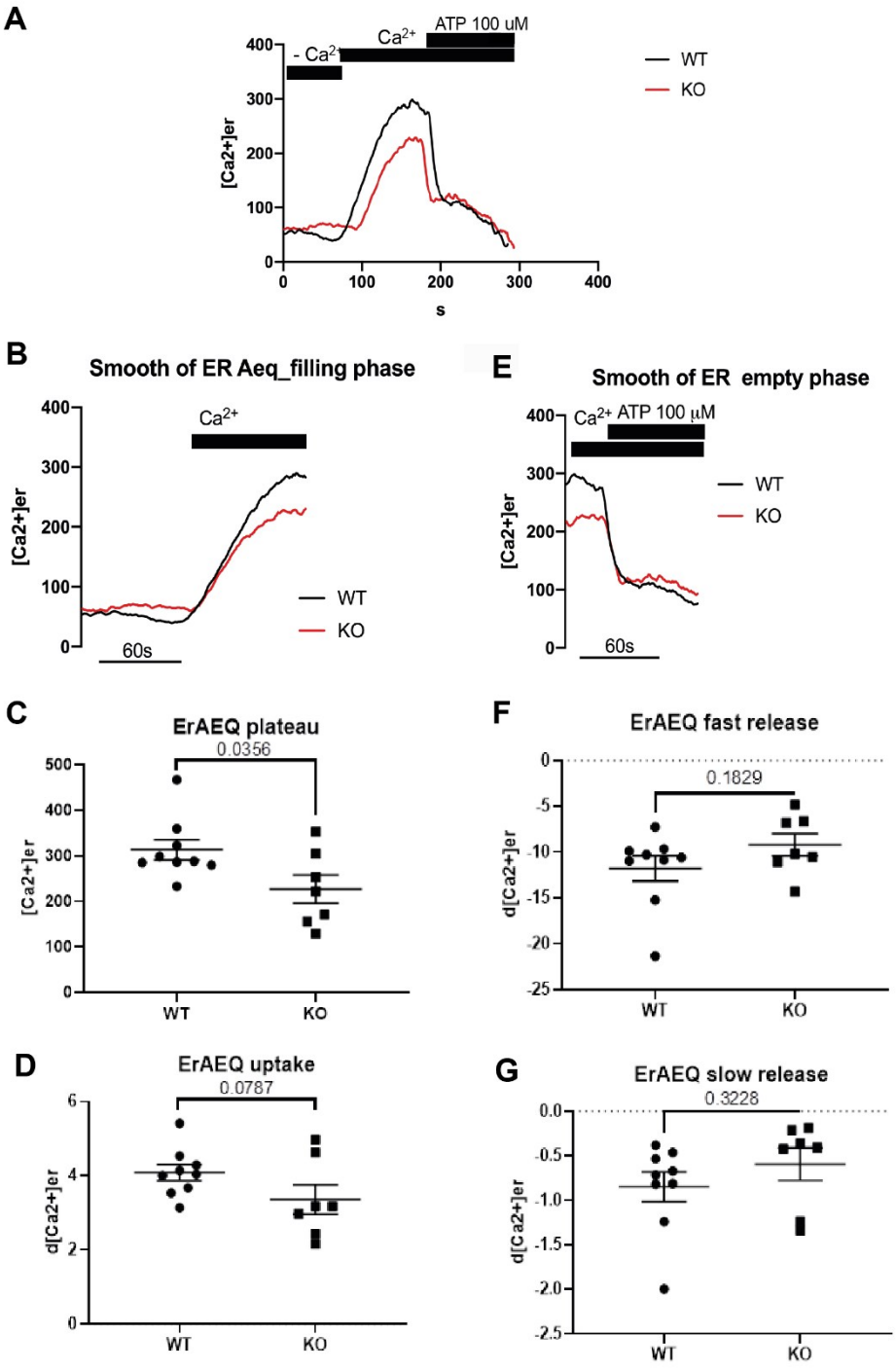
A
- Ca2+
Ca2+
ATP 100 uM
WT
KO
[Ca2+]er
s
B
Smooth of ER Aeq_filling phase
Ca2+
60s
E
Smooth of ER empty phase
Ca2+ ATP 100 µM
C
ErAEQ plateau
0.0356
D
ErAEQ uptake
0.0787
F
ErAEQ fast release
0.1829
G
ErAEQ slow release
0.3228
d[Ca2+]er

FIGURE 11

Figure 12. Mitochondria respiration and Ca^{2+} uptake are impaired in PC2-defective cholangiocytes.

(A) Oxygen consumption rates (OCR) and ATP production are reduced in mitochondria of Pkd2KO cholangiocytes. OCR was analyzed in real time using the Seahorse XF96 extracellular flux analyzer for WT (black trace) and Pkd2KO cells (red trace). A representative experiment is shown. When Oligomycin A is added, the ATP synthase complex is inhibited, therefore the respiratory chain-associated oxygen consumption is inhibited. Addition of the ATP synthesis uncoupler FCCP induces the maximal oxygen consumption by the respiratory chain. Addition of rotenone and antimycinA (Rot/AntA, complex I and III inhibitors, respectively) blocks the electron transfer as well as oxygen consumption by the respiratory chain. (B) Bar graph shows the parameters that can be measured and used to determine mitochondrial respiratory function in WT and *Pkd2-KO* cholangiocytes. Basal respiration (OCR-BASAL), ATP production (OCR-ATP), spare respiratory capacity (OCR-SRC) and maximal respiration (OCR-MMR). The reduced OCR-BASAL, OCRATP, OCR-MMR, and OCR-SRC in Pkd2KO (red bar) compared with WT cholangiocytes (black bar) indicate an overall impaired mitochondria-linked aerobic respiration and ATP production in Pkd2KO cells. (Bar plots show the mean± S.E.M. of n=8 replicates. **p<0.01 vs WT) (C) Mitochondrial calcium uptake is decreased in PC2-defective cholangiocytes in absence of external calcium. Representative traces show averages of mitochondrial Ca^{2+} uptake upon ATP-stimulation in WT (black trace) and *Pkd2-KO* cholangiocytes (red trace). (D) Averaged mitochondrial calcium uptake response after 100uM of $CaCl_2$ stimulus measured with aequorin-based probe. Differences were determined not significant by unpaired t test. (E) Mitochondrial calcium uptake is decreased in PC2-defective cholangiocytes in absence of external calcium. Representative traces show averages of mitochondrial Ca^{2+} uptake upon ATP-stimulation in WT (black trace) and *Pkd2-KO* cholangiocytes (red trace). (F) Averaged mitochondrial calcium uptake response after 100uM of $CaCl_2$ stimulus measured with aequorin-based probe in absence of external calcium. *Pkd2-KO* cholangiocytes show a significant decrease of calcium uptake compared to WT cells. (p=0.06 vs WT, n=5)

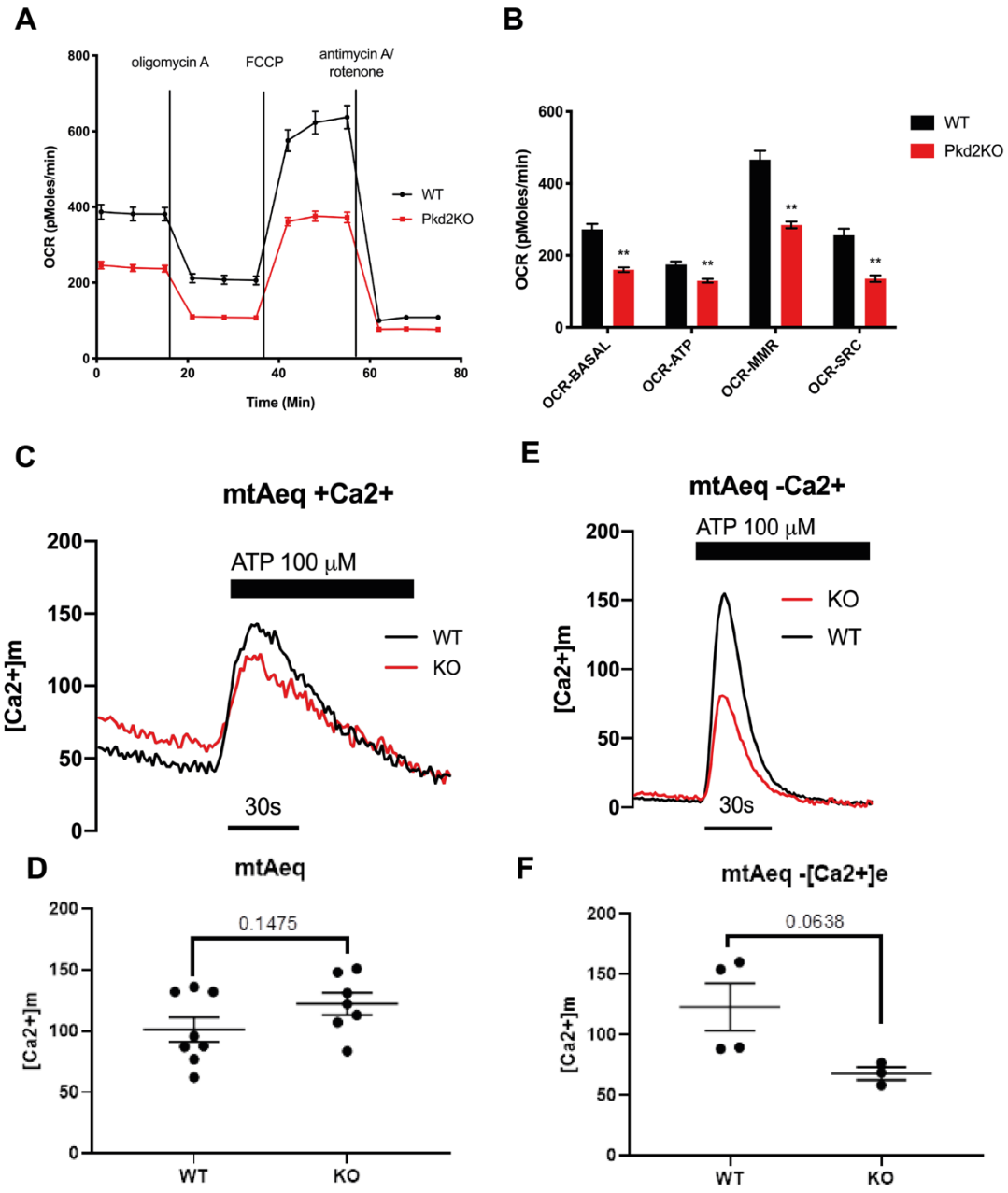
A
oligomycin A
FCCP
antimycin A/
rotenone
OCR (pMoles/min)
Time (Min)
WT
Pkd2KO
B
OCR (pMoles/min)
WT
Pkd2KO
OCR-BASAL
OCR-ATP
OCR-MMR
OCR-SRC
C
mtAeq +Ca2+
ATP 100 μM
[Ca2+]m
WT
KO
30s
D
mtAeq
0.1475
[Ca2+]m
WT
KO
E
mtAeq -Ca2+
ATP 100 μM
[Ca2+]m
KO
WT
30s
F
mtAeq -[Ca2+]e
0.0638
[Ca2+]m
WT
KO

FIGURE 12

Figure 13. Altered intracellular signaling in PLD-ADPKD (working model).

In PC2-defective cholangiocytes, store- operated Ca^{2+} entry is inhibited and cells respond to an acute reduction in endoplasmic reticulum (ER) Ca^{2+} levels with stromal interacting molecule 1 (STIM1)-dependent and adenylyl cyclase 5 (AC5)-dependent stimulation of cAMP production, which drives PKA- dependent activation of ERK1/ERK2 and VEGF-A secretion. In turn, cAMP activates the PKA–Ras–Raf–ERK pathway and stimulates vascular endothelial growth factor (VEGF) production through an mTOR–HIF1α- mediated mechanism. mTOR has a central role in IGF-1-stimulated proliferation of cystic cholangiocytes. IGF-1, a growth factor secreted by the cystic epithelium and by cholangiocyte under stress, binds to its receptor IGF1-R and activates the PI3K/AKT/mTOR pathway; mTOR stimulates proliferation through a HIF1-α /VEGF-dependent autocrine loop. In a paracrine way, VEGF produced by cystic cholangiocytes increases perivascular microvascular density and cholangiocyte proliferation through binding with VEGF receptor 2 (VEGFR2). *(Modified from Fabris L. et al., Nature Review Gastroenterology and Hepatology, 2019).*

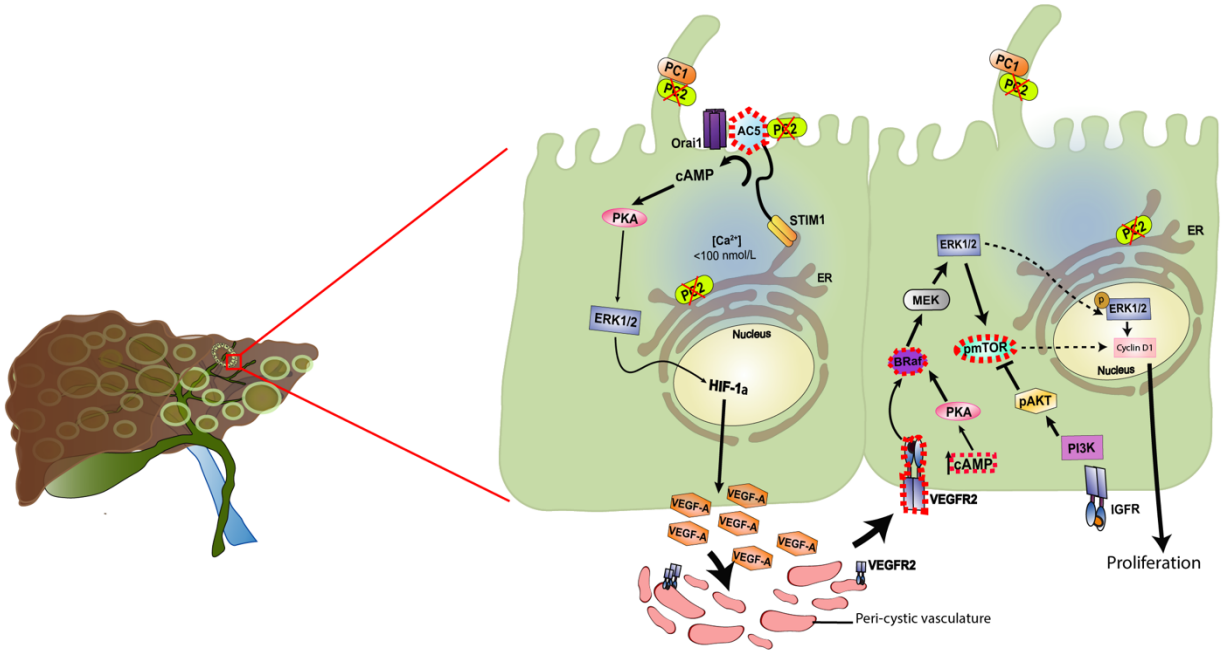
PC1
PC2
Orai1
AC5
PE2
cAMP
PKA
STIM1
[Ca2+]
<100 nmol/L
ER
ERK1/2
Nucleus
HIF-1a
VEGF-A
VEGFR2
Peri-cystic vasculature
MEK
BRaf
pmTOR
pAKT
PI3K
IGFR
Cyclin D1
Proliferation

FIGURE 13

Table 3 | Sample Profiles

Cystic Area

Sample	Mean±SD (% Cystic Area)	*p Value*	*n*
Pkd2-KO Ctrl	5.29±0.85		*9*
Pkd2-KO + SQ22,536	2.95±0.46	***p<.0001	*6*
Pkd2/AC6-KO Ctrl	6.52±0.47		*5*
Pkd2/AC6-KO + SQ22,536	3.56±1.19	***p<.0001	*4*

Liver/Body Weight

Sample	Mean±SD (g)	*p Value*	*n*
Pkd2-KO Ctrl	0.064±0.004		*9*
Pkd2-KO + SQ22,536	0.045±0.003	***p<.0001	*6*
Pkd2/AC6-KO Ctrl	0.073±0.007	n.s.	*5*
Pkd2/AC6-KO + SQ22,536	0.042±0.004	***p<.0001	*4*

cAMP

Sample	Mean±SD (pmol/mg protein)	*p Value*	*n*
WT Ctrl	0.15±0.10		*9*
WT + TPEN	0.39±0.17	*p<.05	*9*
WT + TPEN + SQ22,536	0.089±0.008	*p<.05	*3*
WT + SQ22,536	0.093±0.003		*3*
WT + TPEN + NKY80	0.11±0.014	*p<.05	*3*
WT + NKY80	0.10±0.008		*3*
Pkd2-KO Ctrl	0.44±0.21		*9*
Pkd2-KO + TPEN	1.19±0.45	***p<.0001	*9*
Pkd2-KO + TPEN +SQ22,536	0.28±0.033	***p<.0001	*3*

Pkd2-KO + SQ22,536	0.18±0.005		*3*
Pkd2-KO + TPEN + NKY80	0.29±0.016	***p<.0001	*3*
Pkd2-KO + NKY80	0.20±0.010		*3*
Pkd2/AC6-KO Ctrl	0.39±0.12		*9*
Pkd2/AC6-KO + TPEN	1.04±0.18	***p<.0001	*9*
Pkd2/AC6-KO + TPEN+ SQ22,536	0.24±0.039	***p<.0001	*3*
Pkd2/AC6-KO + SQ22,536	0.15±0.015		*3*
Pkd2/AC6-KO + TPEN+ NKY80	0.41±0.073	**p<.001	*3*
Pkd2/AC6-KO + NKY80	0.20±0.005		*3*

VEGF

Sample	**Mean±SD (ng/mg protein)**	***p Value***	***n***
WT Ctrl	211±50		*3*
WT + Thapsi	291±80	*p<.05	*3*
WT + Thapsi + SQ22,536	229±43	n.s.	*3*
WT + SQ22,536	204±69		*3*
Pkd2-KO Ctrl	666±112		*3*
Pkd2-KO + Thapsi	1469±247		*3*
Pkd2-KO + Thapsi +SQ22,536	453±85	**p<.001	*3*
Pkd2-KO + SQ22,536	267±65	**p<.001	*3*
Pkd2/AC6-KO Ctrl	575±98		*3*
Pkd2/AC6-KO + Thapsi	1449±184		*3*
Pkd2/AC6-KO + Thapsi+SQ22,536	492±58	***p<.0001	*3*
Pkd2/AC6-KO + SQ22,536	252±100	*p<.05	*3*

Cysts Organoids Volume

Sample	Mean±SD (μm^3)	*p Value*	*n*
WT Ctrl	$1.78x10^7 \pm 3.81x10^6$		*8*
WT + SQ22,536	$1.62x10^7 \pm 5.12x10^6$	n.s.	*5*
WT + NKY80	$2.09x10^7 \pm 1.94x10^6$	n.s.	*4*
Pkd2-KO Ctrl	$3.33x10^7 \pm 4.07x10^6$	*p<.05	*8*
Pkd2-KO + SQ22,536	$7.68x10^6 \pm 2.17x10^7$	**p<.001	*5*
Pkd2-KO + NKY80	$6.48x10^6 \pm 6.98x10^6$	**p<.001	*4*
Pkd2/AC6-KO Ctrl	$2.73x10^7 \pm 6.95x10^6$	*p<.05	*8*
Pkd2/AC6-KO + SQ22,536	$5.83x10^6 \pm 1.75x10^6$	*p<.05	*5*
Pkd2/AC6-KO + NKY80	$6.58x10^6 \pm 5.31x10^6$	*p<.05	*4*

Box 1| Measurement of [Ca^{2+}] in ER compartment using *erAEQmut*

1. Cells were perfused with KRB (without $CaCl_2$)+ EGTA 100uM for at least 30 seconds to obtain a stable signal, and the lower value was considered as background. Use peristaltic pump (standard flow rate: 2.5 ml min-1).

2. To reload the stored Ca^{2+} cells were perfused with modified KRB (with 1mM $CaCl_2$).

3. To activate the Ca^{2+} pathways, Ca^{2+} -mobilizing solution (CMS, KRB + 1mM $CaCl_2$) in which ATP (100uM) is dissolved was perfused. After addition of agonist, light emission (counts per second ,c.p.s. values) rapidly decreases.

4. Wait until there is no further change in the c.p.s. value for ~20–30 s. Pause perfusion, and change the medium to lysis solution (0.1% TritonX-100). A large increase in luminescence (c.p.s. value) will be observed.

5. To accurately determine the total aequorin content, wait until the c.p.s. value returns to the basal level recorded at the beginning of the experiment. Stop the analysis system and the perfusion

Box 2| Measurement of [Ca^{2+}] in Mitochondrial compartment using *mtAEQmut*

- With external Ca2+ :

1. Cell were perfused with modified KRB (with 1mM $CaCl_2$) for at least 60 sec to obtain a stable signal, and the lower value was considered as background. Use peristaltic pump (standard flow rate: 2.5 ml min-1).

- Without external Ca^{2+} :

1. Cell were perfused with modified KRB (without $CaCl_2$)+ EGTA 100uM for at least 60 sec to obtain a stable signal, and the lower value was considered as background. Use peristaltic pump (standard flow rate: 2.5 ml min-1).

2. To activate the Ca^{2+} pathways, Ca^{2+} -mobilizing solution (CMS, KRB + 1mM $CaCl_2$) in which ATP (100uM) is dissolved was perfused. Raise the rate of perfusion from 2.5 to 5 ml min-1 to allow rapid equilibration of the compounds in the perfusion chamber. After addition of agonist, light emission (c.p.s. values) rapidly increases, reaches a peak and then starts to decline. The c.p.s. value will return to almost basal values within 2 min.

3. To accurately determine the total aequorin content, wait until the c.p.s. value returns to the basal level recorded at the beginning of the experiment. Stop the analysis system and the perfusion.

PART II

β-catenin and IL-1β dependent CXCL10 production drives progression of disease in a mouse model of Congenital Hepatic Fibrosis

BACKGROUND

Fibropolycystic diseases, i.e. Autosomal recessive polycystic kidney disease (ARPKD), Congenital Hepatic Fibrosis (CHF) and Caroli Disease (CD) are rare hereditary hepatorenal fibrocystic disorder characterized by intra-hepatic biliary duct dilatation and markedly enlarged kidney, which cause the major cause of pediatric morbidity and mortality[18, 52]. The reported incidence in the America continent is 1 in 26.500 live births, corresponding to carrier frequency of ~1 in 70 in the general population. ARPKD occurs equally in boys and girls. After birth, the mortality of the infants is ~30-40% due to an incomplete development of the lungs (i.e. pulmonary hypoplasia)[128]. However, for patients surviving to adulthood the prognosis of 10-year survival is estimated around 82%. The spectrum of symptoms of surviving patients with ARPKD is highly variable and includes systemic and portal hypertension, congenital hepatic fibrosis, biliary dysgenesia, segmental ductal dilations and progressive end-stage renal failure (ERAD) due to fusiform dilatation of the renal collecting ducts of the kidney[49, 128].

These disease-associated phenotypes results from disordered terminal differentiation during renal and hepatic development, particularly arising from malformation of the ductal plate (DPM) during early embryogenesis[50]. Of note, similar DPM has been observed in other ciliopathies such as in nephronopthisis, Joubert and Barder-Biedl syndrome, which may also have an ARPKD-like phenotype[129].

Different types of missense or truncating mutation in PKHD1 gene (chromosome 6p12.3-12.2) are responsible for most cases of ARPKD. PKHD1 is a large-size gene, consisting of 12.222bp coding sequence, 67 exons, and long ~470kb, with a high level of allelic heterogeneity (~60% of mutation occurs in-frame, and 40% are truncating mutation)[130-132]. Of note, the complexity of the gene and its mutation further complicate the molecular diagnosis of ARPKD. However, some of this mutation is more common than others, and some are higher in a specific population[133]. For example, T36M is the most common mutation and accounts for ~10-15% of a mutant allele in the European population[133].

Additionally, multiple transcript are generated from the mRNA of PKHD1 by alternative splicing. The longest transcript encodes for the fibrocystin, also known as

polyductin, a 4.074-residue protein comprising a single transmembrane domain, an large extracellular N-domain and short C-terminal cytoplasmic tail. Fibrocystin mainly localize in the primary cilium and in other cellular compartment, including in the basal bodies and mitotic spindle in renal tubular and biliary epithelial cells[131]. Notably, specific motifs in the C-terminal of fibrocystin guarantee its translocation in the ciliary membrane[134]. Whereas, similar to the Notch signaling, the N-terminal of fibrocystin is proteolytically-cleaved to release the C-terminal, which translocate into the nucleus where probably regulate the transcription of downstream genes[135-137]. To date this aspect remain to be better established, however it is considerable to think that the C-terminal of fibrocystin may be regulate genes involved in the ductal dilatation. Furthermore, the C-terminal domains includes putative cAMP/cGMP-dependent protein kinase phosphorylation sites that play an important role in its still unclear intracellular function[136].

Another gene-related disease, encoding for the ciliary transition zone protein DAZ-interacting protein 1-like protein (DZIP1L), has been found to be causative of moderate ARPKD in children that do not have PKHD1 mutation[128, 138]. DZIP1L contain 2.301bp coding sequence, 16 exons, long ~53kb and is a soluble zing-finger proteins localizing in the centrioles and in the basal bodies, similarly to fibrocystin and polycystin-1 and polycystin-2 (PC1 and PC2, respectively)[138]. DZIP1L enters into relation with septin2, which is recognized as a protein designed to support the periciliary diffusion barrier within the ciliary transference zone. Indeed, studies from Bergmann and colleagues shown that absence of DZIP1L results in a defective ciliary-membrane translocation of PC1 and PC2 that results in ARPKD[138]. Importantly, there have been findings that PC1 and PC2 might also be genetically inherited in a recessive way with having one PKD1 or PKD2 hypomorphic allele at minimum, or having some mutation in HNF1B, which provokes a phenotype-like to ARPKD [129].

Mutation in these genes cause the hepatic phenotype characterized by CHF, which occurs in children with ARPKD, in association with non-obstructive dilatation of the intra-hepatic bile ducts (Caroli Disease) and portal hypertension (thrombocytopenia, anemia and/or splenomegaly) or episodes of cholangitis. Furthermore, adult ARPKD patients (>40 years of age) have an increased risk of developing hepatic tumours, specially cholangiocarcinoma[139].

Differently from ADPKD, patients with ARPKD present dilatation of the intra-hepatic bile ducts occurs with concomitant progression of portal fibrosis, the main mechanism of progression in all the cholangiopathies[19, 51]. Thus, understanding the mechanistic relationships between biliary damage and portal fibrosis is of considerable interest.

Caroli disease and CHF are of extreme interest, as they are associated with brisk and progressive peribiliary fibrosis. This fibrosis is not triggered by necroinflammatory damage to the biliary epithelium, but rather is the result of the adaptation of the epithelium itself to the fibrocystin mutation[140].

SUMMARY OF PREVIOUS DATA AND AIM

To gain insight into the cholangiocyte dysfunction and portal fibrosis mechanism of CHF, we used a mouse orthologous of human CHF that harbors a homozygous deletion in exon 4 of *Pkhd1* gene (*Pkhd1*$^{del4/del4}$) that generate an inactive transcript[32, 141].

Pkhd1$^{del4/del4}$ mice develop progressive formation of biliary cysts, portal fibrosis, and splenomegaly. Intrahepatic bile duct lesions are present as early as two weeks post-birth and lead to progressive liver cyst formation and periportal fibrosis after three months. The presence of splenomegaly in more than 50% of the mice already at three months indicates clinically relevant portal hypertension[142].

Although little is known about the biological functions of fibrocystin (FPC), several studies in animal models, including our own, observed that the 3'-5'-cyclic adenosine monophosphate (cAMP) and the mammalian target of rapamycin (mTOR) signaling pathways are activated and, through protein kinase A (PKA) pathway, stimulate cell proliferation and cysts expansion[94, 143]. Increased cAMP/PKA signaling is also a feature of PLD-ADPKD, a condition with a different clinical and pathological features[84, 91]. On the other hand we found that β-catenin signaling is increased only in fibrocystin-defective cholangiocytes[143]. Physiologically, β-catenin is known as a multifunctional protein that serves both as a cell adhesion agent and a transcriptional regulator of the fundamental Wnt signaling pathway, which is responsible for proliferation and differentiation functions in time of organ development. A vital element of this pathway is the management of a scope of cytosolic β-catenin by a selected "destruction" combination. If Wnt signal is "offline" (i.e., there are no Wnt ligands), the set of cytosolic β-catenin becomes isolated by this destruction combination and transforms into phosphorylation at the Ser45 with a help of the casein-kinase 1α (Ck1α), which directs the glycogen synthase kinase 3 (Gsk3)-regulated phosphorylation of β-catenin towards the N-Terminal Tyr41, Ser37 and Ser33 areas. Eventually, this complex of phosphorylation titled as "phospodegron" becomes identified by the F-box-incorporating protein β-trasducin repeat-containing protein (β-TrCP) ubiquitin E3 ligase complex and then redirected towards ubiquitination and proteasomal degradation. In the meantime, binding of Wnt ligands bind with the frizzled (FZD) and the co-receptor low-density-lipoprotein-related protein

5/6 (LRP5/6), triggers the Wnt signal pathway activation. In the Wnt “ON” state, dephosphorylated β-Catenin moves towards the nucleus, initiating the T-cell factor (TCF) or lymphoid enhancer-binding factor 1(LEF), which are transcription factors aimed to make the target genes of β-Catenin active (**Fig.**14)[144, 145]. This includes c-Myc and Zeb-1 that functionally contribute to cell proliferation and mobility, accordingly[146, 147].

Several recent studies have shown that cAMP/PKA-mediated phosphorylation of β-Catenin at Ser522 and Ser675 residue results in increased β-catenin transcription activity since its dissociate from the destruction complex[148]. We have shown that in *Pkhd1*$^{del4/del4}$ cholangiocytes, phosphorylation at Ser-675 enhances β-catenin transcriptional activity. In fact, in the presence of activated Rac-1, p-β-catenin-Ser675 is translocated to the nucleus, becomes transcriptionally active, and is responsible for the down-regulation of E-cadherin and the increased motility of FPC-cholangiocytes[143].

Even if the role of β-catenin in fibrocystin defective cholangiocytes is not completely clear, recent studies have identified β-catenin an emerging regulator of inflammation. For example, by activating pro- and anti-inflammatory mediators, including CXCL2 and CXCL10, β-catenin signaling produces an inflammatory milieu that can affect tumour behavior, such as the aggressiveness of the hepatocellular carcinoma[149]. Interestingly, increased secretion of pro-inflammatory cytokines and chemokines has also been observed in CHF/CD. Indeed, we have shown that fibrocystin-defective cholangiocytes express significantly more CXCL1, CXCL10 CXCL12, and IL-1β than WT cholangiocytes. Furthermore, we showed that inhibition of β-catenin signaling significantly reduces the expression of the CXCL1, CXCL10 CXCL12, and IL-1β, suggesting that β-catenin may also be responsible for increased production of chemokine[142]. We also provided evidence that these chemokines are responsible for the pericystic recruitment of inflammatory mononuclear cells, at an early stage od disease characterized as M1 macrophages that progressively switch to an M2 phenotype[142].

In a recent study, we have demonstrated that in *Pkhd1*$^{del4/del4}$ mice, pericystic fibrosis was associated with progressive accumulation of CD45^{+} cells closely located at the basal side of the biliary dilatation. In *Pkhd1*$^{del4/del4}$ mice, macrophages were identified by Flow cytometric analysis (FACS) as the main cell subset of CD45^{+} cells

using co-expression markers CD11b and F4/80. The relative proportion of other subsets, such as neutrophils ($CD45^+/Ly^-6G^+$) and monocytes ($CD45^+/CD11b^+/F4/80^-$), was generally lower than 5%[142].

The recruited macrophages ultimately secrete TNFα (an M1 cytokine) and TGF-β1 (an M2 cytokine) that in FPC-defective up-regulate the expression of αvβ6-Integrin, a latent activator of TGF-β1. The expression of αvβ6-Integrin was restricted to the biliary cells, especially in cystic epithelia and was correlated with portal fibrosis and $CD45^+$ cell infiltration [142](**Fig.**15).

Notably, gene expression experiments on whole liver tissue demonstrated that expression of TGFβ1 (an M2 cytokine) is only modestly increased in the early phase, becoming significant at nine months (2.5-folds as respect to WT) of age. In contrast, TNFα (an M1 cytokine) mRNA is strongly up-regulated since the early stage of the disease, reaching nearly 5-fold expression with respect to WT in one month. This time-dependent cytokine expression is consistent with a phenotypic switch from M1 (pro-inflammatory) to M2 (pro-fibrotic) macrophages the course of the disease[142]. The relevance of the chemotactic effect of CXCL1 and CXCL10 on macrophage was highlighted by the significant reduction of macrophage migration after administration of anti-CXCL1 and anti-CXCL10 blocking antibodies in cultured FPC-cholangiocytes.

The pathophysiological relevance of M2 macrophages in fibrosis deposition was confirmed by in vivo clodronate or vehicle treatment in *Pkhd1*$^{del4/del4}$ mice and WT littermates. Macrophages depletion with clodronate given for three months in *Pkhd1*$^{del4/del4}$ mice, reduced the inflammatory infiltrate, decreased αvβ6-Integrin expression on biliary structures and with a significant reduction of collagen fibers deposition and splenomegaly[142].

Based on these observation, we concluded that, similar to reactive cholangiocytes, the genetic defect of FPC in cholangiocytes induces the secretion of a number of growth factors, cytokines, and chemokines, that recruit macrophages in the portal microenvironment and initiate a chronic inflammatory loop, defined by Medzhitov as *"parainflammation"*, aimed at restoring a normal cellular homeostasis rather than an overt cell injury[140, 150].

The CXCL10 chemokine is a chemoattractant for different inflammatory cells, including monocytes/macrophages, T cells, Natural Killer (NK) cells and dendritic cells and perform its function by binding to the cell surface receptor CXC chemokine receptor family 3 (CXCsR3)[151-153]. The role of CXCR10 in promoting liver fibrosis

by mediating the recruitments of macrophages in toxic induced liver fibrosis models have been recently established[154].

In part II of this Ph.D. thesis, we aimed to study the mechanisms that promote CXCL10 production in FPC-defective cholangiocytes and to test *in vivo* if the blockade of the CXCL10/CXCR3 axis may reduce the progression of the CHF/CD disease. Furthermore, these genetic diseases offer a unique opportunity to improve our understanding of the mechanistic relationships between biliary damage and portal fibrosis, the primary mechanism of progression in cholangiopathies.

RESULTS

In vivo CXCL10/CXCR3 axis inhibition leads to reduction in fibrosis, inflammation and growth in cyst in Pkhd1$^{del4/del4}$ mice

We have found that increased secretion of CXCL10 in cholangiocytes isolated from *Pkhd1$^{del4/del4}$* mice triggers the recruitments of macrophages, which play an essential role in fibrosis progression. To gain better insights on the role of CXCL10 in macrophage recruitment and disease progression we studied the effects of CXCR3–CXCL10 axis inhibition in *Pkhd1$^{del4/del4}$* mice. The key chemokines CXCL9, CXCL10, and CXCL11, bind to the interferon-inducible chemokine receptor CXCR3, performing an essential role in recruitment, activation, and differentiation of immune cells. Thus, we thought first to assess the expression of CXCR3 and its ligands in the whole liver and cholangiocytes isolated from *Pkhd1$^{del4/del4}$* mice. Analysis of gene expression from *Pkhd1$^{del4/del4}$* livers showed a not significant difference in CXCL9 and CXCL11 levels while the CXCL10 expression increased with respect to control liver (**Fig.**16A-C). In addition to this, the secretion of CXCL9 and CXCL11 was not detected in FPC-defective cholangiocytes (no data shown). Afterwards, after analyzing the CXCR3 expression in cell from 3-month old mice whole livers, isolated using FACS-sorting, it was evident that there was an increase in CXCR3 expression in respect to the normal cells in fibroblasts (collagen 1^{+} cells) (**Fig.** 16D), macrophages (F4/80^{+} cells) (**Fig.** 16F), and cholangiocytes (K19^{+} cells) isolated from *Pkhd1$^{del4/del4}$* mice (**Fig.** 16H).

Therefore, using AMG-487 (5 mg/kg orally, four times in a week for 3 months), a small molecule CXCR3 agonist or its veichle 20% hydroxypropyl-ß-cyclodextrin (HB-β-CD), we treated 3 months old *Pkhd1$^{del4/del4}$* and WT mice in order to hinder CXCR3 (**Fig.**17A). The results of the treatment indicated a significant reduction in *Pkhd1$^{del4/del4}$*mice disease progression. This is shown by the inflammatory infiltrate reduction (47% reduction in CD45-positive area) (**Fig.** 17B) in the K19-positive cysts amount (37% reduction in K19-positive area) (**Fig.** 17C), in deposition of pericystic collagen (53% reduction in Sirius red–positive area) (**Fig.** 17D), and in splenomegaly (35% reduction in the relative spleen weight), indicating a reduction in the portal hypertension. Next, we analyzed the AMG-487 effects on *Pkhd1$^{del4/del4}$* mice immune CD45^{+} cell subpopulation. From **Fig.**18, it is evident that in comparison to vehicle

treated mice, there was a 40% reduction in macrophage ($CD45^+CD11b^+F4/80^+$) infiltration amount, 50% reduction of T helper Cells ($CD45^+CD11b^-CD4^+$) due to inhibition of CXCL10/CXCR3 axis (**Fig**.18A). On the other hand, there was insignificant or no change in the $CD45^+$ immune subpopulations such as granulocytes ($CD45^+CD11b^+F4/80\text{-}Gr1^+$), natural killer cells ($CD45^+CD11bhi^-NK1.1^+$), CD8 cells ($CD45^+CD11b^-CD8^+$), and B cells ($CD45^+CD11b^-CD19^+$) levels upon the CXCR3 inhibition (**Fig**.18B).

Our published data show that M2 macrophages progressively increase in parallel with the development of peribiliary fibrosis and the establishment of portal hypertension in *Pkhd1*$^{del4/del4}$ mice. In the current study, we show a 60% reduction in the M2 subtype of macrophages ($CD45^+F4/80^+Erg2^+$) (**Fig.** 18D-E), as there is a slight increase in M1 ($CD45^+F4/80^+NOS2^+$) subtype (**Fig**.18C-E) upon inhibition of CXCR3. Consequently, the AMG-487 treatment led to an increase in M1/M2 ration, leading to a conclusion that there was a correlation in the decrease in M2 polarized macrophages and the reduced pericystic collagen deposition, which had been observed in the same mice (**Fig**.18F). Collectively, these data conclude that the CXCL10–CXCR3 axis is a key element in macrophages recruitment and therefore, in the progression of CHF/CD disease. Thus, we considered crucial a better understanding of the mechanisms that lead to the increase in CXCL10 secretion in cholangiocytes from *Pkhd1*$^{del4/del4}$ mice.

CXCL10 secretion is stimulated by β-catenin through promostion of the pSTAT3 nuclear translocation in FPC-defective cholangiocytes

The JAK/STAT pathway is known to regulate CXCL10 secretion. Consequently, using different STAT isoforms we tested the expression and the status of phosphorylation by use of FACS analysis of whole-liver cell extracts and in isolated wild-type and FPC-defective cholangiocytes.

Being STAT3 modulated by β-catenin at transcriptional levels, we decided to first evaluate this isoform. STAT3 activation is due to the phosphorylation of tyrosine residue 705 (pSTAT3-(Tyr705)). pSTAT3-(Tyr705) translocate into the nucleus and, upon binding to specific DNA sequences, start the transcription of several related downstream genes. To assess if this phosphorylation occurs in our models, we performed FACS-sorting for cholangiocyte populations isolated from the whole liver of

wild-type and *Pkhd1*$^{del4/del4}$ mice. We found a significant increase (> 20%) in the number of cholangiocytes (K19^{+} cells) bearing the phosphorylation at the tyrosine 705 in STAT3 (pSTAT3- (Tyr705)) in the liver of 3-month-old *Pkhd1*$^{del4/del4}$ compared to WT liver (**Fig**.19A-B).

Moreover, the increased expression of pSTAT3-(Tyr705) in the cystic epithelium in *Pkhd1*$^{del4/del4}$ mice was further confirmed by immunohistochemistry of mouse liver specimens (**Fig**.19G-H). Primary cystic cholangiocytes isolated from WT and *Pkhd1*$^{del4/del4}$ mice were cultured as monolayer and pSTAT3-(Tyr705) levels were evaluated by immunofluorescence and FACS analysis. Increased pSTAT3-(Tyr705) levels were observed with in FPC-defective cholangiocytes compared to WT cells with both the techniques (**Fig**.19C-D).

The involvement of JAK/STAT3 pathways in the secretion of CXCL10, was confirmed by the treatment with JAK inhibitor (pan-JAK inhibitor, 10 μM) or a STAT3 inhibitor (Static V, 10 μM) in cultured monolayer cholangiocytes for 24 hours. At the end of the treatment, gene expression and secretion of CXCL10 were analyzed by RT-qPCR or ELISA assay, respectively. Both JAK and STAT3 inhibition were able to significantly decrease CXCL10 gene expression and secretion from FPC-cholangiocytes (**Fig**.19E-F). In particular, we observed that CXCL10 gene and secretion decreased by ~50% when treated with the STAT3 inhibitor (**Fig**.19E-F), while JAK inhibitor resulted in an ~80% of reduction at gene level and ~40% of secretion in FPC-defective cholangiocytes compared to untreated cells. Of note, CXCL10 was inhibited only by JAK inhibitor and only at the gene level in WT cells (**Fig**.19E).

We have clearly illustrated that the FPC-defective cholangiocytes response to β-Catenin (ICG-001 or Quercetin) inhibition correlate with a reduction in CXCL10 production. To further confirm the β-catenin-dependent CXCL10 production, we knockdown endogenous β-catenin by using specific siRNA in WT and FPC-defective cholangiocytes. β-catenin was downregulated by 60% at the mRNA level and by 65% at the protein level 48 hours post-transfection (**Fig**.20A-B). In this instance, β-catenin silencing induces a significant reduction of CXCL10 both at the mRNA level (80% reduction) (**Fig**.20C) and at secreted protein level (50% reduction) in FPC-defective cholangiocytes (**Fig**.20D).

Being phosphorylation of β-catenin at Ser675 dependent on cAMP/PKA signaling, we tested the effect of cAMP stimulation of PKA inhibition on CXCL10 expression and secretion. Our findings show that there was a CXCL10 gene expression and protein secrectio induction with increased cAMP levels, which were abolished with PKA inhibitor (**Fig**.20E, F). Notably, the dependency of the the cAMP/β-catenin on the CXCL10 production was only visible in FPC-defective cholangiocytes, as WT were not affected. Therefore, concluding that there is a direct relationship between the changes observed and the fibrocystin function.

Afterwards, we went further to determine if β-catenin downregulation affected STAT3 phosphorylation. The β-catenin depletion caused by siRNA showed that β-Catenin was required for pSTAT3-(Tyr705) nuclear translocation in FPC-defective cholangiocytes (**Fig**.21A). Similar results were obtained by treating cultured FPC-defective cholangiocytes with ICG-001, a β-catenin inhibitor (10 μM) (**Fig**.21B-C). However, these effects were only observed in FPC-defective cholangiocytes but not in WT cells (**Fig**.21B-C).

We have previously shown that Rac1 facilitates β-catenin nuclear translocation in FCP-defective cholangiocytes. To validate its involvement also in the nuclear translocation of pSTAT3-(Tyr705), we observed the direct effect of Rac1 inhibition on pSTAT3-(Tyr705) nuclear translocation. Western blot analysis showed that inhibition of Rac1 significantly reduced the levels of pSTAT3-(Tyr705) in the nucleus of FPC-defective cholangiocytes (**Fig**.21D).

These latter findings suggested to us that β-catenin and STAT3 physically interact. To address this hypothesis, we used an *in situ* proximity ligation assay (PLA) which allows the detection of two protein of interest when in close proximity (< 40nm) by generating a fluorescent dot. The quantification of the generated dots indicates an interaction between β-catenin and STAT3 in FPC-defective cells, while the formation of the complex results absents in WT cells (**Fig**.21E).

These results are in agreement with our previous finding showing that Rac1 facilitated β-Catenin nuclear translocation in FPC– cholangiocytes and with other studies showing that Rac1 is required for STAT3 nuclear translocation. Collectively our data indicate that STAT3 and β-Catenin bind together as a complex and that Rac1 facilitate its nuclear translocation. Notably, we found out that, among the STATs, only

STAT3 dependent on β-Catenin in our models. For instance, during β-catenin knockdown, there was no decrease in the pSTAT1-(Tyr701) levels compared to untreated FPC-defective cells (**Fig**.22A, B). Furthermore, the inhibition of STAT1 and STAT5 upon IL-1β stimulation do no decrease Cxcl10 gene expression in FPC-defective cholangiocytes (**Fig**.22C).

Increase in IL-1β stimulates secretion of CXCL10 through STAT3 in FPC-defective cholangiocytes.

Together with an increased gene expression of *Cxcl10*, we previously reported an increased expression of IL-1β in biliary K19-positive structures isolated from 3-month-old *Pkhd1*$^{del4/del4}$ mice by laser capture microdissection (LCM). Since it is known that pro- IL-1β may further induce the expression and secretion of CXCL10, we studied if this was indeed the case in our models. We found that in cholangiocytes (sorted with FACS as EpCAM^{+}- positive fraction) isolated from *Pkhd1*$^{del4/del4}$ *mice* at one month of age, the gene expression of pro-IL-1β was significantly increased (**Fig**. 23A) compared to cholangiocytes isolated from WT mice at the same age. On the other hand, we found that levels of *Cxcl10* gene expression were not significantly different between *Pkhd1*$^{del4/del4}$ cholangiocytes and WT cholangiocytes isolated at one month of age (**Fig**.23B). These findings were further confirmed by immunofluorescence of liver specimens of wild-type and *Pkhd1*$^{del4/del4}$ mice. We found that IL-1β colocalizes with K19^{+} cystic cholangiocytes in 1-month-old *Pkhd1*$^{del4/del4}$mice but not in WT mice at the same age (**Fig**.23C). CXCL10 expression was not detected in K19^{+} cells in 1-month-old WT and *Pkhd1*$^{del4/del4}$ mice (**Fig**.23D), but CXCL10 colocalizes with IL-1β only in cysts cholangiocytes in 3-month-old *Pkhd1*$^{del4/del4}$mice (**Fig**.23E).

To test the hypothesis that IL-1β modulates CXCL10 production in FPC-defective cholangiocytes, we first analyzed the expression and secretion of IL-1β in cultured monolayer cholangiocytes. We observed that both pro-IL-1β mRNA levels and IL-1β secreted in media culture were significantly increased (**Fig**.24A-B). Interestingly, the secretion of IL-1β by isolated FPC-defective cells indicates that this is a cell-autonomous phenomenon, possibly a consequence of defective fibrocystin. Furthermore, treatment of WT and FCP-defective cholangiocytes with IL-1β (5ng/mL)

for 24hours, resulted in a 16-fold increase in CXCL10 gene expression and 2-fold increase of CXCL10 secretion in FPC-defective cholangiocytes but not in WT cells (**Fig**.24C-D).

To study if IL-1β induces CXCL10 secretion in FPC-defective cholangiocytes through STATs, we treated cells with IL-1β alone or in combination with STAT3 inhibitor for 24 hours. From our results, it was noted that STAT3 (10 μM, Static-V) inhibition, led to a 90% decrease and a 40% reduction of IL-1β-induced CXCL10 expression at the gene level and at the protein level, respectively (**Fig**.24C, D). Further, the treatment with IL-1β alone led to an increase in pSTAT3-Tyr705 in FPC-defective cholangiocytes (**Fig**.24E), while there was a significant reduction of pSTAT3-Tyr705 (**Fig**.24F) when cells were treated with IL-1β and JAK inhibitor (JAK/Tyk2 inhibitor). Collectively, these data indicate that, through JAK/pSTAT3 pathway activation and nuclear translocation mediation, IL-1β and β-Catenin work together to increase production of CXCL10.

NF-kβ-mediated NLRP3 Inflammasome activation controls expression of pro-IL-1β and secrection of IL-1β in Pkhd1$^{del4/del4}$ mice.

IL-1β is produced at an inactive state, pro-IL-1β; therefore, to be active a specific enzymatic cleavage is needed. We tested the upregulation of the main factors involved in IL-1β gene expression (NF-kB) and protein secretion (inflammasome) in FPC-defective cholangiocytes.

NF-kB transcription factor family consists of 5 proteins that differentially associate when transcriptionally active. The most abundant of the NF-kB transcription factor family is the p50/p65 heterodimer. Phosphorylation of p65 at site Ser276 and Ser536 further enhance the binding NF-kB to DNA and its transcriptional activity. We tested the p65 phosphorylation status by western blot of the nuclear fraction of WT and FPC-defective cholangiocytes.

We found a significant higher phosphorylation at Ser276 and ser536 residues of p65 in FPC-defective cholangiocytes compared to WT cells (**Fig**.25A). This result correlate with an higher NF-kB transcriptional activity measured in FPC-defective cells compared to WT cells (**Fig**.25B). Furthermore, we found that NF-kB inhibition lead to 60% of IL-1β gene expression reduction (**Fig**.25C) and 50% reduction of its secretion

(**Fig**.25D) in FPC-defective cholangiocytes. Interestingly, the increased NF-kB transcriptional activity in isolated cholangiocytes was β-catenin/STAT3-dependent, as shown by the 50% reduction in NF-kB transcriptional activity caused by β-catenin silencing (**Fig**.25E) or the 80% reduction upon STAT3 inhibition (**Fig**.25F) in FPC-defective cholangiocytes. Collectively, from the data, we can draw a conclusion that CXCL10 production regulation is managed by β-catenin, which act on the nuclear import of pSTAT3-(Tyr705) and by increasing IL-1β gene expression through NF-kB activation. Since bioactivation of IL-1β require the proteolytical cleavage by the activated caspase-1 (p10) and expression of Nlrp3 (**Fig**.26A), we measured cleaved caspase-1 by Western Blot and Nlrp3 expression, as readout of inflammasome activation, in WT and FPC-defective cholangiocytes. In comparison to WT cholangiocytes, we described an increase in 2 fold and 4 fold in cleaved caspase-1 protein levels (**Fig**.26B) and in Nlrp3 gene expression (**Fig**.26C) in FPC-defective cholangiocytes. In addition to this, there was a significant decrease (40% reduction) in IL-1β secretion in FPC-defective unlike in WT, cholangiocytes (**Fig**.26D) caused by MCC950 (10 μM), an inhibitor of the NLRP3 inflammasome. In conclusion, these data indicate that increased bioactive IL-1β results from either NF-kB and the NLRP3 inflammasome activation in FPC-defective cholangiocytes.

DISCUSSION

It is noted that congenital hepatic fibrosis (CHF) as well as Caroli disease (CD) are recognized as genetic cholangiopathies provoked by mutations in PKHD1 gene[44]. In turn, PKHD1 is viewed as the gene that is encoded for fibrocystin, a protein with indistinctive biological role yet the one produced within cilia and biliary epithelial cells' centromeres[131]. Fibrocystin (FPC) is involved in a variety of cell functions, such as proliferation, tubulogenesis, and cell–matrix interactions, but its precise cellular function remains unknown[132]. CHF and CD are characterized by biliary dysgenesis, segmental ductal dilations, and progressive portal fibrosis with portal hypertension, which eventually leads to liver decompensation and death[44]. Investigating the parameters and patterns associated with this interrelation should assist in designing and practicing innovative therapeutic approaches for portal fibrosis, which is a key factor of illness development in most cholangiopathy cases.

Relying on the *Pkhd1*$^{del4/del4}$ mouse known as an orthologous sample of CHF/CD, it was identified that cystic cholangiocytes in an isolated form tend to generate a set of cytokines, including IL-1β, along with some chemokines, such as MCP-1, CXCL1, CXCL5, CXCL10, and CXCL12, which role is the concentration and replenishment of inflammatory cells. In most cases, it represents a group of M1 macrophages, which, in turn, progressively transform into M2 macrophages phenotype[142]. Such transformation is attributed to raised TGF-β secretion as well as other factors of growth (TNFα, for instance) that stimulate recruitment of collagen-manufacturing cells in addition to deposition of extracellular matrix[40, 155, 156]. In fact, the replacement of paracrine factors could cause an impact on cross-interaction between cholangiocytes and inflammatory/mesenchymal cells, which provoke the disease's ongoing development. Understanding these vital patterns should bring a clearer awareness about the molecular mechanisms that might tie epithelial dysfunction to the inflammation process and eventual form of fibrosis. It was our decision to stay focused on CXCL10, since its proinflammatory and profibrotic function in progressing liver illness is well identified[152, 154, 157].

In order to clarify whether CXCL10 contributes to disease progression *in vivo,* we inhibited the CXCR3–CXCL10 axis (AMG-487); and assessed its role in blocking

macrophage recruitment. Inhibition of CXCR3 *in vivo* reduced the infiltration with CD45+ immune cells and collagen deposition, and modified the M1/M2 ratio by reducing the amount of M2 macrophages. This resulted in a reduction of the progression of the disease. Importantly to note, other CXCR3 ligands, specifically identified as CXCL9 and CXCL11, were not found active in terms of upregulation in liver tests relating to *Pkhd1*$^{del4/del4}$ mice. To be specific, CXCR3 inhibition caused a general decrease of all macrophages (F4/80-low/CD11-high infiltrating macrophages) in addition to common reduction of pro-inflammatory T-cells, improving the mechanisms of decreasing inflammatory cells' sample instead of influencing the macrophages (M2) only. Moreover, the inhibition of fibrosis and inflammation was concomitant with a significant reduction in splenomegaly (index of portal hypertension) and in liver cysts, which is in accordance with the reduction of disease progression as described upon clodronate-induced macrophage depletion[142].

By identifying an important pathogenetic role of CXCL10 in CHF, it was decided to explore the pattern of managing its manufacturing by cholangiocytes. We have shown that CXCL10 generation was dependent on β-catenin in FPC identified and marked as defective cholangiocytes. Indeed, both gene expression and secretion of CXCL10 were diminished by two different inhibitors of β-catenin transcriptional activity (quercetin and ICG-001)[142]. Downregulation of endogenous β-catenin confirmed the specific relevance of β-catenin, signaling, mediating inflammation by siRNA. It was identified that the so-called downregulation of β-catenin led to a decrease of CXCL10 gene manifestation. This pattern was marked for FPC cells identified as defective, since no vivid transformations in CXCL10 secretion were determined within silent and non-active β-catenin WT cells. In addition, manifestation and secretion of CXCL10 gene was eliminated under PKA inhibition (PKI) in defective FPC cells. In the past, the cAMP/PKA pathway was responsible for activating β-catenin within FPC cholangiocytes[143]. In this sense, there is a big likelihood that the cAMP's impact on CXCL10 is achieved through interaction with β-catenin.

Knowledge of the molecular mechanism through which β-catenin mediates CXCL10 production may lead to the identification of possible targets for therapy.

Control of CXCL10 production has been demonstrated to be under the signal transducers and activators of the transcription (STATs) family[158]. Among the

different STATs we tested (STAT1, STAT3, and STAT5), only increased tyrosine 705 phosphorylation of STAT3 (pSTAT3-Tyr705) in nuclear fraction of FPC-defective cells, as compared to WT cells. Activation of the STAT3 signaling pathway is primarily mediated by (pSTAT3-Tyr705), which induces dimerization, nuclear translocation, and thereby activates transcription.

Interestingly, downregulation or inhibition of β-catenin signaling blocked pSTAT3-Tyr705 nuclear translocation in FPC-defective cells, without affecting the protein levels of total STAT3. These findings suggest the involvement of β-catenin in mediating nuclear translocation of pSTAT3-Tyr705, an event apparently specific for FPC-defective cells.

It is noteworthy that the reduction of nuclear pSTAT3-Tyr705 levels was also observed upon Rac1 inhibition in FPC-defective cells. Its physical interaction with STAT3 confirmed the role of β-catenin in mediating CXCL10 secretion via modulation of pSTAT3-Tyr705. The outcomes achieved are formally in compliance with our former results indicating that Rac1 contributed to nuclear translocation of β-catenin in FPC-defective cholangiocytes. The outcomes have also been found consistent with findings from other researches, clarifying that Rac1 was necessary for initiating the nuclear translocation of STAT3[159]. A potential explanation of these findings is that β-catenin and STAT3 are structurally bound, meaning that Rac1 stimulates the nuclear translocation of this complex.

Regulation of CXCL10 secretion through IL-1β has been successfully identified in a few cell types, including neural progenitor cells, human astrocytes, interstitial epithelial cells, rat islets and β cell lines[160-162]. The result proposed in this work sheds light on the role played by IL-1β in mediating CXCL10 production in FPC-defective cholangiocytes. It was detected that CXCL10 secretion mediated by IL-1β in defective FPC cholangiocytes is eliminated if JAK and STAT3 inhibition takes place. Moreover, it was noted that IL-1β instantly produced phosphorylation of STAT3 at Tyr705, which was identified as a crucial step for STAT3' transcriptional activation[163]. There are convincing findings that reinforce the study's conclusion: both IL-1β and β-catenin manage STAT3 activity and thus regulate CXCL10 production through processes of phosphorylation and nuclear translocation [162].

IL-1β is produced as an inactive precursor, named pro- IL-1β, that requires bioactivation to be secreted[164]. This is a two-step process involving first an NF-kB-mediated priming signal and a subsequent activation of an NLRP3 inflammasome. Briefly, activated NF-kB induces the transcription and translation of NLPR3 and pro-IL-1β. Activation of the NLRP3 inflammasome is mandatory to the proteolytic cleavage of pro- IL-1β into its mature secreted form. ATP, uric acid, palmitic acid, cholesterol crystals, free fatty acids, glucose, reactive oxygen species, mitochondrial stress, K^+ and Ca^{2+} cell content, ER stress, as well as bacterial-obtained products are typical signals activating and initiating the NLRP3 inflammasome, provoking liver disease[165, 166]. 'Signal 1' is a collective term for all these signals.

Importantly, increased response of NF-kB and hence upregulation of pro-IL-1β gene manifestation have been identified in FPC cholangiocytes marked defective. In particular, intensified numbers of phosphorylation at Ser276 and Ser536 within the p65-NF-kB subunit were detected in defective FPC cholangiocytes in contrast to WT cells. Phosphorylation at Ser276 can be mediated by the catalytic subunit of PKA and results in a conformational shift that allows p300/CREB-binding protein (CBP) to bind with HDCA complexes. Thus, pSer276 enhances the DNA-binding activity of p65[26]. However, phosphorylated Ser536 induces the binding of NF-kB on TATA-binding protein-associated factor II31, a component of transcription factor II D (TFIID)[167]. Phosphorylation of the p65-NF-kB subunit induces conformational change, impacting p65 ubiquitination and protein–protein interaction to result in enhanced transcriptional activity of NF-kB[168].

Some research projects have identified that signaling pathways associated with NF-kB and β-Catenin mutually manage each other via diverse microbiological mechanisms and within quite separate cells, with no exclusion of epithelial cells[149, 169]. Thus, the launch of NF-kB from β-Catenin was recognized as mediation provoked either by the availability of IL-1β, causing a transcriptional interaction between NF-kB and β-Catenin[170], or by the decline of E-cadherin, resulting into accumulation and absorption of cytoplasmic β-catenin, which initiated the response of p38-mediated NF-kB[171]. Defective FPC cholangiocytes were formerly identified with lower E-cadherin manifestation, which implies that an interaction between signal pathways of NF-kB and β-catenin takes place. Moreover, some scientific sources reported about a direct and extra correlation of NF-kB with STAT3. In short, the C-terminal of STAT3 might take a role of a trans-activator, selecting co-activator

CBP/p300. This interplay causes STAT3 acetylation with further nuclear translocation and gene transcription. It also might be heavily responsible for keeping NF-kB within the nucleus[163, 172]. In this perspective, the decline of FPC triggers β-Catenin to manage NF-kB functionality via pSTAT3-Tyr705. It was identified that inhibition of STAT3 reduces the activity of NF-kB.

Being a part of multimeric protein groups recognized as inflammasomes, the intracellular cysteine protease caspase-1 is found as a critically vital protease for bioactivation of IL-1β. When microbial and damage-associated signals (DAMP) are somehow stimulated, inflammasomes are gathering together from self-scaffold proteins through interaction with NATCH domain to eventually extract a primary host defense by cytokines' proteolytic maturation (for example, IL-1β). LRP3 is capable of forming an inflammasome, a macromolecular complex that directs activation of the IL-1-converting enzyme caspase-1, resulting in cleavage and secretion of the proinflammatory mediator IL-1β[173]. The reinforced secretion of active IL-1β by defective FPC cholangiocytes *in vivo* and *in vitro* has clarified that the NLRP3 inflammasome is directly stimulated in our cells, which is proven by and associated with increased manifestation of NLRP3 and procaspase 1.

Active IL-1β secretion in epithelial cells is of high significance because it leads to a self-perturbating loop that sustains inflammatory responses[174]. This phenomenon is the basis of autoinflammatory conditions, caused by either mutation in NLRP3, resulting in unbalanced production of IL-1β and regulatory cytokines, or by deficiency of the interleukin-1-receptor antagonist (DIRA)[175]. IL-1β acts as the major driver and can cause both systemic and organ-specific immune-mediated pathologies. There are evidence reporting that activated aberrant inflammasome is related to liver disease, being linked to factors of liver damage, steatosis, degrees of inflammation, and fibrosis. With reference to diverse cell types where the pattern has been manifested, IL-1β is found to be a mediator of the release of chemokines, cytokines, inflammatory mediators (such as TNF-α), CXCL10, IL-8, inducible nitric oxide synthase, COX-2, prostaglandin E2, nitric oxide, and type 2 phospholipase A[174]. Importantly to indicate, even in low concentrations (2–10 pg/ml)[176], IL-1β can stay active, which implies that early generation in the first stages of the disease development might essentially contribute (directly or indirectly) to production of macrophages via the manufacturing of other chemoattractants, including CXCL10.

All the experimental studies encourage us to clarify a unique case for CXCL10 management in defective FPC cholangiocytes. Several premises of this case can be mentioned: a) CXCL10 generated is regulated by the JAK/STAT3, IL-1β, and β-Catenin pathways; b) β-Catenin triggers pSTAT3-Tyr705 nuclear translocation, while IL-1β functionally stimulates phosphorylation of JAK/STAT3; and c) pro-IL-1β is mediated by NF-kB stimulation dependent on β-Catenin, while intense activity of NLRP3 inflammasome mediates the manufacturing of IL-1β. As a result, the pathophysiological significance of this pathway has been proven in vivo by blockage and isolation of CXCR3, which is known as the receptor of CXCL10. Working model of the mechanism leading to biliary fibrosis in CHF/CD is summarized in **Fig.**27. Therapeutic intervention in relation to CXCR3 delays progression of the disease in the FPC-defective model of CHF/CD by decreasing the infiltration of macrophages, as well as reduction of collagen deposition and cyst expansion.

The outcomes of the study emphasize the status of CHF as an autoinflammatory diseases, proposing new clinical and therapeutic approaches to treatment.

FIGURES

Figure 14. Molecular mechanism of Wnt activation

(1) In absence of Wnt ligant, the canonical Wnt signalling is not active (Wnt off). In this state, β-catenin is located in adherent junctions and cytoplasm of the cell, where it becomes phosphorylated by the destruction complex and undergo to ubiquitination and proteasomal degradation. (2) Canonical Wnt signalling is active in the presence of Wnt ligands (Wnt on), which bind to the FZD–LRP5/LRP6 co-receptor. Phosphorylation of LRP6 induces the recruitment of Axin and Dishevelled (DVL), which blocks Axin-mediated phosphorylation of β-catenin and thereby prevents β-catenin degradation, enabling its accumulation and nuclear translocation. In the nucleus, β-catenin binds to diverse co-effectors, mainly to the TCF/LEF transcription factor, regulating the expression of genes involved in different cellular processes. *(Modified from Perugorria MJ., et al. Nature Review Gastroenterology and Hepatology, 2019)*

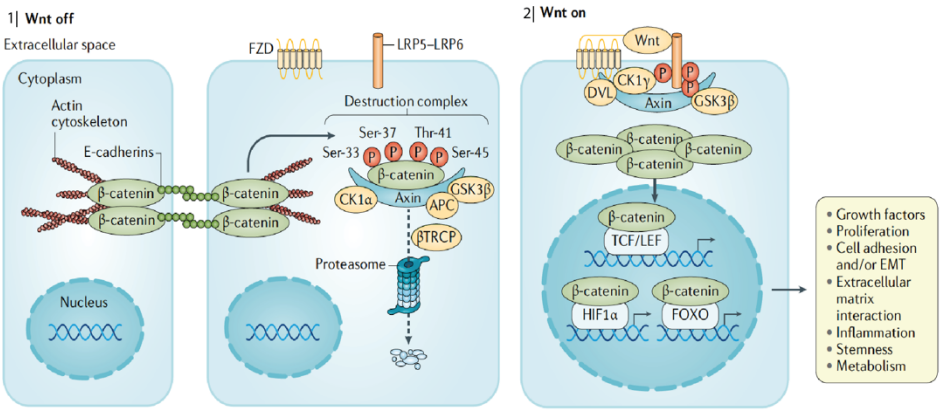
1| Wnt off
Extracellular space
Cytoplasm
Actin cytoskeleton
E-cadherins
β-catenin
β-catenin
β-catenin
β-catenin
Nucleus
FZD
LRP5–LRP6
Destruction complex
Ser-37
Thr-41
Ser-33
Ser-45
β-catenin
CK1α
Axin
APC
GSK3β
βTRCP
Proteasome
2| Wnt on
Wnt
CK1γ
DVL
Axin
GSK3β
β-catenin
β-catenin
β-catenin
β-catenin
TCF/LEF
β-catenin
β-catenin
HIF1α
FOXO
• Growth factors
• Proliferation
• Cell adhesion and/or EMT
• Extracellular matrix interaction
• Inflammation
• Stemness
• Metabolism

FIGURE 14

Figure 15. Summary of previously published observations generated FPC-defective cholangiocytes

In *Pkhd1*$^{del4/del4}$ mice, portal fibrosis is the result of intensive crosstalk between epithelial and inflammatory cells, originating from FPC-deficient cholangiocytes. Overactivation of β-catenin signaling in *Pkhd1*$^{del4/del4}$ cholangiocytes induces the secretion of a range of chemokines, including CXCL1, CXCL10, and CXCL12 (purple arrow and dots) and the recruitment of macrophages in the portal area. In the early phases, this portal infiltrate is mainly composed of M1 macrophages (yellow peribiliary cells), and TNF-α (yellow arrow) is the predominant cytokine released until also TGFβ1 (orange arrow) becomes significantly secreted by M2 macrophages (orange peribiliary cells). Both macrophage-derived cytokines up-regulate avβ6 integrin expression on biliary cysts and this, in turn, activates latent TGFβ1. Once activated, TGFβ1 induces production of collagen by cyst cholangiocytes and, as the disease progresses, by myofibroblasts, ultimately resulting in excessive matrix deposition into the peribiliary region. *(Modified from Locatelli L. et al., Hepatology, 2016)*

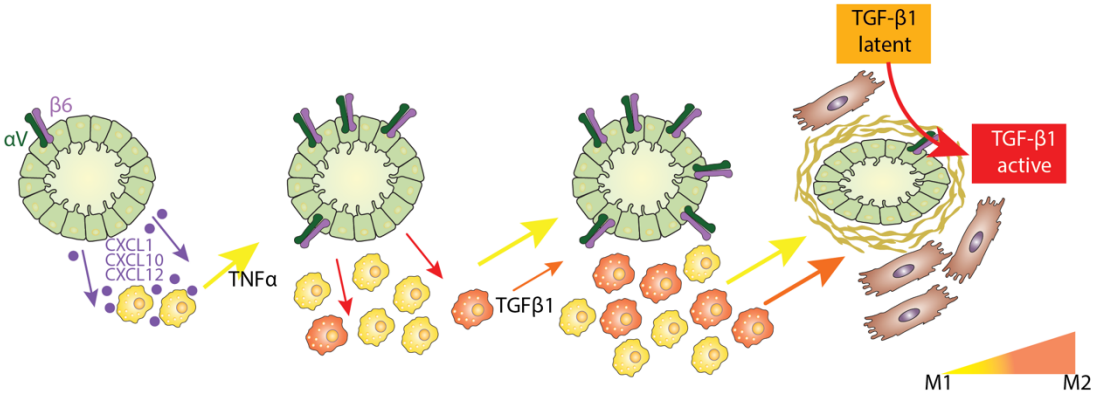
β6
αV
CXCL1
CXCL10
CXCL12
TNFα
TGFβ1
TGF-β1
latent
TGF-β1
active
M1
M2

FIGURE 15

Figure 16. Analysis of cytokine expression in the liver of WT and *Pkhd1*$^{del4/del4}$ mice.

(A-C) CXCL9, CXCL10 and CXCL11 gene expression was quantified in WT and *Pkhd1*$^{del4/del4}$ mice liver samples (WT, n=5 and *Pkhd1*$^{del4/del4}$, n=5). Changes in CXCL9 (A) and CXCL11 (B) gene expression levels were not significantly different in *Pkhd1*$^{del4/del4}$ livers compared with WT. (C) Significant upregulation of CXCL10 expression was instead observed in *Pkhd1*$^{del4/del4}$ liver (*p<.05 *Pkhd1*$^{del4/del4}$ vs WT). (D-H) Representative scatter plots of fluorescence-activated cell sorting (FACS) analysis and relative quantification (%) showed a significant increase in CXCR3 expression in Fibroblast (Collagen1+) (D), Macrophages (F4/80+) (F) and Cholangiocytes (K19+) (H) of *Pkhd1*$^{del4/del4}$ mouse liver samples compared to WT mouse liver sample (WT, n=5 and *Pkhd1*$^{del4/del4}$, n=5) (*p<.05 *Pkhd1*$^{del4/del4}$ vs WT). The results are presented as mean ± SEM.

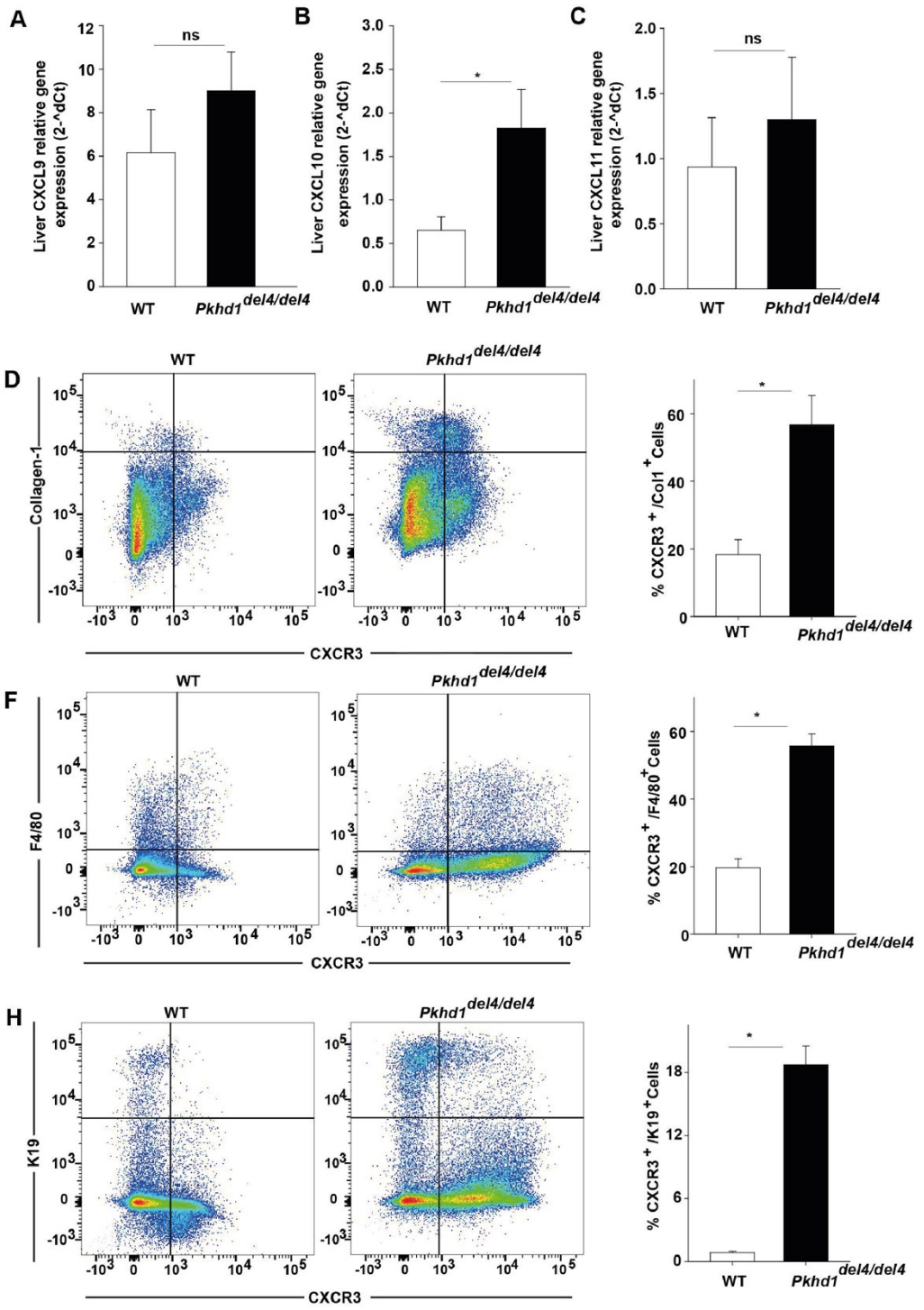
A
Liver CXCL9 relative gene expression (2-^dCt)
ns
WT
Pkhd1del4/del4
B
Liver CXCL10 relative gene expression (2-^dCt)
*
C
Liver CXCL11 relative gene expression (2-^dCt)
ns
D
Collagen-1
CXCR3
% CXCR3+/Col1+Cells
F
F4/80
% CXCR3+/F4/80+Cells
H
K19
% CXCR3+/K19+Cells

FIGURE 16

Figure 17. CXCR3 blockage slowed disease progression in *Pkhd1*$^{del4/del4}$ mice.
(A) Hematoxylin and eosin (H&E) of the AMG-487-treated and vehicle-treated mice (magnification x40). *Pkhd1*$^{del4/del4}$ + vehicle-treatment, n=13 and *Pkhd1*$^{del4/del4}$ + AMG-487-treatment, n=13. AMG-487-treated mice show reduction in (B) the infiltration of immune cells (CD45^{+}) as assessed by immunohistochemistry for CD45 and their respective quantification (magnification x200), (C) the K19-positive area as assessed by immunohistochemistry for K19 and its respective quantification (magnification x100), (D) collagen deposition as assessed by sirius red staining and its respective quantification (magnification x100), CD45-positive, K19-positive, and sirius red–positive areas were quantified with image J by measuring 10 independent fields per liver specimen (*p<.05 *Pkhd1*$^{del4/del4}$ + AMG-487 vs *Pkhd1*$^{del4/del4}$ + vehicle mice).

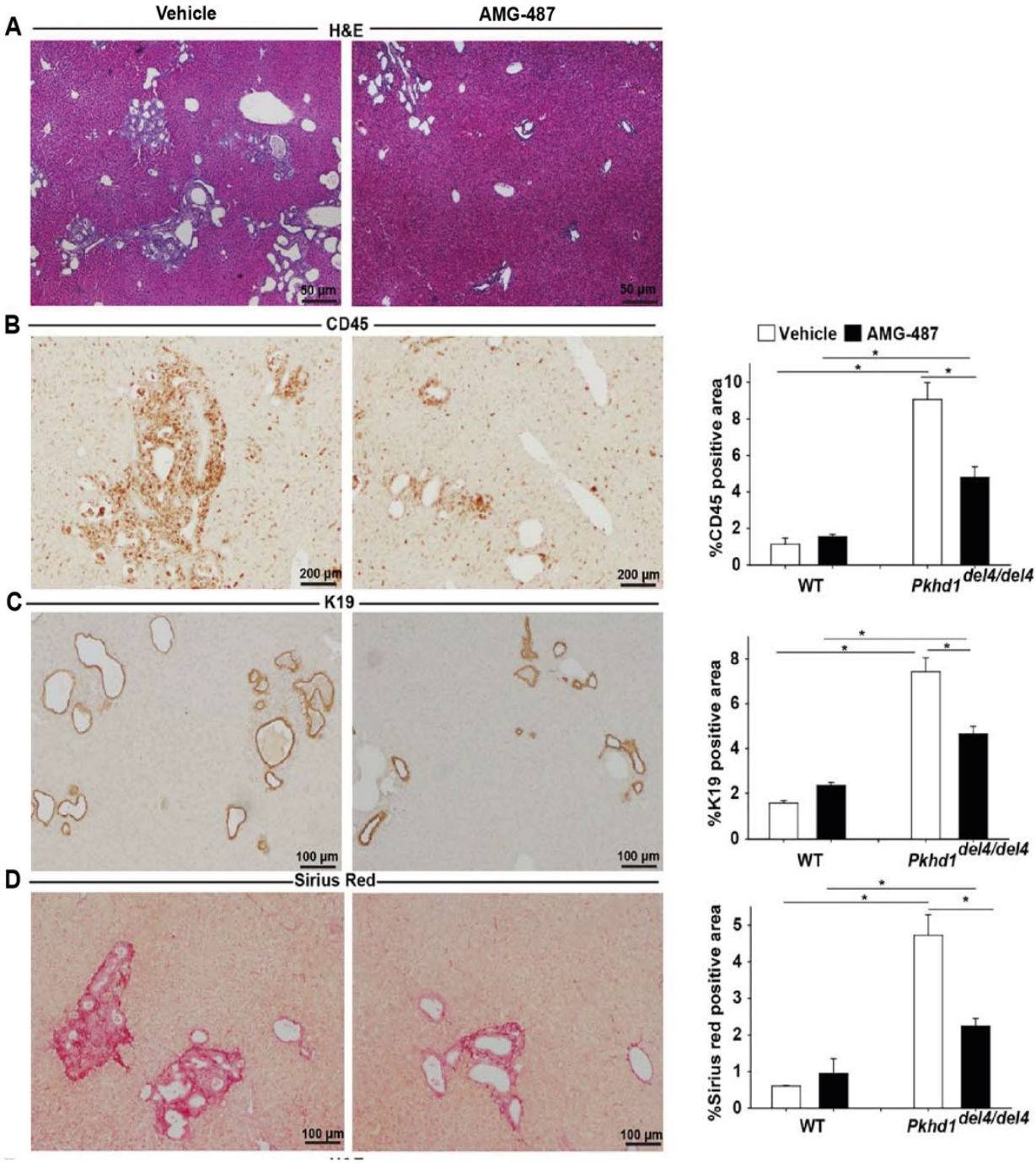
A
Vehicle
AMG-487
H&E
50 μm
50 μm
B
CD45
200 μm
200 μm
C
K19
100 μm
100 μm
D
Sirius Red
100 μm
100 μm
Vehicle
AMG-487
%CD45 positive area
0
2
4
6
8
10
WT
Pkhd1 del4/del4
%K19 positive area
0
2
4
6
8
WT
Pkhd1 del4/del4
%Sirius red positive area
0
1
2
3
4
5
WT
Pkhd1 del4/del4

FIGURE 17

Figure 18. CXCR3 blockage reduced macrophages and T helper cell ($CD4^+$) recruitment in *Pkhd1*$^{del4/del4}$ mice.

(A) Representative scatter plots of fluorescence-activated cell sorting (FACS) analysis of the $CD45^+$ immune cell population in *Pkhd1*$^{del4/del4}$ mice treated with vehicle (top) or AMG-487 (bottom). The y-axis represents forward scatter (FSC-A), where an increased signal can indicate increased cell size. The x-axis indicates CD45 marker, which was used to select subpopulation of inflammatory cells. $F4/80^+$ and CD11b positive staining was used to select the macrophage subpopulation and CD4 was used to identify T-cells in the previously gated CD45+ subpopulation. (B) Quantitative analysis of the percentage of subpopulation of CD45+ cells by FACS analysis ($p<.05$ *Pkhd1*$^{del4/del4}$ + AMG-487 vs *Pkhd1*$^{del4/del4}$ + vehicle mice) showed that macrophages and T-cells were reduced in *Pkhd1*$^{del4/del4}$ mice after treatment with AMG-487). (C,D) Identification of M1 ($F4/80^+$/$NOS2^+$) and M2 ($F4/80^+$/ $Erg2^+$) macrophages subpopulation. Representative scatter plots of flow cytometry staining of surface $F4/80^+$ and intracellular $NOS2^+$ (C) and $Erg2^+$ (D) in *Pkhd1*$^{del4/del4}$ mice treated with vehicle or AMG-487. (E) Quantitative analysis of the percentage of subpopulation of $F4/80^+$-positive cells showing the proportion of M1($NOS2^+$) or M2 ($Erg2^+$) phenotype in *Pkhd1*$^{del4/del4}$ mice treated with vehicle or AMG-487. *Pkhd1*$^{del4/del4}$ mice treated with AMG-487 showed no significant reduction in the M1($NOS2^+$) macrophage phenotype, whereas a significant reduction was observed in M2 ($Erg2^+$) macrophages. No differences have been found in vehicle-treated *Pkhd1*$^{del4/del4}$ mice. ($p<.05$ *Pkhd1*$^{del4/del4}$ + AMG-487 vs *Pkhd1*$^{del4/del4}$ + vehicle mice). (F) The M1/M2 macrophage ratio is increased in AMG-487-treated *Pkhd1*$^{del4/del4}$ mice compared to vehicle-treated *Pkhd1*$^{del4/del4}$ mice ($p<.05$ *Pkhd1*$^{del4/del4}$ + AMG-487 vs *Pkhd1*$^{del4/del4}$ + vehicle mice).

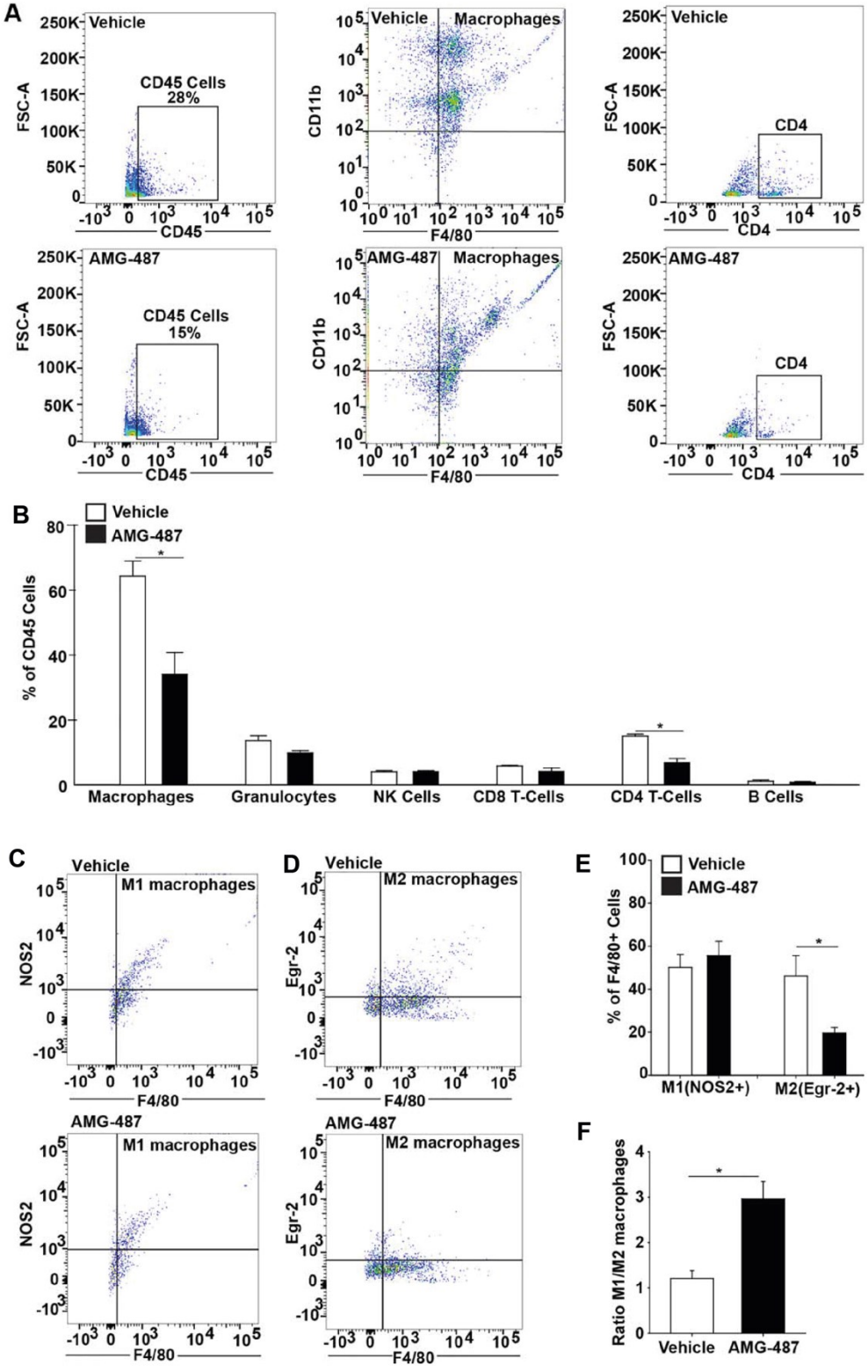
A
Vehicle
CD45 Cells
28%
FSC-A
CD45
Vehicle
Macrophages
CD11b
F4/80
Vehicle
CD4
FSC-A
CD4
AMG-487
CD45 Cells
15%
FSC-A
CD45
AMG-487
Macrophages
CD11b
F4/80
AMG-487
CD4
FSC-A
CD4
B
Vehicle
AMG-487
% of CD45 Cells
Macrophages
Granulocytes
NK Cells
CD8 T-Cells
CD4 T-Cells
B Cells
C
Vehicle
M1 macrophages
NOS2
F4/80
AMG-487
M1 macrophages
NOS2
F4/80
D
Vehicle
M2 macrophages
Egr-2
F4/80
AMG-487
M2 macrophages
Egr-2
F4/80
E
Vehicle
AMG-487
% of F4/80+ Cells
M1(NOS2+)
M2(Egr-2+)
F
Ratio M1/M2 macrophages
Vehicle
AMG-487

FIGURE 18

Figure 19. Increased phosphorylation of STAT3 at Tyr705 site is responsible for CXCL10 production in FPC-defective mice.

(A) Expression of pSTAT3(-Tyr705) in cholangiocytes from WT and *Pkhd1*$^{del4/del4}$ mice at 3-month-old was quantified by FACS analysis. FACS histograms of K19-positive cells (cholangiocytes) showed an increase in the expression of pSTAT3(-Tyr705) in the liver of 3-month-old *Pkhd1*$^{del4/del4}$ mice, compared to WT mice (*Pkhd1*$^{del4/del4}$ mice, n=3 and WT mice, n=3). (B) Quantitative analysis of the percentage of pSTAT3(-Tyr705) in K19-positive cells. ($p<.05$ *Pkhd1*$^{del4/del4}$ mice vs WT mice).

(C) Representative micrographs of immunofluorescence for pSTAT3(Tyr705) (red) in cholangiocytes isolated from WT and FPC-defective cholangiocytes (FPC^{-}). Nuclei were stained with DAPI (blue). pSTAT3(Tyr705) was expressed in the cytoplasm and the nucleus of FPC^{-} cholangiocytes but not in WT. (D) FACS histograms of K19-positive cells (cholangiocytes) show an increase in the expression of pSTAT3(-Tyr705) in FPC-defective cholangiocytes compared to WT cells. The number in the (+) fraction for pSTAT3 is the mean (SD) of the percentage of pSTAT3+ cholangiocytes. (E) In vitro treatment of WT and FPC-defective cholangiocytes with JAK or STAT3 inhibitor for 24 hours significantly reduced *Cxcl10* gene expression assessed by RT-PCR (WT, n=7 and FPC-, n=8; *$p<.05$ JAK-treated cells vs untreated cells, *$p<.05$ STAT3-treated FPC- cells vs untreated FPC-). (F) Quantification of CXCL10 secretion upon JAK or STAT3 inhibition in WT and FPC-defective cells. Significant reduction of CXCL10 secretion was observed only in FPC-defective cholangiocytes (*$p<.05$ FPC-treated vs untreated FPC cells). (G,H) IHC analysis of pSTAT3(Tyr705) in liver specimens from 3-months-old WT and *Pkhd1*$^{del4/del4}$ mice. Quantitative analysis of the number of positive pSTAT3(Tyr705) cysts in the whole lobe showed increased expression of pSTAT3(Tyr705) in FPC-defective cystic cholangiocytes.

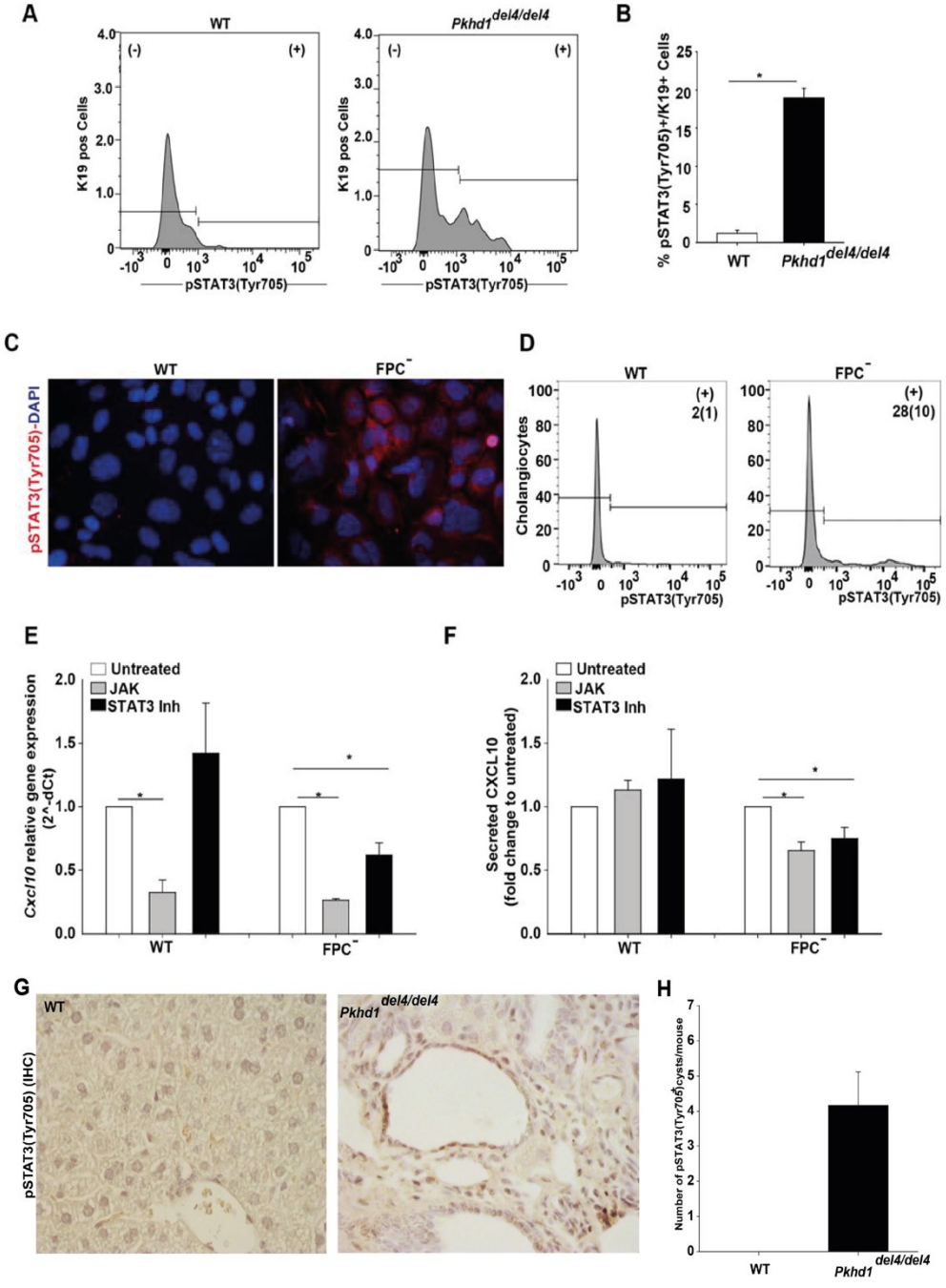
A
WT
Pkhd1 del4/del4
(-)
(+)
K19 pos Cells
pSTAT3(Tyr705)
B
% pSTAT3(Tyr705)+/K19+ Cells
WT
Pkhd1 del4/del4
C
WT
FPC-
pSTAT3(Tyr705)-DAPI
D
WT
FPC-
(+) 2(1)
(+) 28(10)
Cholangiocytes
pSTAT3(Tyr705)
E
Untreated
JAK
STAT3 Inh
Cxcl10 relative gene expression (2^-dCt)
WT
FPC-
F
Untreated
JAK
STAT3 Inh
Secreted CXCL10 (fold change to untreated)
WT
FPC-
G
WT
Pkhd1 del4/del4
pSTAT3(Tyr705) (IHC)
H
Number of pSTAT3(Tyr705) cysts/mouse
WT
Pkhd1 del4/del4

FIGURE 19

Figure 20. CXCL10 gene expression and secretion are β-catenin- and cAMP-dependent.

WT and FPC-defective cholangiocytes (FPC$^-$) were transfected with specific β-catenin siRNAs or with scrambled RNA (scrRNA) as negative control. RNA, protein, and supernatant were collected 48 hours post-transfection. Both β-catenin gene (A) and protein (B) expression was reduced in WT and FPC$^-$ cholangiocytes transfected with the β-catenin siRNA. (C) Cxcl10 gene expression was significantly reduced only in FPC$^-$ cholangiocytes silenced for β-catenin. (D) Similarly, secreted CXCL10 in cell supernatants were reduced only in FPC$^-$ cholangiocytes. (E-F) WT and FPC$^-$ cholangiocytes were treated with cAMP or PKA inhibitor for 24 hours. β-catenin gene expression and secretion were increased upon cAMP treatment and decreased upon inhibition with PKA inhibitor in FPC$^-$ cholangiocytes but not in WT cells (WT n=6 and FPC- n=6; *p<.05 treated FPC$^-$ cells vs untreated FPC- cells).

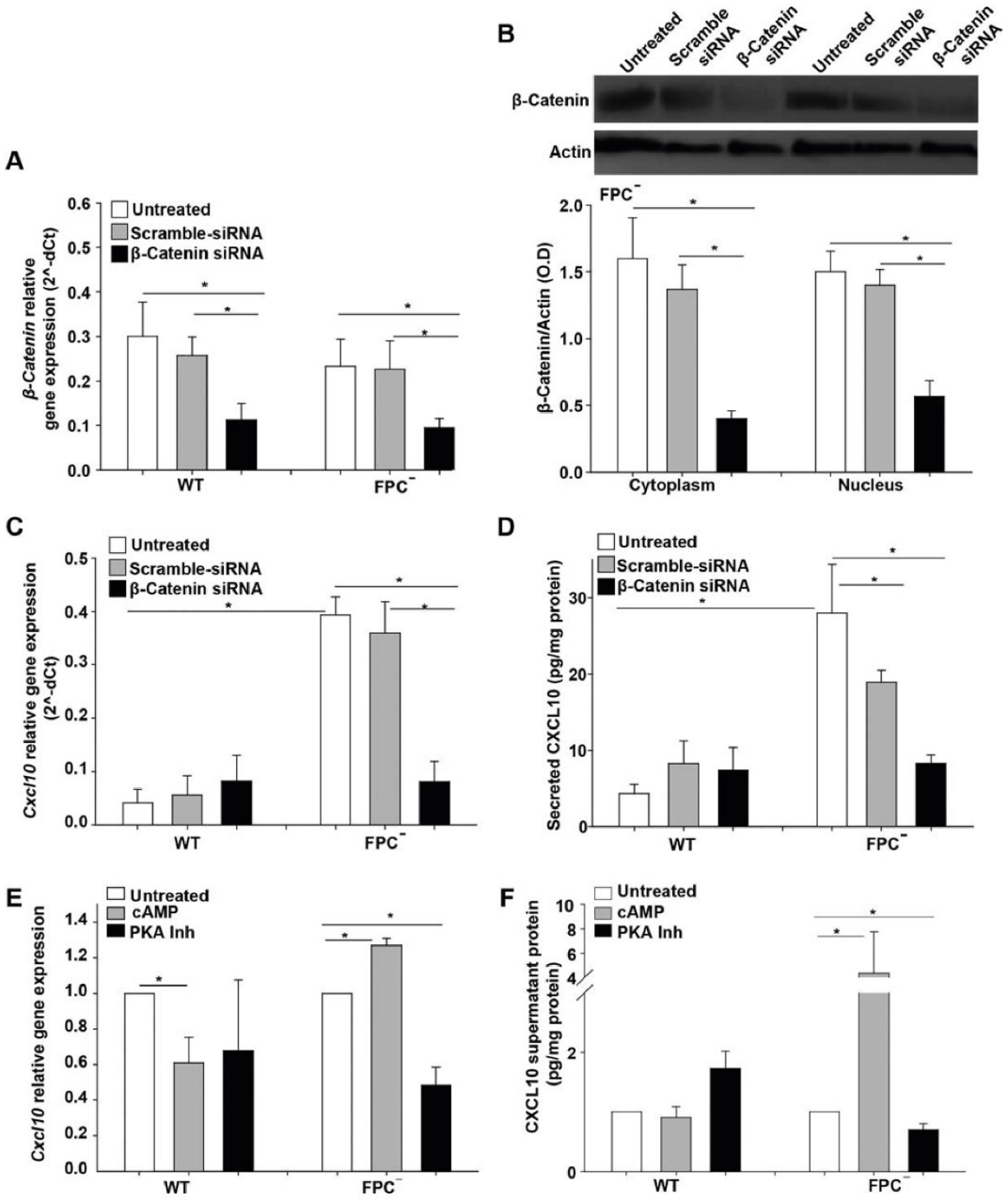
A
β-Catenin relative gene expression (2^-dCt)
Untreated
Scramble-siRNA
β-Catenin siRNA
WT
FPC⁻
B
Untreated
Scramble siRNA
β-Catenin siRNA
β-Catenin
Actin
β-Catenin/Actin (O.D)
Cytoplasm
Nucleus
C
Cxcl10 relative gene expression (2^-dCt)
D
Secreted CXCL10 (pg/mg protein)
E
Cxcl10 relative gene expression
cAMP
PKA Inh
F
CXCL10 supermatant protein (pg/mg protein)

FIGURE 20

Figure 21. β-catenin silencing or inhibition blocked pSTAT3(Tyr705) nuclear translocation in FPC-defective cholangiocytes.

(A) Western blot analysis for pSTAT3(Tyr705) and STAT3 in nuclear and cytoplasmic extracts of FPC-defective cholangiocytes (FPC-). Actin was used as a loading control, lamin B was used as nuclear fraction control and pyruvate kinase muscle (PKM) as cytoplasm fraction. The relative quantification showed a reduction in nuclear pSTAT3(Tyr705) protein expression upon β-Catenin silencing (n=5, p<.05 siRNA β-catenin vs control cells). (B) Western blot analysis for pSTAT3(Tyr705) and STAT3 in nuclear and cytoplasmic extracts of WT and FPC$^-$ cholangiocytes upon β-catenin inhibition with (ICG-001). The relative quantification show a reduction in nuclear pSTAT3(Tyr705) in FPC$^-$ cholangiocytes upon β-Catenin silencing (n=5, *p<.05 siRNA β-catenin vs control cells). (C) Representative micrographs for pSTAT3(Tyr705) (red) in WT and FPC$^-$ cholangiocytes treated for 1 hour with β-Catenin inhibitor (ICG-001). Nuclei were stained with DAPI (blue). Decreased nuclear pSTAT3(Tyr705) expression is observed in FPC-defective cholangiocytes upon inhibition of β-Catenin. (D) Western blot analysis for pSTAT3(Tyr705) and STAT3 in nuclear and cytoplasmic extracts of WT and FPC$^-$ cholangiocytes upon Rac-1 inhibition. The relative quantification showed a reduction in the nuclear expression of pSTAT3(Tyr705) upon Rac-1 inhibition (n=3, p<.05 Rac1 Inhib vs control cells). Relative quantifications of the cytoplasm fraction are not shown. (E) Fluorescence imaging of in-situ proximity ligation assay (PLA), showed increased interaction of β-Catenin and pSTAT3 (green dots) in FPC$^-$ cells compared to WT cells. (n=4, p<.05 FPC- vs WT cells)

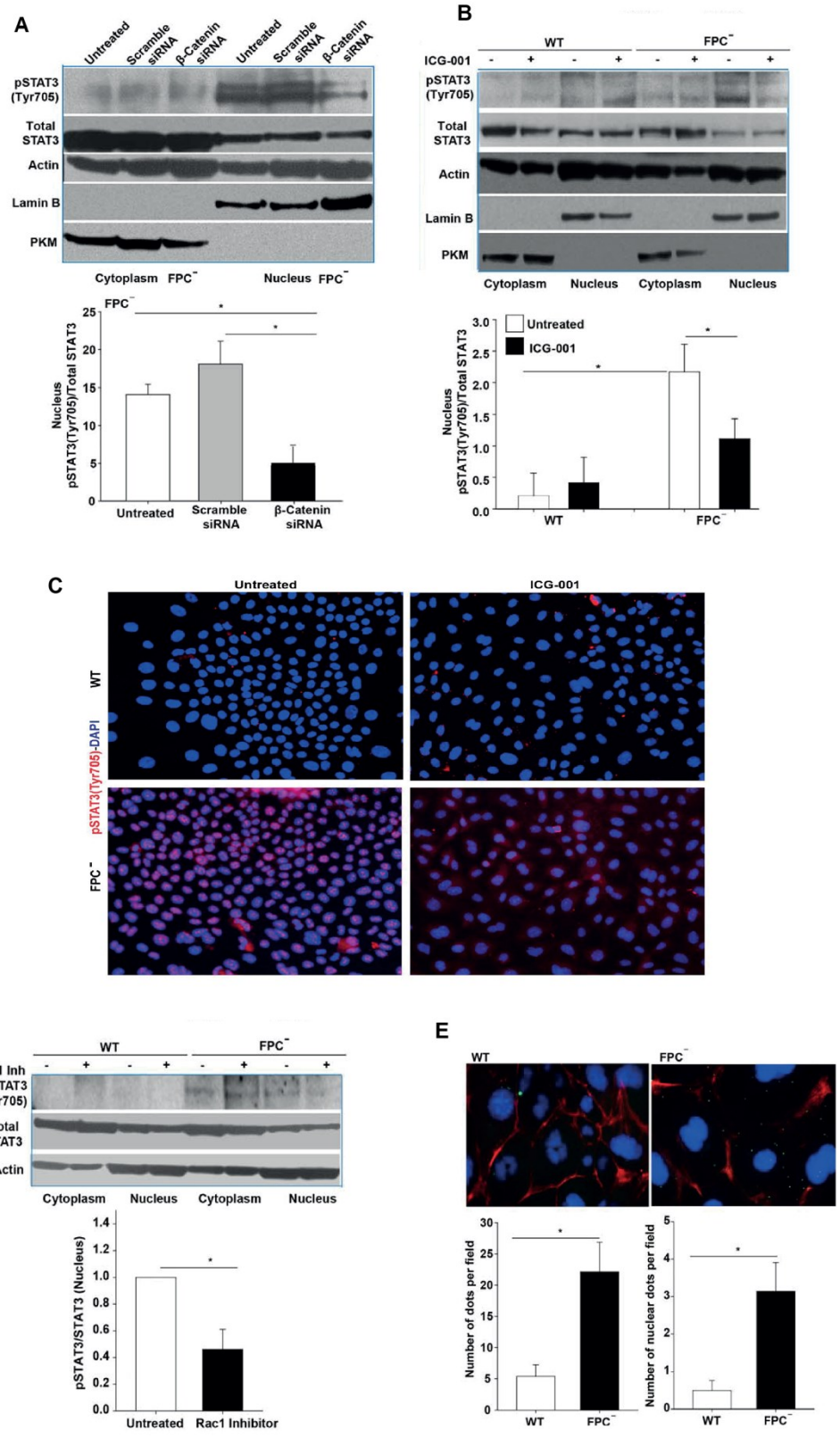
A
Untreated
Scramble siRNA
β-Catenin siRNA
Untreated
Scramble siRNA
β-Catenin siRNA
pSTAT3 (Tyr705)
Total STAT3
Actin
Lamin B
PKM
Cytoplasm FPC⁻
Nucleus FPC⁻
FPC⁻
Nucleus pSTAT3(Tyr705)/Total STAT3
Untreated
Scramble siRNA
β-Catenin siRNA
B
WT
FPC⁻
ICG-001
pSTAT3 (Tyr705)
Total STAT3
Actin
Lamin B
PKM
Cytoplasm
Nucleus
Cytoplasm
Nucleus
Untreated
ICG-001
Nucleus pSTAT3(Tyr705)/Total STAT3
WT
FPC⁻
C
Untreated
ICG-001
WT
pSTAT3(Tyr705)-DAPI
FPC⁻
D
WT
FPC⁻
Rac-1 Inh
pSTAT3 (Tyr705)
Total STAT3
Actin
Cytoplasm
Nucleus
Cytoplasm
Nucleus
pSTAT3/STAT3 (Nucleus)
Untreated
Rac1 Inhibitor
E
WT
FPC⁻
Number of dots per field
Number of nuclear dots per field
WT
FPC⁻
WT
FPC⁻

FIGURE 21

Figure 22. β-catenin silencing does not affect pSTAT1(Tyr701) nuclear translocation in FPC-defective cholangiocytes.

(A) Representative Western blot for pSTAT1(Tyr701) and STAT1 in nuclear and cytoplasmic extracts of FPC^{-} cholangiocytes upon β-catenin silencing. (B) The relative quantification showed no reduction of nuclear pSTAT3(Tyr705) upon β-catenin silencing (n=5). (C) IL-1β induced CXCL10 gene expression was not affected upon inhibition of STAT1 and STAT5 for 24 hours. The results are presented as mean±SEM, (n=3).

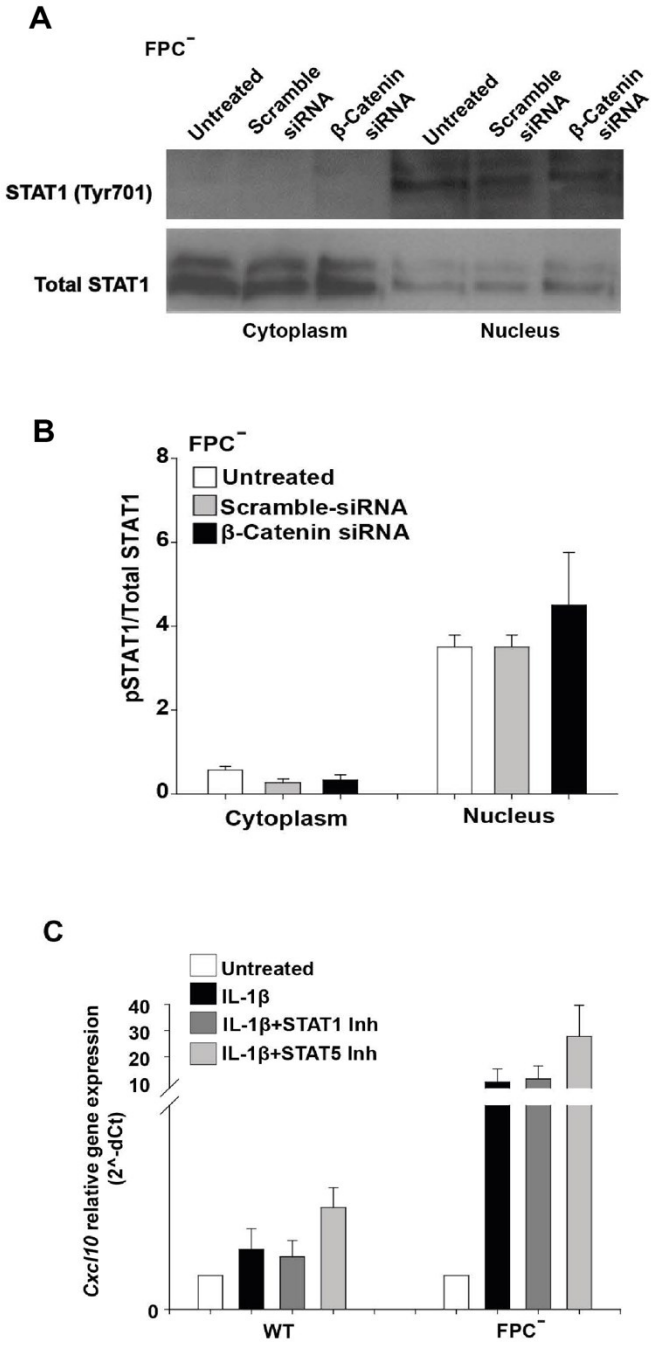
A
FPC⁻
Untreated
Scramble siRNA
β-Catenin siRNA
Untreated
Scramble siRNA
β-Catenin siRNA
STAT1 (Tyr701)
Total STAT1
Cytoplasm
Nucleus
B
FPC⁻
Untreated
Scramble-siRNA
β-Catenin siRNA
pSTAT1/Total STAT1
8
6
4
2
0
Cytoplasm
Nucleus
C
Untreated
IL-1β
IL-1β+STAT1 Inh
IL-1β+STAT5 Inh
Cxcl10 relative gene expression (2^-dCt)
40
30
20
10
0
WT
FPC⁻

FIGURE 22

Figure 23. IL-1β is produced earlier than CXCL10 in *Pkhd1*$^{del4/del4}$ cholangiocytes in vivo.

Analysis of pro-IL-1β and Cxcl10 expression in EpCAM+ cells (cholangiocyte population) isolated by FACS from WT and *Pkhd1*$^{del4/del4}$ mice. (A) pro-IL-1β and (B) Cxcl10 gene expression were significantly higher in EpCAM+ cells isolated from 1month old *Pkhd1*$^{del4/del4}$ mice compared to age-matched WT mice. (C-D) Liver tissue from 1 month old WT and *Pkhd1*$^{del4/del4}$ mice was double-stained with the cholangiocyte-specific marker K19 and with IL-1β or CXCL10. Co-localization of IL-1β with K19 was evident only in *Pkhd1*$^{del4/del4}$ mice but not in WT mice. Whereas, CXCL10 expression was absent in cystic cholangiocytes of WT and *Pkhd1*$^{del4/del4}$ mice at 1 month of age. (E) Representative micrographs of IL-1β and CXCL10 expression in liver specimens from 3 months old *Pkhd1*$^{del4/del4}$ mice. Clear co-localizatio of CXCL10 and IL-1β is evident, suggesting that CXCL10 expression was increased and colocalized with IL-1β. Magification x20, insert: x60.

Magification x20, insert: x60.

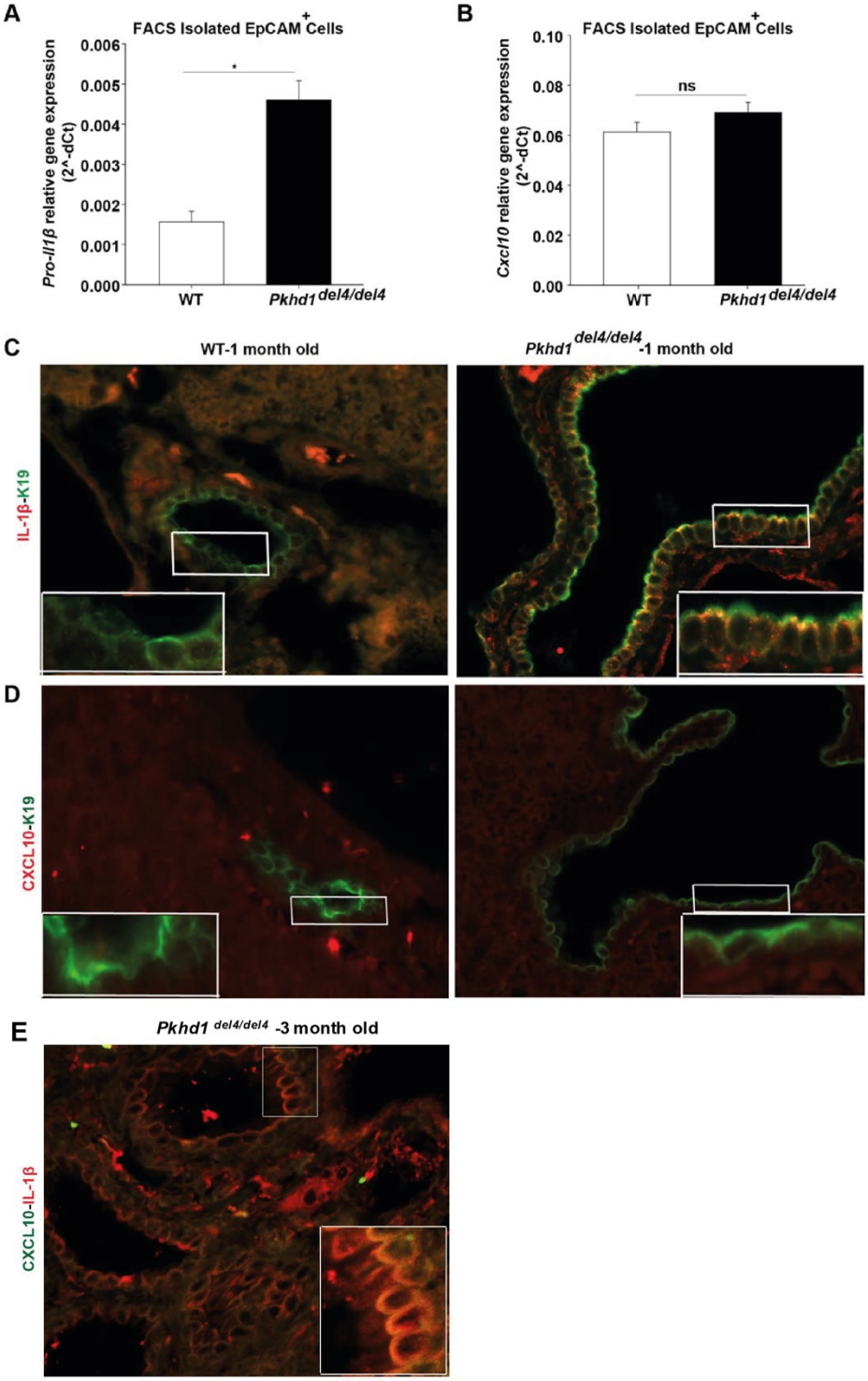
A
FACS Isolated EpCAM+ Cells
Pro-Il1β relative gene expression (2^-dCt)
0.006
0.005
0.004
0.003
0.002
0.001
0.000
*
WT
Pkhd1 del4/del4
B
FACS Isolated EpCAM+ Cells
Cxcl10 relative gene expression (2^-dCt)
0.10
0.08
0.06
0.04
0.02
0.00
ns
WT
Pkhd1 del4/del4
C
WT-1 month old
Pkhd1 del4/del4 -1 month old
IL-1β-K19
D
CXCL10-K19
E
Pkhd1 del4/del4 -3 month old
CXCL10-IL-1β

FIGURE 23

Figure 24. IL-1β was increased in FPC⁻ cholangiocytes and was responsible for increased CXCL10 through the JAK/STAT3 pathway.

(A) Pro-IL-1β gene expression was significantly increased in FPC-defective cholangiocytes (FPC–) compared to WT cells (n=8, p<.05 FPC- vs WT cells). (B) IL-1β protein levels measured by enzyme-linked immunosorbent assay in cell supernatants were increased in FPC⁻ defective cholangiocytes compared to WT cells in vitro (n=8). (C,D) Treatment with STAT3 inhibitor inhibited IL-1β-induced Cxcl10 gene and protein expression in FPC⁻ cholangiocytes, but not in WT (n=8). (E) Quantitative analysis of the percentage of pSTAT3(-Tyr705) in FPC⁻ cholangiocytes treated with recombinant IL-1β. IL-1β treatment induced a significant increase of pSTAT3(-Tyr705) in FPC⁻ cholangiocytes. (n=3,*p<.05 IL-1β treated vs untreated cells). (F) Western blot of pSTAT3 and STAT3 in WT and FPC⁻ cholangiocytes upon JAK inhibition (JAK/Tyk2 inhibitor) and treatment with recombinant IL-1β. Actin was used as loading control. The relative quantification of nuclear fraction showed that the induction of pSTAT3 upon IL-1β treatment was abolished in the presence of JAK/Tyk2 inhibitor in FPC- cholangiocytes (n=3, p<.05 IL-1β +JAK/Tyk2 inhibitor vs IL-1β FPC-treated cells). Relative quantification of nuclear fraction of WT cells is not shown.

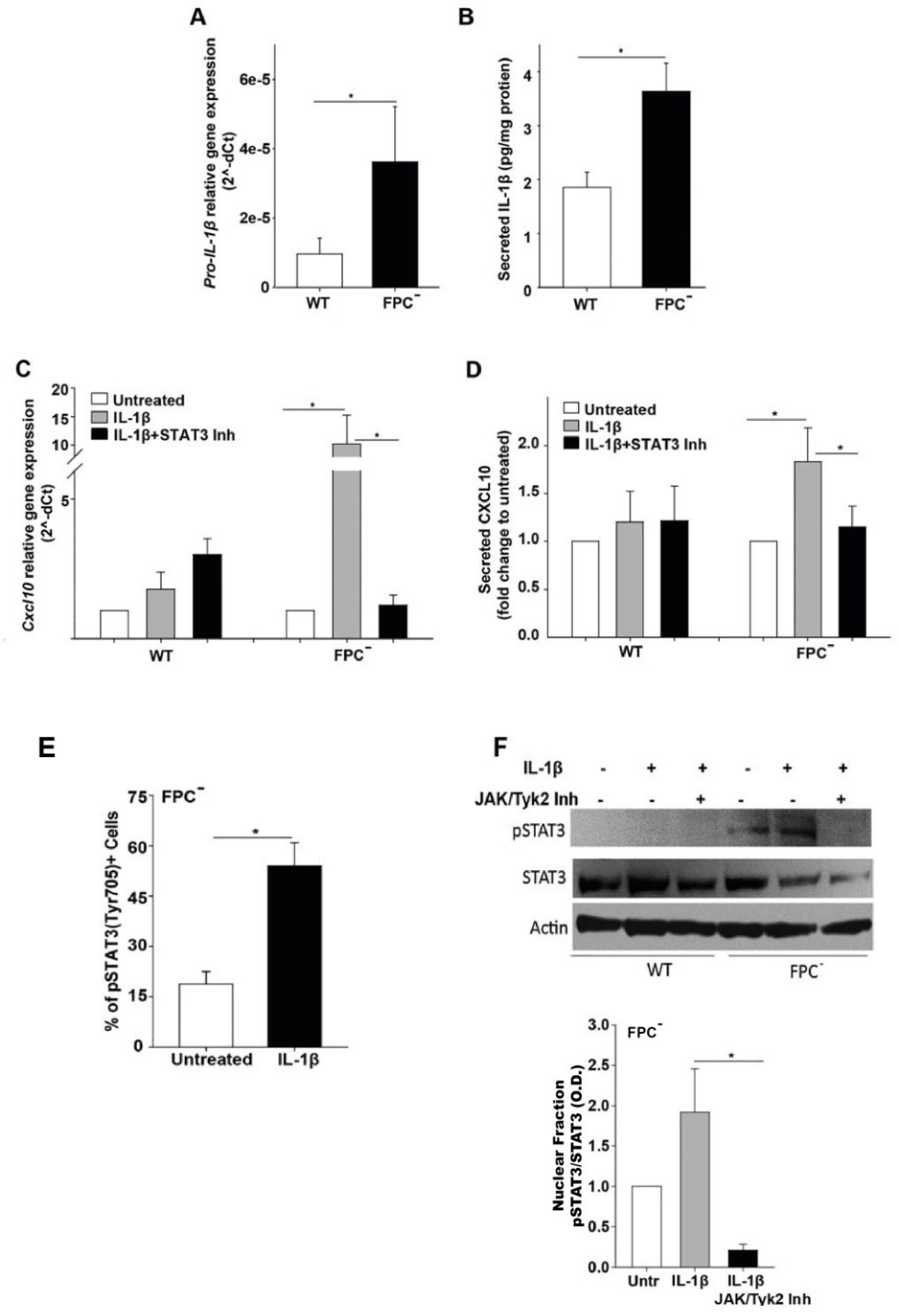
A
Pro-IL-1β relative gene expression (2^-dCt)
6e-5
4e-5
2e-5
0
WT
FPC⁻
B
Secreted IL-1β (pg/mg protien)
4
3
2
1
0
WT
FPC⁻
C
Cxcl10 relative gene expression (2^-dCt)
20
15
10
5
Untreated
IL-1β
IL-1β+STAT3 Inh
WT
FPC⁻
D
Secreted CXCL10 (fold change to untreated)
2.0
1.5
1.0
0.5
0.0
Untreated
IL-1β
IL-1β+STAT3 Inh
WT
FPC⁻
E
FPC⁻
% of pSTAT3(Tyr705)+ Cells
75
60
45
30
15
0
Untreated
IL-1β
F
IL-1β
JAK/Tyk2 Inh
pSTAT3
STAT3
Actin
WT
FPC⁻
FPC⁻
Nuclear Fraction pSTAT3/STAT3 (O.D.)
3.0
2.5
2.0
1.5
1.0
0.5
0.0
Untr
IL-1β
IL-1β JAK/Tyk2 Inh

FIGURE 24

Figure 25. NF-kB transcriptional activity is β-Catenin dependent and regulates IL-1β production and secretion.

(A) Western blot analysis for phosphorylated p65 fraction of NF-kB (Ser276 and Ser536) in nuclear fraction of WT and FPC-defective cholangiocytes (FPC^{-}). Actin was used as loading control. The relative quantification showed increased phosphorylated p65 either at Ser276 and Ser536 in FPC^{-} cholangiocytes compared to WT. (B) Nf-kB transcriptional activity, assessed by luciferase report assay, significantly increased in FPC^{-} cholangiocytes. (n=5, p<.05 FPC- cells vs WT cells), (C) Pro-IL-1β gene expression was reduced only in FPC^{-} but not in WT cholangiocytes treated with the NF-kB inhibitor for 24 hours (ACHP) (n=8). (D) Treatment with Nf-kB inhibitor significantly reduced secreted IL-1β levels in FPC^{-} but not in WT cholangiocytes (n=5, p<.05 FPC- cells vs WT cells). (E) NF-kB transcriptional activity was reduced upon β-Catenin silencing as well as with STAT3 inhibition (F) in FPC^{-} cholangiocytes compared to the relative controls (n=4, p<.05 treated-cells vs untreated cells). (G) Silencing of β-Catenin significantly reduced Pro-IL-1β and gene expression in FPC^{-} cholangiocytes compared to controls (n=6, p<.05 treated-cells vs untreated cells). (H) Silencing of β-Catenin decreased the secretion of IL-1β only in FPC-defective cholangiocytes (n=6, p<.05 treated-cells vs untreated cells). The results are presented as mean±SEM.

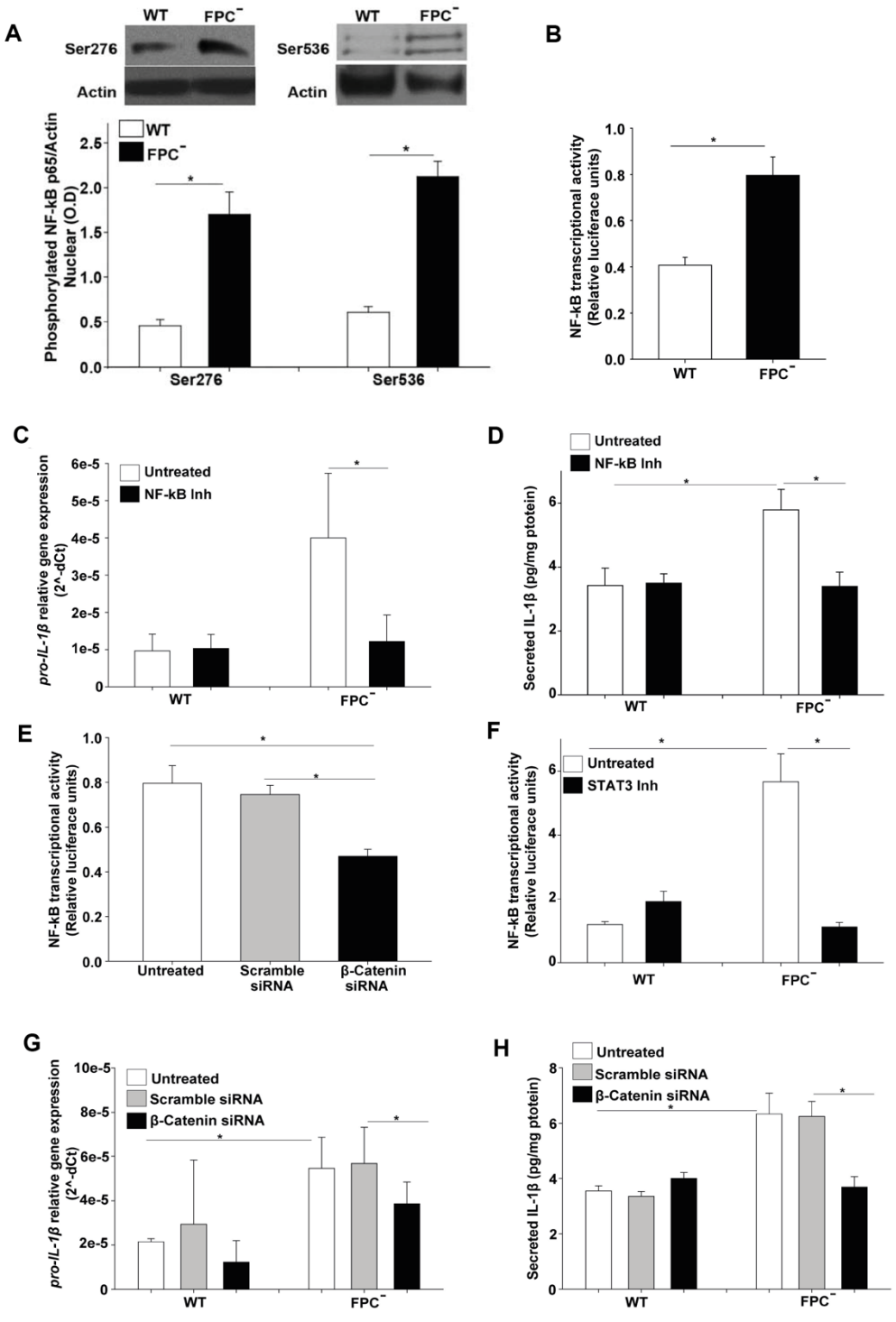
A
WT
FPC⁻
Ser276
Actin
Ser536
Phosphorylated NF-kB p65/Actin Nuclear (O.D)
B
NF-kB transcriptional activity (Relative luciferace units)
C
pro-IL-1β relative gene expression (2^-dCt)
Untreated
NF-kB Inh
D
Secreted IL-1β (pg/mg ptotein)
E
Scramble siRNA
β-Catenin siRNA
F
STAT3 Inh
G
H

FIGURE 25

Figure 26. Inflammasome activation is increased in FPC-defective cholangiocytes and is responsible for IL-1β secretion.

(A) Representative working model of inflammasome activation and production of IL-1β (two-steps). Signal 1 is delivered via activation of pattern recognition receptors, signal 2 is delivered by diverse stimuli including particulates and adenosine triphosphate. Upon signal 2, the protein complex NLRP3/ASC/Procaspase1 (inflammasome) forms. The inflammasomes activate caspase 1, which proteolytically bioactivates the pro-inflammatory cytokines interleukin-1β (IL-1β).

(B) Western blot analysis for cleaved caspase-1 (p10), marker of inflammasome activation, in WT and FPC-defective cholangiocytes (FPC^{-}). The relative quantification showed a significantly higher levels in FPC^{-} cholangiocytes compared to WT (n=6, p<.05 FPC- vs WT cells). (B) Nlrp3 gene expression assessed by RT-PCR was increased in FPC^{-} cholangiocytes compared to WT (=8, <.05 FPC- vs WT cells). (C) Analysis of IL-1β secretion, assessed by ELISA assay, in WT and FPC^{-} cholangiocytes upon treatment with NLRP3 inhibitor. Bar graphs show a significant decrease in IL-1β secretion upon blockage of NLRP3 inflammasome in FPC-cholangiocytes compared to WT (n=6, p<.05 FPC-treated vs untreated FPC- cells).

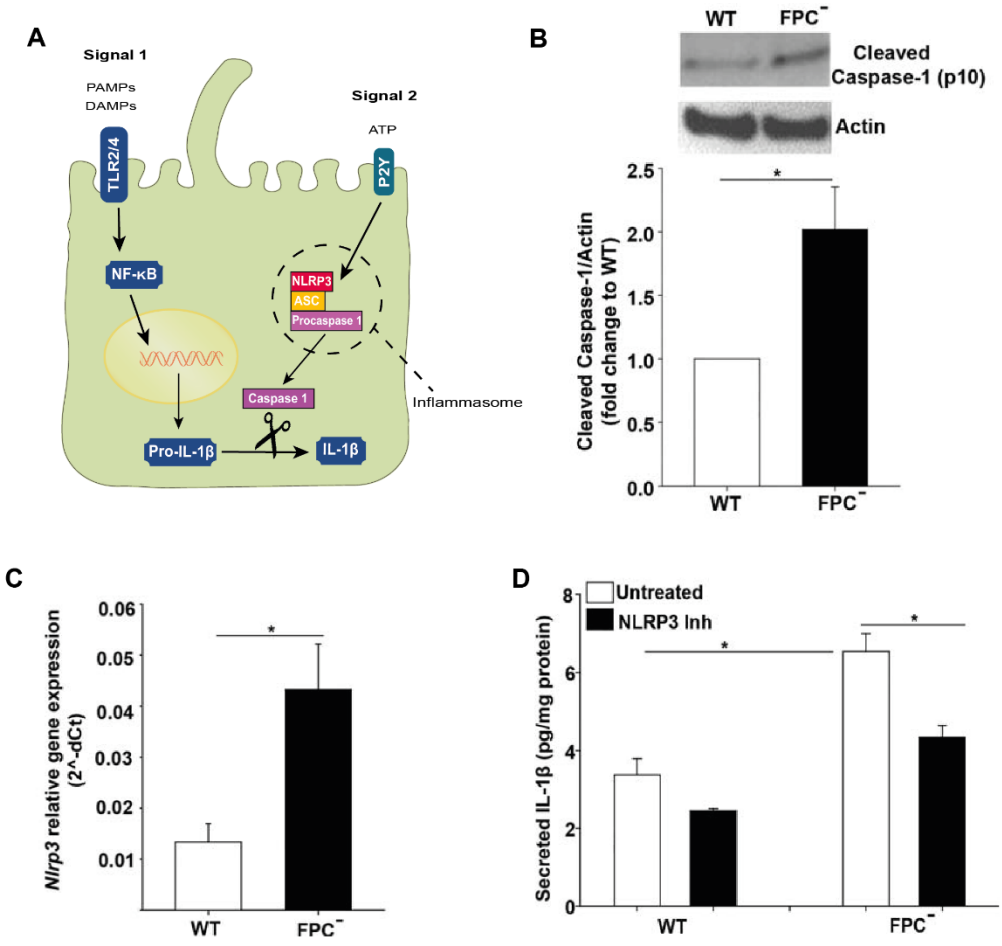
A
Signal 1
PAMPs
DAMPs
TLR2/4
NF-κB
Signal 2
ATP
P2Y
NLRP3
ASC
Procaspase 1
Caspase 1
Pro-IL-1β
IL-1β
Inflammasome
B
WT
FPC⁻
Cleaved Caspase-1 (p10)
Actin
Cleaved Caspase-1/Actin (fold change to WT)
2.5
2.0
1.5
1.0
0.5
0.0
*
WT
FPC⁻
C
Nlrp3 relative gene expression (2^-dCt)
0.06
0.05
0.04
0.03
0.02
0.01
*
WT
FPC⁻
D
Untreated
NLRP3 Inh
Secreted IL-1β (pg/mg protein)
8
6
4
2
0
*
*
WT
FPC⁻

FIGURE 28

Figure 27. Mechanism of biliary fibrosis in CHF and CD (working model).

In FPC^{-} cholangiocytes, increased levels of cAMP activate protein kinase A (PKA)-dependent phosphorylation of β- catenin (β-Cat) that leads to its nuclear translocation and transcriptional activation. This mechanism mediates the secretion of CXC-chemokine ligand 1 (CXCL1), CXCL10 and CXCL12 that recruit inflammatory cells, mostly M1 and then M2 macrophages, around the pericystic microenvironment. Macrophages secrete transforming growth factor- β (TGFβ) and TNF and stimulate the expression of αVβ6 integrins on cystic cholangiocytes that in turn activate latent TGFβ. CXCL10 secretion is further increased by NLRP3 inflammasome-mediated secretion of IL-1β, through the activation of the Janus kinase (JAK)–signal transducer and activator of transcription 3 (STAT3) pathway. *(Modified from Fabris L. et al., Nature Review Gastroenterology and Hepatology, 2019).*

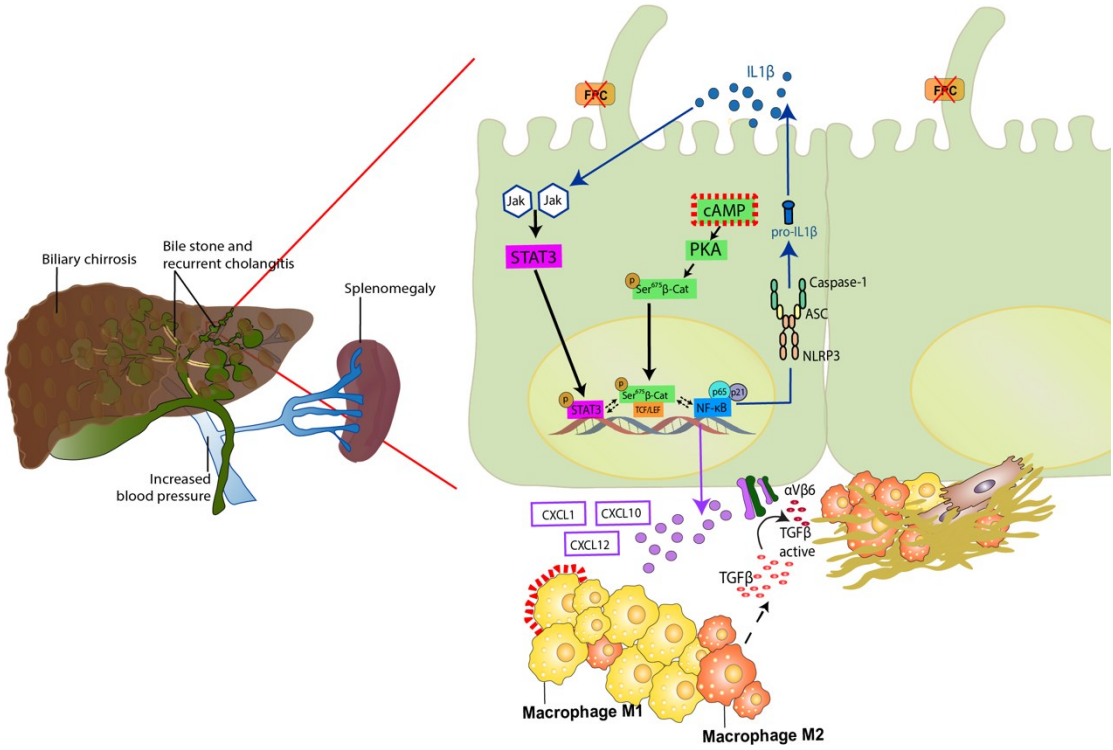
Biliary chirrosis
Bile stone and recurrent cholangitis
Splenomegaly
Increased blood pressure
IL1β
FFC
FFC
Jak
Jak
STAT3
cAMP
PKA
pro-IL1β
Caspase-1
ASC
NLRP3
Ser675β-Cat
STAT3
Ser675β-Cat
TCF/LEF
NF-κB
p65
p21
CXCL1
CXCL10
CXCL12
αVβ6
TGFβ active
TGFβ
Macrophage M1
Macrophage M2

FIGURE 27

CONCLUSION

Studies in inherited and congenital cholangiopathies generated new information and insights into cholangiocyte pathobiology that are relevant also to acquired cholangiopathies.

The central mechanism of cholangiopathies pathobiology is persistent inflammation with ongoing biliary damage, proliferation and repair, resulting in progressive portal fibrosis, and evolution to biliary cirrhosis. These processes require the reactivation of morphogenetic mechanisms that were involved in biliary development[177]. Our lab has investigated a number of genetically-determined cholangiopathies, and found that some of them involve the activation of a specific morphogenetic pathway. For example, VEGF/VEGFR2 signaling is activated in Polycystic Liver Disease, Wnt–β-catenin signaling in Congenital hepatic fibrosis, and Notch signalling in Alagille Syndrome (not discussed in this thesis).

This Ph.D. thesis focused on the molecular mechanism driving the the progression of Polycystic and Fibropolycystic Liver Diseases (specifically, Polycystic Liver Disease associated to ADPKD and Congenital Hepatic Fibrosis) with the aim to understand their pathophysiology and identify novel therapeutic approaches potentially applicable in the clinical setting.

Prior studies in PLD-ADPKD have highlighted the fundamental role of primary cilia, organelles that were previously neglected in biliary physiology. The cilium hosts many proteins (including PC1 and PC2, the proteins mutated in PLD-ADPKD) that are able to sense physical and chemical properties of the biliary milieu, and its dysfunction is associated with increased cholangiocyte proliferation and profound changes in cholangiocyte intracellular signalling and biliary morphology[19, 71, 73, 81]. The studies discussed in this thesis shifts this paradigm in the sense that focus ADPKD pathogenesis on cellular Ca^{2+} homeostasis and on the role of the endoplasmic reticulum (ER) and possibly of the mitochondria. Using PC2-defective mice, we have unveiled novel mechanisms in which loss of Ca^{2+} homeostasis in the ER might increase cAMP levels via AC5, when PC2 expression is absent or heavily reduced. This novel mechanism ultimately leads to increased cholangiocyte proliferation via the activation of intracellular ERK1/2 signaling and autocrine/paracrine VEGF/VEFGR2 signaling,

Indeed, studying PLD, we have also understood the role played by VEGF and VEGFR2 in regulating autocrine biliary proliferation and paracrine peribiliary vascularization. In fact, we have provided evidence that biliary proliferation and pericystic vascularization, that further support cyst growth are mediated by the autocrine and paracrine effects of VEGF via the Ras/Raf/ ERK1/2/mTOR signaling pathway[30, 31, 91]. The importance of this pathway is further highlighted by the reduction of cyst volume achieved using competitive VEGFR2 (SU5416) inhibitor, by using a specific mTOR(Rapamycin), or by inhibiting both Raf-1 tyrosine kinase (Sorafenib) and adenyl cyclases (somatostatin)[30, 31, 91, 178, 179]. As angiogenic factors also play a fundamental role in biliary repair by increasing cholangiocyte proliferation and providing a clue for neoangiogenesis, these therapeutic strategies could be applicable also to acquired cholangiopathies.

Furthermore, we have shown that that in ADPKD, the loss of Ca^{2+}homeostasis in the ER, enhances cAMP levels through AC5 activation[180]. Thus, blocking AC5, using specific inhibitors, might represent a novel alternative approach to prevent or minimize pathological angiogenesis. Of note, interventions aimed at reducing proliferation by increasing intracellular Ca^{2+} levels in cystic cholangiocytes is currently under investigation also by other groups (including the administration of ursodeoxycholic acid (UDCA) treatment with transient receptor potential cation channel subfamily V (TRPV4) agonists)[181]. On the other hand, studies on rat models as well as clinical trials have validated the use of two somatostatin analogues (pasireotide and octreotide), able to bind the somatostatin receptor and to block cAMP signaling and resulting in decreased biliary cysts growth and to a lesser extent, fibrous deposition.

Portal fibrosis is the main mechanism of progression of both acquired and inherited cholangiopathies. Fibrosis is usually the result of pathologic repair due to chronic necro-inflammatory damage. In genetic cholangiopathies the stimulus for chronic inflammation does not derive only from cell necrosis. In fact, “the effort of adapting to the loss of homeostasis in epithelial cells (secondary to the mutated gene) generates a sequence of events directed towards the re-establishment of new homeostatic set-points. As a result, epithelial cells secrete numerous molecules and factors that are able to instruct immune cells or generate an inflammatory response[177].

Therefore, besides being the target of the disease, cholangiocytes might also be the originators of an inflammatory response and immune reaction as an attempt to repristinate cell homeostasis. This scenario is evident in CHF/CD (Part II of this Ph.D. thesis) where the absence of fibrocystin fosters the β-catenin dependent activation of NLRP3 inflammasome, the production of IL1β and of other chemokines including CXCL10, able to attract macrophages, and to orchestrate the process of pericystic and portal fibrosis. Indeed, we also showed that a reduction of macrophages recruitment was also achieved by blocking the CXC-chemokine receptor 3 (CXCR3) of the chemokine CXCL10[182]. This further confirms the key role played by infiltrating macrophages in fibropolycystic liver disease. Thus, the recruitment of inflammatory cells in the pericystic microenvironment is essential for the initiation and the progression of fibrosis deposition. Thus, another promising approach to treat ARPKD and CHF is to target this cell milieu. Specifically, the block of monocyte-macrophage transdifferentiation by clodronate administration in *Pkhd1*$^{del4/del4}$ mice resulted in a reduced number of macrophages infiltrating the portal space. These effects were also accompanied by a reduction in fibrosis in the peribiliary area and by a decrease in cysts growth.

Moreover, this new information will help to better understand the pathophysiology of acquired cholangiopathies, such as primary sclerosing cholangitis, primary biliary cirrhosis and biliary atresia. Approaches aimed at reducing the recruitment of inflammatory cells are also being applied to acquired liver diseases, such as in primary biliary cholangitis (PBC)[183, 184] and primary sclerosing cholangitis (PSC)[156, 185]. Altogether, the studies presented in this Ph.D. thesis have led to the understanding of new important pathobiological mechanisms as well as in the identification of new possible therapeutic approaches that have been listed in Table 4. It is expected that further research efforts in studying the pathobiology of these complex diseases will be more informative and valuable, bringing an expanded awareness about the functionality of the healthy biliary epithelium.

TABLE 4 | THERAPEUTIC TARGETS IN GENETIC CHOLANGIOPATHIES

Disease	Target	Drug Name
PLDs	- Somatostatin Receptor (Inhibitor) - AC5 (Inhibitor) - VEGFR2 (Inhibitor) - BRAF - Intracellular Calcium -pmTOR	Octreotide Lanreotide Pasireotide SQ22,536 SU5416 Sorafenib UDCA Rapamycyn
CHF/CD	- Somatostatin Receptor (Inhibitor) - Intracellular Calcium I - Macrophage (depletion) - CXCR3 (Inhibitor)	Octreotide Pasireotide UDCA Clodronate AMG-487

MATERIAL AND METHODS

MATERIAL AND METHODS of PART I

Materials and reagents

Culture media, Dulbecco modified Eagle's minimal essential medium, Ham's F12, fetal bovine serum, minimal essential medium nonessential amino acid solution, minimal essential medium vitamin solutions, glyceryl monostearate, chemically defined lipid concentrate, soybean trypsin inhibitor, penicillin/streptomycin, gentamycin, and glutamine were purchased from Invitrogen (Carlsbad, CA). Epidermal growth factor, dexamethasone, triiodothyronine, EDTA, collagenase IV, forskolin, tamoxifen, thapsigargin, TPEN and NKY80 (2-amino-7-(2-furanyl)-7,9-dihydro-5(6H)-quinazolinone) were purchased by Sigma-Aldrich. 16% Paraformaldehyde (PFA) was purchased from Electron Microscopy Sciences; HEPES and TritonX-100 were purchased by American Bioanalytical. SQ22,536 (9-(tetrahydro-2-furanyl)- 9H-purin-6-amine) was purchased from Cayman Chemical. The protease inhibitor cocktail was purchased by Biovision. The NE-PER nuclear and cytoplasmic extraction reagent, total cell lysis reagent, ultra-V block and the Coomassie reagent for protein measurement were purchased from Thermo Scientific. The rat anti-mouse K19 antibody (TROMA-III) was obtained from the Developmental Studies Hybridoma Bank (University of Iowa).

Mouse models

All mice use in the experiments were housed at the Yale Animal Care facility and animal experimental protocols were approved by the Yale Animal Care and Use Committee (IACUC) and the Office of Animal Research Support (OARS).

- ***Pkd2$^{flox/-}$:pCxCreER^{TM}***

Pkd2$^{flox/-}$:pCxCreER^{TM} mouse (*Pkd2-KO)* (a kind gift from Dr. S. Somlo, Yale University) is an ADPKD mouse model yet characterized by previous studies[30, 31]. This conditional knock-out mouse is generated by an inducible defect in polycystin 2 (*Pkd2$^{flox/-}$:pCxCre^{ERTM}*), targeted through a Cre system, fused to the ligand-binding domain of a mutated estrogen receptor, as previously described[31].The deletion of floxed PC2 alleles is achieved 28 days after birth by exposing the mice to tamoxifen

(0.2 mg/g/day) for five days. *Pkd2-KO* mice developed a liver phenotype resembling human ADPKD.

- **Generation of *Pkd2$^{fl/fl}$/AC6$^{-/-}$* mice**

AC6 knock-out mice (a kind gift from Dr. M.H. Nathanson, Yale University) were generated by disruption of the AC6 gene by homologous recombination with a targeting vector containing exon1 replaced by the PGKneo-bpA cassette. *AC6 $^{-/-}$* mice were fertile, and no physical abnormalities were obvious[186]. *Pkd2-KO* mice were double crossed with *AC6$^{-/-}$* mouse to generate *Pkd2$^{fl/fl}$/AC6$^{-/-}$* mice. Mice with this genotype were treated with tamoxifen (0.2 mg/g/day) for five days in order to obtain *Pkd2$^{-/-}$/AC6$^{-/-}$* mice. Successful deletion of AC6 was assessed by RT/qPCR. Moreover, the levels of expression of AC6 were assessed by RT-PCR in liver tissues as well as in cholangiocytes isolated from WT, Pkd2 and Pkd2/AC6 KO mice (**Fig.**4A).

In vivo Treatments

Pkd2-KO and *Pkd2/AC6-KO* mice were treated with AC5 inhibitor, SQ22,536 (300µg/Kg) or with vehicle (Phosphate Buffered Saline) intraperitoneally (i.p.) every day for 8 weeks, starting 1 week after induction with tamoxifen.

At the end of the treatments, mice were anesthetized with Ketamine (100mg/Kg) in combination with Xylazine (10mg/Kg) in 1M PBS by i.p. Blood samples were taken by direct cardiac puncture, and serum was stored for analysis. Liver tissue (two main lobes) was harvested and fixed in formalin and then embedded in paraffin for histochemical analysis; the small lobes were snap frozen in liquid nitrogen; 5µm thick liver slides were processed and stained with hematoxylin/eosin or other specific markers

Isolation of mouse cholangiocytes and establishment of primary cell lines

Mice were anaesthetized as described above, the portal vein was cannulated and the liver perfused in situ with 250 ml of cold-ringer-HCO_3 buffer (KRB) for 5 minutes. Then, about 2-3 ml of liquid trypan blue agar was injected into the portal vein. Interlobular and primary branches of portal vein, hepatic artery and bile ducts were exposed by removing surface hepatocytes by forceps. Bile ducts were micro-dissected under a dissecting microscope, by using the blue agar-filled portal vein and hepatic artery for reference (bile ducts are usually run adjacent to the circulation). Residual hepatocytes,

component of the portal veins and hepatic arteries, and excess of connective tissues were removed. The isolated bile ducts or liver cysts, in the case of *Pkd2-KO* and *Pkd2/AC6-KO* mice, were plated into petri dishes on a rat-tail collagen layer. In one-two weeks biliary cells usually start out-growing out of the explant. Once subconfluent, cells were plated into 25cm^2 tissue culture flasks coated with rat-tail collagen and cultured on an enriched medium (see table). Cells were characterized by immunocytochemistry for the biliary marker K19 (polyclonal rat anti-K-19 Troma III clone). When cultured in 0.4 μm pore size cell culture inserts (BD Biosciences, San Jose, CA, USA) cholangiocytes formed a polarized epithelium and showed the presence of primary cilia (monoclonal mouse anti-acetylated tubulin primary antibody (Sigma). Establishment of a confluent monolayer with competent tight junction was routinely checked by measuring transepithelial resistance and membrane potential difference (Millicell ERS system). One week after confluence, transepithelial resistance was > 1000 $\Omega \cdot$ cm^2.

RNA Interference Silencing and Real-Time PCR

Silencing of AC5 and AC6: Gene silencing was performed using commercially available siRNAs against AC5 (50nM) and AC5 (50nM)(Ambion). Scramble RNAs (50 nM) were used as control for non-specific silencing effects (Dharmacon). *Pkd2-KO* cholangiocytes were grown on 6 well plates and 6hours after plating were transfected with siRNAs for AC5, AC6 or both using the Lipofectamine 2000 transfection reagent (Invitrogen), according to the manufacturer's protocol.

Cells were harvested and processed for isolation of RNA, 48 hours after transfection in order to verify the efficiency of gene silencing. Data were analyzed with the ΔΔCt method with normalization of the raw data relative to *Gapdh* gene expression.

RNA isolation and Real-time PCR

Total RNA was isolated using Trizol reagent (Invitrogen) and quantified with Nanodrop 1000 spectrometer (Thermo Scientific) with an absorbance of 270 nm. 1 μg RNA was converted into PCR template with the High capacity cDNA reverse Transcription kit (Applied Biosystem). 50 ng of total PCR template was then combined with the TaqMan® Universal PCR Master Mix (Applied Biosystem), and real-time PCR was performed using an ABI 7500 termalcycler (Applied Biosystem). TaqMan probes

(labeled with 5'-FAM) and primers for all genes analyzed in this study were designed to cover the exons terminals in order to exclude genomic DNA co-amplification (Applied Biosystem).

Immunohistochemical studies

Paraffin-fixed liver sections (5µm thick) were deparaffinized and treated with specific antigen retrieval before proceeding with the staining. Blocking for non-specific binding was performed using V-block (Vector Labs) for 10min before incubation with specific primary antibodies. A K19 antibody was used to identify the biliary cysts area, while the nuclear antigen (PCNA) antibody was used to quantify the percentage of cystic cholangiocytes entering the cell cycle and therefore to assess cell proliferation. IHC was also performed to analyze pERK1/2 expression in liver section of *Pkd2-KO* and *Pkd2/AC6-KO* mice.

Liver sample were incubated for 1 hour at RT with specific primary antibodies in DAKO-Antibody Diluent. After 3 brief washing with PBS/Triton-100x (PBST) 0.2%, slides were incubated with the proper the proper secondary HRP-conjugated antibody (EnVision, DAKO) for 30 min at RT and then were developed with 3,3'-Diaminobenzidine (DAB) for 5min (CellSignaling). Peroxidase immunolabelling was analyzed with a Nikon Ecliple TE2000U microscope (Nikon, Bloomfield, CT, USA) supply with a motorized stage system (Rockland, MA, USA). Images were collected using a photometric cool snap HQ digital camera (Roper Scientific, Tucson, AZ, USA). Five random non overlapping fields per each slide were recorded by a digital camera at 20x magnification.For all immunoreactions, negative controls were also included and showed no staining.

Quantitative analysis of the PCNA immunohistochemical staining was made by counting an average of 500 nuclei per each mouse, and the percentage of PCNA-positive nuclei was then calculate. K19, and pERK1/2 staining underwent to morphometric quantization (see below).

Antibody used are listed in Table 5.

Morphometric quantization of K19 and pERK1/2 positive structures

Liver section stained for K19 and pERK1/2 underwent computer-assisted morphometric analysis using a motorized stage system to scan the whole liver lobes at 4x magnification and the Metamorph software (Molecular devices). Data were

expressed as the percentage of the whole liver lobe area occupied by K19 and pERK1/2 positive cells. The setup consisted in a Nikon Eclipse TE2000U microscope (Nikon), a motorized stage system (Rockland) and a photometric cool snap HQ digital camera (Roper Scientific).

Intracellular cAMP Assay

Pkd2-KO and *Pkd2/AC6-KO* cholangiocytes were stimulated with N',N',N'-tetrakis-(2- pyridylmethyl)-ethylenediamide (TPEN; 20 lM or 1 mM)[12] for 5 minutes at 37°C, then lysed with HCl (0.1 M) for nucleotide extraction. Total protein concentrations were determined by the Lowry assay (Bio-Rad). Cellular cAMP levels were measured by using an enzyme immunoassay (EIA) procedure (cAMP-EIA kit; Cayman Chemical Company), following the manufacturer's instructions. Assays were performed in duplicate for each sample, and intracellular cAMP concentrations were expressed as picomoles/mg proteins.

Generation of biliary organoids

Mouse cholangiocytes isolated from WT, *Pkd2-KO* and *Pkd2/AC6-KO* mice were cultured in Matrigel (BD Biosciences) in a non-attaching 8 well chamber. Culture medium was based on DMEM/F12 (GIBCO) supplemented with 1% N2 and 1% B27 (GIBCO) and the growth factors: 50 ng/ml EGF (SIGMA),100 ng/ml FGF4 (R&D), 25 ng/ml HGF (R&D), 10 mM Nicotinamide (Sigma) and 10 uM FSK (SIGMA). Culture medium was supplemented with 30% Wnt3α (R&D), during the first 3 days. When cultured in these conditions, cells grew as organoids and maintained the expression of cholangiocyte markers such as K19, SOX9 and showed the presence of primary cilia. The growth of WT, *Pkd2-KO* and *Pkd2/AC6-KO* organoids was followed for 10 days and images were taken using an Axio Observer.Z1 Zeiss Microscope at 10× magnification. The AC5 inhibitors, SQ22,536 (1uM) and NKY80 (1uM) were added at day 5 in culture. To assess the volume of organoids, three diameters were measured from eight random organoids every day for the following 5 days.

Transmission Electron Microscopy

Biliary derived organoids samples used for transmission electron microscopy (TEM) were collected and fixed with 2.0% PFA/2.5% EM grade glutaraldehyde in 0.1 M sodium cacodylate buffer (pH 7.4) at 4°C for 30 minute and other 30 minute at RT.

After fixation, samples were placed in 2% osmium tetroxide in 0.1 M sodium cacodylate buffer (pH 7.4), dehydrated in a graded series of ethyl alcohol and embedded in Epon resin. Sections were cut and mounted on Formvar/carbon-coated slot grids. They were stained with uranyl acetate and lead citrate and were examined using a Jeol 100× TEM.

Western Blotting

Total cell lysates were extracted by using a lysate buffer (50 mM Tris-HCl, 1% NP40, 0.1% SDS, 0.1% Deoxycholic acid, 0.1 mM EDTA, 0.1 mM EGTA) containing protease and phosphatase inhibitor cocktails (Sigma, St Louis, CA). Nuclear and cytosolic fractions were isolated using the NE-PER Kit (Pierce, Rockford, IL), following the manufacturer's instructions. Protein concentration was measured using the Comassie protein assay reagent (Pierce). Equal amounts of proteins were applied to a 4-12% NuPAGE Novex Bis-Tris gel (Invitrogen) and electrophoresed. Proteins were transferred to nitrocellulose membrane (Invitrogen). Membranes were blocked with 5% non-fat dry milk (Bio-Rad Laboratories) in phosphate- buffered saline containing 0.05 % Tween-20 (PBST) for 1h and then incubated with specific primary antibodies (see table 5). Nitrocellulose membranes were washed three times with PBST and then incubated with horseradish peroxidase-conjugated secondary antibodies for 1h. Proteins were visualized by enhanced chemiluminescence (ECL Plus kit; AmershamBiosciences). The intensity of the bands was determined by scanning video densitometry using the Total lab TI120DM software (Nonlinear USA Inc).

Measurement of VEGF secretion in cells in culture

Quantification of VEGF secretion from *Pkd2-KO* and *Pkd2/AC6-KO* cells was assessed upon treatment with Thapsigargin (2uM) alone or in co-treatment with SQ22,536(1uM).

An enzyme-linked immunosorbent assay (ELISA, R&D Systems) was used to quantify VEGF in culture medium collected from isolated cholangiocytes, as described [31] and ELISA was performed as suggested by supplier. A standard curve was generated for each individual experiment. Readings were normalized for the total protein in the well.

Immunofluorescence and confocal microscopy

Polarized WT, *Pkd2-KO* and *Pkd2/AC6-KO* cholangiocytes were grown on transwell insert until confluence and stained using antibody against Orai-1, STIM-1 and AC5. Briefly, cells were washed with PBS 1X and then fixed for 5 minutes in methanol 100%/acetone (1:1). After 3 brief washing with PBS 1X, the membranes were permeabilized for 10 min in PBST 0.2%. Unspecific binding sites were blocked with DAKO-Blocking Solution for 10 minutes at RT.

Cells were incubated overnight at 4°C with specific primary antibodies in DAKO-Antibody Diluent. After 3 brief washing with PBS 1X, cells were incubated with the proper secondary antibody conjugated with AlexaFluor 488, 555 or 594 for 1 hour at RT. Cells were then mounted using a Vectashield Kit (Vector Laboratories) with 4',6-diamidino-2- phenylindole (DAPI).Confocal analysis was performed using a Zeiss LSM 710 Duo confocal microscope and a 63x objective.

Antibody used are listed in Table 5.

Proximity Ligation Assay (PLA)

PLA experiments were done using Duolink In Situ reagents (Olink Bioscience).

WT, Pkd2- KO and *Pkd2/AC6-KO* cholangiocytes were seeded on collagen coated coverslips. Once confluent, cells were pre-treated or not with Thapsigarging (2uM) and then fixed with Methanol 100% /Acetone (1:1), washed using PBS, and permeabilized with PBST 0.2%. Upon permeabilization, cells were incubated with blocking solution (Olink Bioscience) for 30 minutes and then with one (negative control) or two primary antibodies for 1h at RT. Coverslips were then incubated with secondary antibodies linked to PLA oligonucleotide probes PLUS and MINUS (Olink Bioscience) for 1 h at 37 °C. The samples were then incubated with the ligase solution for 30 min at 37 °C to hybridize oligonucleotides tagged on probes. The coverslips were then incubated with the amplification polymerase solution for 100 min at 37 °C to amplify hybridized oligonucleotides and fluorescently label (Alexa Fluor 488) the amplification products. Cells were then stained with Rhodamine conjugate Phalloidin (Invitrogen) for 20 minutes and coverslips were mounted on slides with Duolink. In Situ Mounting Medium with DAPI. Imaging was done using a Zeiss LSM 710 Duo confocal microscope. Below the representative working model of the PLA assay.

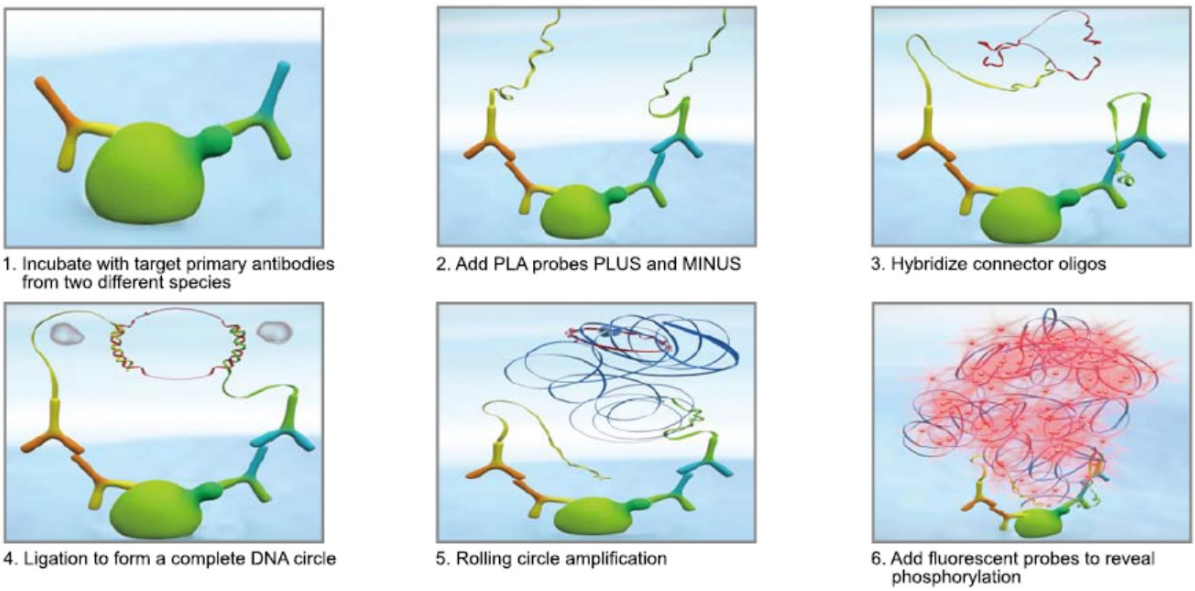

(Modified from Duolink PLA Kit protocol from Sigma-Aldrich Corp, St.Louis, USA)

Antibody used are listed in Table 5.

Oxygen Consumption Rate (OCR) analysis

Different parameters of mitochondrial respiration were measured with the 96-well XF analyzer and the XF cell mito stress kit (Seahorse Bioscience). Assay was done as suggested by the manufacturer. Twelve hours before assay, XF sensor cartridges were hydrated with the supplied calibrant and incubated at 37 °C without CO_2 (pH to 7.4 at 37 °C). Unbuffered XF assay medium was prepared and plated from a 60-well dish to the 96-well XF assay plate at a cell density of 3×10^4 cells per well. Thirty minutes before the assay, the plates were washed with the assay medium and incubated at 37 °C without CO_2. Oligomycin (1 µM), FCCP (1.5 uM) and a mix of Antimycin A and Rotenone (1 µM each) were added into the appropriate ports of the cartridge and calibrated in the instrument. After the calibration of the cartridge, cell culture plate was loaded in the instrument and the assay was run as per the standard template and OCR was measured.

Aequorin Measurements

All aequorin measurements were performed in cells transfected with the appropriate aequorin chimera targeted to the endoplasmic reticulum (*erAEQmut*) and the mitochondria (*mtAEQmut*).

Brief description of the compartment-specific aequorin chimeras:

- *Endoplasmic reticulum (erAEQmut):* The encoded polypeptide includes the leader sequence (L), the VDJ and CH1 domains of an Igg2b heavy chain (HC) and the HA1-tagged aequorin at the C-terminus. In this chimera, retention in the ER depends on the presence of the CH1 domain at the N terminus of aequorin. This domain is known to interact with the luminal ER protein BiP, thus causing the retention of the Igg2b HC in the lumen. In the absence of the immunoglobulin light chain, the polypeptide is retained in this compartment.
- *Mitochondria (mtAEQmut):* Mitochondrial pre-sequence of subunit VIII of cytocrome *c* oxidase (COX) is fused to the HA1-tagged aequorin, the point mutation (Asp119Ala) that affects the second EF-hand domain, produces a mutated aequorin, which can be used to measure [Ca^{2+}] in the range of 10–500 μM.

"AEQmut" refers to a low affinity D119A mutant of aequorin for Ca^{2+}.

1. Measurement of [Ca^{2+}] in high-[Ca^{2+}] compartments (*Endoplasmic reticulum (erAEQmut):* To reconstitute *erAEQmut* with high efficiency, the luminal [Ca^{2+}] of the ER first had to be reduced. This was achieved by incubating cells for 1 hour at 4°C in Krebs-Ringer buffer (KRB) supplemented with 5 μM coelenterazine, 5 μM Ca^{2+} ionophore ionomycin (Sigma-Aldrich), and 600 μM EGTA. After this incubation, cells were extensively washed with KRB supplemented with 2% bovine serum albumin and then transferred to the perfusion chamber.
2. Measurement of [Ca^{2+}] in low-[Ca^{2+}] compartments (*Mitochondria (mtAEQmut):* For the experiments with *mtAEQmut*, cells were incubated with 5 μM coelenterazine for 1.5–2 hour in KRB medium supplemented with $CaCl_2$ (1mM) at at 37 °C in a 5% CO2 atmosphere for complete equilibration of coelenterazine.

A 13 mm coverslip with transfected cells was placed in a perfused thermostatic chamber located in close proximity to a low noise photomultiplier with a built-in amplifier/discriminator. All aequorin measurements were carried out in KRB supplemented with either 1 mM $CaCl_2$ (*mtAEQmut*) or 100 μM EGTA (*erAEQmut*). Agonist was added to the same medium as specified in Box 1 and Box 2. The experiments were terminated by lysing cells with 2% BSA in a hypotonic Ca^{2+}-

containing solution (10 mM $CaCl_2$ in H2O), thus discharging the remaining aequorin pool. The output of the discriminator was captured by a Thorn EMI photon-counting board and stored in an IBM-compatible computer for further analyses. The aequorin luminescence data were calibrated offline into [Ca^{2+}] values using a computer algorithm based on the Ca^{2+} response curve of wild-type and mutant aequorins.

Statistical Analysis

Results are shown as mean $\pm$ standard deviation. Statistical comparisons were made using Student's t tests, or one-way analysis of variance (ANOVA), where appropriate. Statistical analysis was performed using SAS software (SAS Institute). p values <.05 were considered significant.

MATERIAL AND METHODS of PART II

Materials and reagents

Please refer to Material and Methods section of Part1 for detailed protocol.

STAT3 Inhibitor (STATIC V), JAK inhibitor I, NLRP3 inflammasome inhibitor (MCC950) were purchased by Millipore. β-Catenin inhibitor (ICG-001) was purchased by Selleckchem (Houston, TX). NF-kB Inhibitor (ACHP), CXCR3 antagonist (AMG-487) and PKA inhibitor (14-22 Amide) were purchased by Tocris. Rac1 Inhibitor (NSC 23766) and PKA inhibitor was purchased from Cayman. IL-1β was purchased by R&D. Cytofix/cytoperm kit, Perm/Wash Buffer, Streptavidin-Pacific blue, DAPI were purchased by BD Bioscience (San José, CA), ACK Lysing Buffer was purchased by Thermo Scientific. The Dual-Luciferase® Reporter (DLR™) Assay System for the measurement of NF-kB transcriptional activity was purchased by Promega.

Mouse models

All mice use in the experiments were housed at the Yale Animal Care facility and animal experimental protocols were approved by the Yale Animal Care and Use Committee (IACUC) and the Office of Animal Research Support (OARS).

- ***Pkhd1*$^{del4/del4}$ mice**

Pkhd1$^{del4/del4}$ mouse model is a well-established model for human CHF and ARPKD disease and was a kind gift from S. Somlo (Yale University). The *Pkhd1*$^{del4/del4}$ mouse, of a mixed C57BL6/129Sv background, is a carrier for inactivating deletion in the exon 4 of the Pkhd1 gene. These mice mimic the human hepatic disease, developing cysts, splenomegaly, and progressive portal fibrosis in the liver as described[142].

In vivo Treatments

Littermate, sex and age matched WT and *Pkhd1*$^{del4/del4}$ mice were treated with a small molecule CXCL10/CXCR3 antagonist, AMG-487, (5mg/Kg) [187] or with vehicle (20% hydroxypropyl-ß-cyclodextrin) orally every other day for 12 weeks, starting 3 months after birth.

At the end of the treatments, mice were anesthetized with Ketamine (100mg/Kg) in combination with Xylazine (10mg/Kg) in 1M PBS by i.p. Blood samples were taken by direct cardiac puncture, and serum was stored for analysis. Liver tissue (two main lobes) was harvested and fixed in formalin and then embedded in paraffin for histochemical analysis; the small lobes were snap frozen in liquid nitrogen; 5μm thick liver slides were processed and stained with hematoxylin/eosin or other specific markers.

Isolation of mouse cholangiocytes and establishment of primary cell lines

Please refer to Material and Methods section of Part I for detailed protocol.

RNA Interference Silencing and Real-Time PCR

For silencing of β-catenin a pool of 4 pre-designed custom short-interfering RNAs (siRNAs) (50nM) from Dharmacon, were used for β-catenin silencing. Target sequences are listed in Table 6. WT and *Pkhd1*$^{del4/del4}$ cholangiocytes were plated at 15-75% confluency in 24-well plates and were grown overnight. The next day cells were transfected using the Lipofectamine 2000 transfection reagent (Invitrogen) according to the manufacturer's protocol. Cells were harvested and processed for isolation of RNA, 48 hours after transfection in order to verify the efficiency of gene silencing.

RNA isolation and Real-time PCR

Please refer to Material and Methods section of Part I for detailed protocol.

The Nlrp3 gene expression was analyzed using the following unconjugated probes: (F: CGG ATG TTA TTC TGG CAA CA, R: CGC TTT GGA GAT GGA TCT GT) in combination with SYBR Green master mix (Applied Biosystems). Data were analyzed with the ΔΔCt method with normalization of the raw data relative to *Hprt* housekeeping gene.

Western Blotting

Please refer to Material and Methods section of Part I for detailed protocol.

Antibody used are listed in Table 5.

Immunohistochemical studies

Please refer to Material and Methods section of Part I for detailed protocol.

A K19 antibody was used to identify the biliary cysts area, while CD45 antibody was used to assess the immune-inflammatory infiltrate. IHC was also performed to analyze IL-1β and CXCL10 expression in liver section of 3-month age old *Pkhd1*$^{del4/del4}$ and WT littermates.

Quantitative analysis CD45 staining underwent to morphometric quantization (see below).

Antibody used are listed in Table 5.

Morphometric quantization of CD45 positive structures

Liver section stained for CD45 underwent computer-assisted morphometric analysis using a motorized stage system to scan the whole liver lobes at 4x magnification and the Metamorph software (Molecular devices). Data were expressed as the percentage of the whole liver lobe area occupied by CD45 positive cells. The setup consisted in a Nikon Eclipse TE2000U microscope (Nikon), a motorized stage system (Rockland) and a photometric cool snap HQ digital camera (Roper Scientific).

Immunofluorescence and confocal microscopy

WT and *Pkhd1*$^{del4/del4}$ cholangiocytes grown on 6-wells plates, were fixed on cold methanol for 10 minutes at -20°C. Cells were permeabilized with 0.2% triton X-100 in PBS (PBS/t) and then unspecific binding sites were blocked by incubation with 3% BSA in PBS for 1h at room temperature. Cell were stained using antibody against pSTAT3-Tyr705, β-Catenin and p-NF-kB-Ser276 and p-NF-kB-Ser536.

Cells were incubated overnight at 4°C with specific primary antibodies in DAKO-Antibody Diluent. After 3 brief washing with PBS 1X, cells were incubated with the proper secondary antibody conjugated with AlexaFluor 555 for 1 hour at RT. Cells were then mounted using a Vectashield Kit (Vector Laboratories) with 4',6-diamidino-2- phenylindole (DAPI).Confocal analysis was performed using a Zeiss LSM 710 Duo confocal microscope and a 63x objective.

Antibody used are listed in Table 5.

Proximity Ligation Assay (PLA)

Please refer to Material and Methods section of Part I for detailed protocol.

WT and *Pkhd1*$^{del4/del4}$ cholangiocytes were seeded on collagen coated coverslips. Once confluent, cells were fixed on PFA 4% for 10 minutes at Room temperature, washed using PBS, and permeabilized with PBST 0.2%.
Antibody used are listed in Table 5.

Measurement of IL-1β and CXCL10 secretion in cells in culture

Please refer to Material and Methods section of Part1 for detailed protocol.
Quantification of IL-1β and CXCL10 secretion from WT and *Pkhd1*$^{del4/del4}$ cells was assessed upon treatment with JAK inhibitor (Pan-JAK-Tyk2 inhibitor, 10 μM), STAT3 Inhibitor (10 μM), NF-kB Inhibitor (1 μM), PKA inhibitor (14-22 Amide, 1 μM), Rac1 Inhibitor (50 μM), NLRP3 inflammasome inhibitor (10 μM) and recombinant mouse IL-1β (5 ng/ml), β-catenin siRNA (50nM) or their combinations.

Liver Cell Isolation and Fluorescence-Activated Cell Sorting Analysis

Fluorescence-activated cell sorting analysis was performed to characterize the different cell subsets contributing to the portal inflammatory cell infiltrate and to characterize the cell populations expressing pSTAT3 and CXCR3, as described (). In detail, liver cells were isolated from *Pkhd1*$^{del4/del4}$ and WT mice at different ages. The liver was perfused with collagenase type IV and the non-parenchymal cells (NPC) and the biliary tree were isolated. The biliary tree was cut in small pieces and it was digested with a digestion media (3% FBS, 1% BSA, 0.06% Collagenase type IV, 0.3% Pronase, 0.06% DNAase in a-MEM) for 30 min at 37^{O}C in agitation. The solution was filtered with a 70 μm cell strainer and after centrifugation (10 min at 1500 RPM, 8˚C), the biliary tree pellet was combined with the NPC pellet and red blood cell lysis was performed with ACK Lysing Buffer (A1049201, Thermo scientific). After washing with PBS, the cells were resuspended in FACS buffer (1XPBS, 3% FBS and 0.05% sodium azide). 0.5-1x10^{6} cells/ml were used for each staining. For surface staining, cells were blocked with Fc blocker (CD16/32, 2.4G2) for 20 min on ice, then incubated on ice for 30 minutes with primary monoclonal rat anti-mouse conjugated-antibodies (EpCAM-Brilliant Violet 421, CD19-FITC, CD11b-PE/Cy7, CD11b-APC, CD45-Pacific blue, CD45-PerCP, NK1.1-APC, CXCR3-APC, CD4-APC, CD8-FITC, Gr-1-PE, F4/80-FITC) or a corresponding isotype control. For intracellular staining, cells were permeabilized using a cytofix/cytoperm kit (561651, BD Biosciences) for 20 min on

ice. Then a primary unconjugated antibody of pSTAT3(Tyr705), and anti-mouse monoclonal conjugated antibodies of Egr2-APC, NOS2-PE, K19-PE and Collagen-biotin), were diluted in perm/wash and added to the corresponding well. Following incubation for at least 30 min at 4°C in the dark, cells were washed with perm/wash buffer twice (CRF at 1500 rpm for 5 min). Cells were then incubated for 20-30 minutes at 4^{o}C with a fluorochrome-labeled secondary antibody (1:1000) or Streptavidin-Pacific blue (1:1000) diluted in perm/wash buffer. After washing in PBS, the pellet was resuspended in PBS (500 ul), transferred in a FACS tube and analyzed on a BD LSRII Flow Cytometer (BD, NJ). Data were processed using FlowJo Software. To identify myeloid-cell subsets in the liver, cells were selected based on CD45 staining following by sequential gating strategy for specific markers: macrophages (MΦ) (CD11b^{+} F4/80^{+}), granulocytes (CD11b^{+} Ly-6G/Ly-6C^{+}F4/80^{-}), NK1.1 Cells (CD11b^{hi-} NK-1.1^{+}), T-CD4 cells (CD11b^{-} CD4^{+}), T-CD8 cells (CD11b^{-} CD8^{+}), B Cells (CD11b^{-} CD19^{+}). For M1 and M2 macrophages after gating the CD45 cells, M1 were the NOS2^{+} F4/80^{+} cells and the M2 were the Erg2^{+} F4/80^{+} [142].

Antibody used are listed in Table 5.

Statistical Analysis

Results are shown as mean±standard error. Statistical comparisons were made using Student's t tests, or one-way analysis of variance (ANOVA), where appropriate. Statistical analysis was performed using SAS software (SAS Institute). p values <.05 were considered significant.

TABLE 5 | LIST ANTIBODIES USED AND SUPPLIERS

ANTIBODIES	SOURCE	CAT.NO.	ASSAY
β-Actin	Sigma, S. Louis MO	A4700	WB
β-Catenin	Cell Signaling	9562	WB
Caspase-1 (p10)	Santa cruz	sc-514	WB
CD11b-PE-Cy7	Bio legend	101215	FACS
CD11b-APC	BD Bioscience	101211	FACS
CD16/32, 2.4G2	BD Pharmingen	553141	FACS
CD19-FITC	BD Bioscience	557398	FACS
CD45	BD Pharmigen,	550539	FACS
CD45-Pacific blue	Bio legend	103125	FACS
CD45-PerCP	Bio legend	103129	FACS
CD4-APC	Bio legend	100411	FACS
CD8-FITC	Bio legend	100726	FACS
Collagen 1-biotin	Rockland	600-406-103	FACS
CXCL10	Bioss	Bs-1502R	IF
CXCR3-APC	R&D	FAB1685A	FACS,IF
Egr2-APC (clone erongr2)	E Bioscience	17-6691-80	FACS
EpCAM-Brilliant Violet 421	Bio legend	118225	FACS
F4/80-FITC	Bio legend	123108	FACS
Gr-1-PE	Bio legend	108407	FACS
IL-1β	InvivoGen	15F01-MM	WB,IF
K19-PE	Novus	SPM561	FACS
Lamin-B	Abcam	ab133741	WB
NFkB (Ser276)	Thermo Scientific	PA5-37718	WB
NFkB (Ser536)	Abcam	ab86299	WB
NK-1.1 APC	Bio legend	108710	FACS
NOS2-PE	E Bioscience	12-5920-80	FACS
PKM	Cell signaling	3190T	FACS
Pstat3(Tyr705) (D3A7)	Cell Signaling	9145	WB,IF
Pstat3(Tyr705) (Y705)	Cell Signaling	4113S	WB,IF
Total STAT3	Cell Signaling	12640	WB,PLA
Mouse anti-STIM-1	ProSci (Poway, CA)	49-4119	IF,PLA

STIM-1	ProSci (Poway, CA)	4119	IF,PLA
AC5	SCBT (Santa Cruz, CA)	Sc-74300	IF,PLA
ORAI1	ProSci (Poway, CA)	4041	IF,PLA
K19(TROMA III)	Developmental Studies Hybridoma Bank (DSHB) (Iowa City, CA)	TROMA-III	IHC
PCNA	SCBT (Santa Cruz, CA)	56	IHC
pERK1/2	Cell Signaling Technology (Danvers, MA)	4377	IHC,WB
ERK1/2	Cell Signaling Technology (Danvers, MA)	9201	WB
Duolink® In Situ PLA® Probe Anti-Rabbit PLUS Affinity purified Donkey anti-Rabbit IgG (H+L)	Sigma-Aldrich (St Louis, MO)	DUO92002	PLA
Duolink® In Situ PLA® Probe Anti-Mouse MINUS Affinity purified Donkey anti-Mouse IgG (H+L)	Sigma-Aldrich (St Louis, MO)	DUO92004	PLA
Duolink® In Situ PLA® Probe Anti-Goat MINUS Affinity purified Donkey anti-Mouse IgG (H+L)	Sigma-Aldrich (St Louis, MO)	DUO92006	PLA
Phalloidin	Invitrogen (Carlsbad,CA)	R415	PLA
Sox9	EMD Millipore Corporation (Temecula, CA)	AB5535	IF
Tubulin Acetylated	Sigma-Aldrich (St Louis, MO)	T6793	IF
ZO1	Thermo Scientific (Rockford, IL)	617300	IF

TABLE 6 | β-CATENIN TARGET SEQUENCES

#1	3'-GUGAAAUUCUUGGCUAUUA-5'
#2	3'-GCGCUUGGCUGAACCAUCA-5'
#3	3'-AGCAAAUCAUGCGCCUU-5'
#4	3'-AAGCUGACCUGAUGGAGUU-5'

REFERENCES

[1] M. Strazzabosco, L. Fabris, Functional anatomy of normal bile ducts, Anat Rec (Hoboken) 291(6) (2008) 653-60.

[2] S. Glaser, H. Francis, S. Demorrow, G. Lesage, G. Fava, M. Marzioni, J. Venter, G. Alpini, Heterogeneity of the intrahepatic biliary epithelium, World J Gastroenterol 12(22) (2006) 3523-36.

[3] M. Strazzabosco, L. Fabris, C. Spirli, Pathophysiology of cholangiopathies, J Clin Gastroenterol 39(4 Suppl 2) (2005) S90-S102.

[4] C.M. Morell, L. Fabris, M. Strazzabosco, Vascular biology of the biliary epithelium, J Gastroenterol Hepatol 28 Suppl 1 (2013) 26-32.

[5] E. Gaudio, A. Franchitto, L. Pannarale, G. Carpino, G. Alpini, H. Francis, S. Glaser, D. Alvaro, P. Onori, Cholangiocytes and blood supply, World J Gastroenterol 12(22) (2006) 3546-52.

[6] J.H. Tabibian, A.I. Masyuk, T.V. Masyuk, S.P. O'Hara, N.F. LaRusso, Physiology of cholangiocytes, Compr Physiol 3(1) (2013) 541-65.

[7] J.L. Boyer, Bile formation and secretion, Compr Physiol 3(3) (2013) 1035-78.

[8] A. Caligiuri, S. Glaser, R.E. Rodgers, J.L. Phinizy, W. Robertson, E. Papa, M. Pinzani, G. Alpini, Endothelin-1 inhibits secretin-stimulated ductal secretion by interacting with ETA receptors on large cholangiocytes, Am J Physiol 275(4) (1998) G835-46.

[9] A.Y. Gong, P.S. Tietz, M.A. Muff, P.L. Splinter, R.C. Huebert, M.Z. Strowski, X.M. Chen, N.F. LaRusso, Somatostatin stimulates ductal bile absorption and inhibits ductal bile secretion in mice via SSTR2 on cholangiocytes, Am J Physiol Cell Physiol 284(5) (2003) C1205-14.

[10] M. Strazzabosco, R. Fiorotto, S. Melero, S. Glaser, H. Francis, C. Spirli, G. Alpini, Differentially expressed adenylyl cyclase isoforms mediate secretory functions in cholangiocyte subpopulation, Hepatology 50(1) (2009) 244-52.

[11] A. Mennone, D. Biemesderfer, D. Negoianu, C.L. Yang, T. Abbiati, P.J. Schultheis, G.E. Shull, P.S. Aronson, J.L. Boyer, Role of sodium/hydrogen exchanger isoform NHE3 in fluid secretion and absorption in mouse and rat cholangiocytes, Am J Physiol Gastrointest Liver Physiol 280(2) (2001) G247-54.

[12] C. Spirli, A. Granato, K. Zsembery, F. Anglani, L. Okolicsanyi, N.F. LaRusso, G. Crepaldi, M. Strazzabosco, Functional polarity of Na+/H+ and Cl-/HCO3- exchangers in a rat cholangiocyte cell line, Am J Physiol 275(6) (1998) G1236-45.
[13] J.M. Banales, J. Prieto, J.F. Medina, Cholangiocyte anion exchange and biliary bicarbonate excretion, World J Gastroenterol 12(22) (2006) 3496-511.
[14] M. Strazzabosco, C. Spirli, L. Okolicsanyi, Pathophysiology of the intrahepatic biliary epithelium, J Gastroenterol Hepatol 15(3) (2000) 244-53.
[15] M. Kool, M. van der Linden, M. de Haas, G.L. Scheffer, J.M. de Vree, A.J. Smith, G. Jansen, G.J. Peters, N. Ponne, R.J. Scheper, R.P. Elferink, F. Baas, P. Borst, MRP3, an organic anion transporter able to transport anti-cancer drugs, Proc Natl Acad Sci U S A 96(12) (1999) 6914-9.
[16] M.H. Nathanson, A.D. Burgstahler, A. Mennone, J.L. Boyer, Characterization of cytosolic Ca2+ signaling in rat bile duct epithelia, Am J Physiol 271(1 Pt 1) (1996) G86-96.
[17] K.N. Lazaridis, L. Pham, P. Tietz, R.A. Marinelli, P.C. deGroen, S. Levine, P.A. Dawson, N.F. LaRusso, Rat cholangiocytes absorb bile acids at their apical domain via the ileal sodium-dependent bile acid transporter, J Clin Invest 100(11) (1997) 2714-21.
[18] K.N. Lazaridis, M. Strazzabosco, N.F. Larusso, The cholangiopathies: disorders of biliary epithelia, Gastroenterology 127(5) (2004) 1565-77.
[19] M. Strazzabosco, L. Fabris, Development of the bile ducts: essentials for the clinical hepatologist, J Hepatol 56(5) (2012) 1159-70.
[20] M.M. Richardson, J.R. Jonsson, E.E. Powell, E.M. Brunt, B.A. Neuschwander-Tetri, P.S. Bhathal, J.B. Dixon, M.D. Weltman, H. Tilg, A.R. Moschen, D.M. Purdie, A.J. Demetris, A.D. Clouston, Progressive fibrosis in nonalcoholic steatohepatitis: association with altered regeneration and a ductular reaction, Gastroenterology 133(1) (2007) 80-90.
[21] A.D. Clouston, E.E. Powell, M.J. Walsh, M.M. Richardson, A.J. Demetris, J.R. Jonsson, Fibrosis correlates with a ductular reaction in hepatitis C: roles of impaired replication, progenitor cells and steatosis, Hepatology 41(4) (2005) 809-18.
[22] L. Fabris, M. Strazzabosco, Epithelial-mesenchymal interactions in biliary diseases, Semin Liver Dis 31(1) (2011) 11-32.

[23] L. Fabris, C. Spirli, M. Cadamuro, R. Fiorotto, M. Strazzabosco, Emerging concepts in biliary repair and fibrosis, Am J Physiol Gastrointest Liver Physiol 313(2) (2017) G102-G116.
[24] V.J. Desmet, Ductal plates in hepatic ductular reactions. Hypothesis and implications. III. Implications for liver pathology, Virchows Arch 458(3) (2011) 271-9.
[25] M. Yasoshima, N. Kono, H. Sugawara, K. Katayanagi, K. Harada, Y. Nakanuma, Increased expression of interleukin-6 and tumor necrosis factor-alpha in pathologic biliary epithelial cells: in situ and culture study, Lab Invest 78(1) (1998) 89-100.
[26] P. Wang, F. Zhu, N.H. Lee, K. Konstantopoulos, Shear-induced interleukin-6 synthesis in chondrocytes: roles of E prostanoid (EP) 2 and EP3 in cAMP/protein kinase A- and PI3-K/Akt-dependent NF-kappaB activation, J Biol Chem 285(32) (2010) 24793-804.
[27] F. Meng, Y. Yamagiwa, Y. Ueno, T. Patel, Over-expression of interleukin-6 enhances cell survival and transformed cell growth in human malignant cholangiocytes, J Hepatol 44(6) (2006) 1055-65.
[28] D. Alvaro, V.D. Metalli, G. Alpini, P. Onori, A. Franchitto, B. Barbaro, S.S. Glaser, H. Francis, A. Cantafora, I. Blotta, A.F. Attili, E. Gaudio, The intrahepatic biliary epithelium is a target of the growth hormone/insulin-like growth factor 1 axis, J Hepatol 43(5) (2005) 875-83.
[29] M. Gatto, V. Drudi-Metalli, A. Torrice, G. Alpini, A. Cantafora, I. Blotta, D. Alvaro, Insulin-like growth factor-1 isoforms in rat hepatocytes and cholangiocytes and their involvement in protection against cholestatic injury, Lab Invest 88(9) (2008) 986-94.
[30] C. Spirli, S. Okolicsanyi, R. Fiorotto, L. Fabris, M. Cadamuro, S. Lecchi, X. Tian, S. Somlo, M. Strazzabosco, Mammalian target of rapamycin regulates vascular endothelial growth factor-dependent liver cyst growth in polycystin-2-defective mice, Hepatology 51(5) (2010) 1778-88.
[31] C. Spirli, S. Okolicsanyi, R. Fiorotto, L. Fabris, M. Cadamuro, S. Lecchi, X. Tian, S. Somlo, M. Strazzabosco, ERK1/2-dependent vascular endothelial growth factor signaling sustains cyst growth in polycystin-2 defective mice, Gastroenterology 138(1) (2010) 360-371 e7.
[32] V. Mariotti, M. Strazzabosco, L. Fabris, D.F. Calvisi, Animal models of biliary injury and altered bile acid metabolism, Biochim Biophys Acta Mol Basis Dis 1864(4 Pt B) (2018) 1254-1261.

[33] V. Mariotti, M. Cadamuro, C. Spirli, R. Fiorotto, M. Strazzabosco, L. Fabris, Animal models of cholestasis: An update on inflammatory cholangiopathies, Biochim Biophys Acta Mol Basis Dis 1865(5) (2019) 954-964.
[34] C. Hall, K. Sato, N. Wu, T. Zhou, K. Kyritsi, F. Meng, S. Glaser, G. Alpini, Regulators of Cholangiocyte Proliferation, Gene Expr 17(2) (2017) 155-171.
[35] R. Weiskirchen, S. Weiskirchen, F. Tacke, Organ and tissue fibrosis: Molecular signals, cellular mechanisms and translational implications, Mol Aspects Med 65 (2019) 2-15.
[36] A. Charrier, R. Chen, S. Kemper, D.R. Brigstock, Regulation of pancreatic inflammation by connective tissue growth factor (CTGF/CCN2), Immunology 141(4) (2014) 564-76.
[37] T. Kisseleva, D.A. Brenner, Mechanisms of fibrogenesis, Exp Biol Med (Maywood) 233(2) (2008) 109-22.
[38] A. Mallat, S. Lotersztajn, Cellular mechanisms of tissue fibrosis. 5. Novel insights into liver fibrosis, Am J Physiol Cell Physiol 305(8) (2013) C789-99.
[39] A.D. Urribarri, P. Munoz-Garrido, M.J. Perugorria, O. Erice, M. Merino-Azpitarte, A. Arbelaiz, E. Lozano, E. Hijona, R. Jimenez-Aguero, M.G. Fernandez-Barrena, J.P. Jimeno, M. Marzioni, J.J. Marin, T.V. Masyuk, N.F. LaRusso, J. Prieto, L. Bujanda, J.M. Banales, Inhibition of metalloprotease hyperactivity in cystic cholangiocytes halts the development of polycystic liver diseases, Gut 63(10) (2014) 1658-67.
[40] M. Zeisberg, C. Yang, M. Martino, M.B. Duncan, F. Rieder, H. Tanjore, R. Kalluri, Fibroblasts derive from hepatocytes in liver fibrosis via epithelial to mesenchymal transition, J Biol Chem 282(32) (2007) 23337-47.
[41] R.A. Reilkoff, R. Bucala, E.L. Herzog, Fibrocytes: emerging effector cells in chronic inflammation, Nat Rev Immunol 11(6) (2011) 427-35.
[42] E.L. Herzog, R. Bucala, Fibrocytes in health and disease, Exp Hematol 38(7) (2010) 548-56.
[43] T. Kisseleva, D.A. Brenner, The phenotypic fate and functional role for bone marrow-derived stem cells in liver fibrosis, J Hepatol 56(4) (2012) 965-72.
[44] K.N. Lazaridis, N.F. LaRusso, The Cholangiopathies, Mayo Clin Proc 90(6) (2015) 791-800.
[45] M. Spada, S. Riva, G. Maggiore, D. Cintorino, B. Gridelli, Pediatric liver transplantation, World J Gastroenterol 15(6) (2009) 648-74.

[46] A. Srivastava, Progressive familial intrahepatic cholestasis, J Clin Exp Hepatol 4(1) (2014) 25-36.
[47] T.J. Gevers, J.P. Drenth, Diagnosis and management of polycystic liver disease, Nat Rev Gastroenterol Hepatol 10(2) (2013) 101-8.
[48] T. Masyuk, A. Masyuk, N. LaRusso, Cholangiociliopathies: genetics, molecular mechanisms and potential therapies, Curr Opin Gastroenterol 25(3) (2009) 265-71.
[49] D.A. Braun, F. Hildebrandt, Ciliopathies, Cold Spring Harb Perspect Biol 9(3) (2017).
[50] P. Raynaud, J. Tate, C. Callens, S. Cordi, P. Vandersmissen, R. Carpentier, C. Sempoux, O. Devuyst, C.E. Pierreux, P. Courtoy, K. Dahan, K. Delbecque, S. Lepreux, M. Pontoglio, L.M. Guay-Woodford, F.P. Lemaigre, A classification of ductal plate malformations based on distinct pathogenic mechanisms of biliary dysmorphogenesis, Hepatology 53(6) (2011) 1959-66.
[51] M.C. Veigel, J. Prescott-Focht, M.G. Rodriguez, R. Zinati, L. Shao, C.A. Moore, L.H. Lowe, Fibropolycystic liver disease in children, Pediatr Radiol 39(4) (2009) 317-27; quiz 420-1.
[52] P.C. Harris, V.E. Torres, Polycystic kidney disease, Annu Rev Med 60 (2009) 321-37.
[53] M. Strazzabosco, S. Somlo, Polycystic liver diseases: congenital disorders of cholangiocyte signaling, Gastroenterology 140(7) (2011) 1855-9, 1859 e1.
[54] R.M.M. van Aerts, L.F.M. van de Laarschot, J.M. Banales, J.P.H. Drenth, Clinical management of polycystic liver disease, J Hepatol 68(4) (2018) 827-837.
[55] S. Khan, A. Dennison, G. Garcea, Medical therapy for polycystic liver disease, Ann R Coll Surg Engl 98(1) (2016) 18-23.
[56] A.B. Chapman, O. Devuyst, K.U. Eckardt, R.T. Gansevoort, T. Harris, S. Horie, B.L. Kasiske, D. Odland, Y. Pei, R.D. Perrone, Y. Pirson, R.W. Schrier, R. Torra, V.E. Torres, T. Watnick, D.C. Wheeler, P. Conference, Autosomal-dominant polycystic kidney disease (ADPKD): executive summary from a Kidney Disease: Improving Global Outcomes (KDIGO) Controversies Conference, Kidney Int 88(1) (2015) 17-27.
[57] C.G. Iglesias, V.E. Torres, K.P. Offord, K.E. Holley, C.M. Beard, L.T. Kurland, Epidemiology of adult polycystic kidney disease, Olmsted County, Minnesota: 1935-1980, Am J Kidney Dis 2(6) (1983) 630-9.
[58] M. Levy, J. Feingold, Estimating prevalence in single-gene kidney diseases progressing to renal failure, Kidney Int 58(3) (2000) 925-43.

[59] V.E. Torres, S. Rossetti, P.C. Harris, Update on autosomal dominant polycystic kidney disease, Minerva Med 98(6) (2007) 669-91.
[60] E. Cornec-Le Gall, V.E. Torres, P.C. Harris, Genetic Complexity of Autosomal Dominant Polycystic Kidney and Liver Diseases, J Am Soc Nephrol 29(1) (2018) 13-23.
[61] B. Porath, V.G. Gainullin, E. Cornec-Le Gall, E.K. Dillinger, C.M. Heyer, K. Hopp, M.E. Edwards, C.D. Madsen, S.R. Mauritz, C.J. Banks, S. Baheti, B. Reddy, J.I. Herrero, J.M. Banales, M.C. Hogan, V. Tasic, T.J. Watnick, A.B. Chapman, C. Vigneau, F. Lavainne, M.P. Audrezet, C. Ferec, Y. Le Meur, V.E. Torres, H.P.o.P.K.D.G. Genkyst Study Group, D. Consortium for Radiologic Imaging Studies of Polycystic Kidney, P.C. Harris, Mutations in GANAB, Encoding the Glucosidase IIalpha Subunit, Cause Autosomal-Dominant Polycystic Kidney and Liver Disease, Am J Hum Genet 98(6) (2016) 1193-1207.
[62] E. Cornec-Le Gall, R.J. Olson, W. Besse, C.M. Heyer, V.G. Gainullin, J.M. Smith, M.P. Audrezet, K. Hopp, B. Porath, B. Shi, S. Baheti, S.R. Senum, J. Arroyo, C.D. Madsen, C. Ferec, D. Joly, F. Jouret, O. Fikri-Benbrahim, C. Charasse, J.M. Coulibaly, A.S. Yu, K. Khalili, Y. Pei, S. Somlo, Y. Le Meur, V.E. Torres, G. Genkyst Study, H.P.o.P.K.D. Group, D. Consortium for Radiologic Imaging Studies of Polycystic Kidney, P.C. Harris, Monoallelic Mutations to DNAJB11 Cause Atypical Autosomal-Dominant Polycystic Kidney Disease, Am J Hum Genet 102(5) (2018) 832-844.
[63] C. Bergmann, J. von Bothmer, N. Ortiz Bruchle, A. Venghaus, V. Frank, H. Fehrenbach, T. Hampel, L. Pape, A. Buske, J. Jonsson, N. Sarioglu, A. Santos, J.C. Ferreira, J.U. Becker, R. Cremer, J. Hoefele, M.R. Benz, L.T. Weber, R. Buettner, K. Zerres, Mutations in multiple PKD genes may explain early and severe polycystic kidney disease, J Am Soc Nephrol 22(11) (2011) 2047-56.
[64] J.P. Drenth, R.H. te Morsche, R. Smink, J.S. Bonifacino, J.B. Jansen, Germline mutations in PRKCSH are associated with autosomal dominant polycystic liver disease, Nat Genet 33(3) (2003) 345-7.
[65] M.J. Janssen, J. Salomon, R.H. Te Morsche, J.P. Drenth, Loss of heterozygosity is present in SEC63 germline carriers with polycystic liver disease, PLoS One 7(11) (2012) e50324.
[66] A. Li, S. Davila, L. Furu, Q. Qian, X. Tian, P.S. Kamath, B.F. King, V.E. Torres, S. Somlo, Mutations in PRKCSH cause isolated autosomal dominant polycystic liver disease, Am J Hum Genet 72(3) (2003) 691-703.

[67] S. Davila, L. Furu, A.G. Gharavi, X. Tian, T. Onoe, Q. Qian, A. Li, Y. Cai, P.S. Kamath, B.F. King, P.J. Azurmendi, P. Tahvanainen, H. Kaariainen, K. Hockerstedt, O. Devuyst, Y. Pirson, R.S. Martin, R.P. Lifton, E. Tahvanainen, V.E. Torres, S. Somlo, Mutations in SEC63 cause autosomal dominant polycystic liver disease, Nat Genet 36(6) (2004) 575-7.
[68] W. Besse, K. Dong, J. Choi, S. Punia, S.V. Fedeles, M. Choi, A.R. Gallagher, E.B. Huang, A. Gulati, J. Knight, S. Mane, E. Tahvanainen, P. Tahvanainen, S. Sanna-Cherchi, R.P. Lifton, T. Watnick, Y.P. Pei, V.E. Torres, S. Somlo, Isolated polycystic liver disease genes define effectors of polycystin-1 function, J Clin Invest 127(5) (2017) 1772-1785.
[69] W.R. Cnossen, R.H. te Morsche, A. Hoischen, C. Gilissen, M. Chrispijn, H. Venselaar, S. Mehdi, C. Bergmann, J.A. Veltman, J.P. Drenth, Whole-exome sequencing reveals LRP5 mutations and canonical Wnt signaling associated with hepatic cystogenesis, Proc Natl Acad Sci U S A 111(14) (2014) 5343-8.
[70] V.E. Torres, P.C. Harris, Y. Pirson, Autosomal dominant polycystic kidney disease, Lancet 369(9569) (2007) 1287-1301.
[71] A.I. Masyuk, T.V. Masyuk, N.F. LaRusso, Cholangiocyte primary cilia in liver health and disease, Dev Dyn 237(8) (2008) 2007-12.
[72] G. Wu, S. Somlo, Molecular genetics and mechanism of autosomal dominant polycystic kidney disease, Mol Genet Metab 69(1) (2000) 1-15.
[73] S.M. Nauli, F.J. Alenghat, Y. Luo, E. Williams, P. Vassilev, X. Li, A.E. Elia, W. Lu, E.M. Brown, S.J. Quinn, D.E. Ingber, J. Zhou, Polycystins 1 and 2 mediate mechanosensation in the primary cilium of kidney cells, Nat Genet 33(2) (2003) 129-37.
[74] F. Qian, F.J. Germino, Y. Cai, X. Zhang, S. Somlo, G.G. Germino, PKD1 interacts with PKD2 through a probable coiled-coil domain, Nat Genet 16(2) (1997) 179-83.
[75] A. Hofherr, M. Kottgen, TRPP channels and polycystins, Adv Exp Med Biol 704 (2011) 287-313.
[76] K.H. Banner, F. Igney, C. Poll, TRP channels: emerging targets for respiratory disease, Pharmacol Ther 130(3) (2011) 371-84.
[77] M. Trebak, L. Lemonnier, J.T. Smyth, G. Vazquez, J.W. Putney, Jr., Phospholipase C-coupled receptors and activation of TRPC channels, Handb Exp Pharmacol (179) (2007) 593-614.

[78] G.I. Anyatonwu, M. Estrada, X. Tian, S. Somlo, B.E. Ehrlich, Regulation of ryanodine receptor-dependent calcium signaling by polycystin-2, Proc Natl Acad Sci U S A 104(15) (2007) 6454-9.
[79] Y. Li, J.M. Wright, F. Qian, G.G. Germino, W.B. Guggino, Polycystin 2 interacts with type I inositol 1,4,5-trisphosphate receptor to modulate intracellular Ca2+ signaling, J Biol Chem 280(50) (2005) 41298-306.
[80] E. Sammels, B. Devogelaere, D. Mekahli, G. Bultynck, L. Missiaen, J.B. Parys, H. De Smedt, Unraveling the role of polycystin-2/inositol 1,4,5-trisphosphate receptor interaction in Ca signaling, Commun Integr Biol 3(6) (2010) 530-2.
[81] A. Torrice, V. Cardinale, M. Gatto, R. Semeraro, C. Napoli, P. Onori, G. Alpini, E. Gaudio, D. Alvaro, Polycystins play a key role in the modulation of cholangiocyte proliferation, Dig Liver Dis 42(5) (2010) 377-85.
[82] L. Fabris, M. Cadamuro, L. Libbrecht, P. Raynaud, C. Spirli, R. Fiorotto, L. Okolicsanyi, F. Lemaigre, M. Strazzabosco, T. Roskams, Epithelial expression of angiogenic growth factors modulate arterial vasculogenesis in human liver development, Hepatology 47(2) (2008) 719-28.
[83] L. Fabris, M. Cadamuro, R. Fiorotto, T. Roskams, C. Spirli, S. Melero, A. Sonzogni, R.E. Joplin, L. Okolicsanyi, M. Strazzabosco, Effects of angiogenic factor overexpression by human and rodent cholangiocytes in polycystic liver diseases, Hepatology 43(5) (2006) 1001-12.
[84] T. Yamaguchi, S. Nagao, D.P. Wallace, F.A. Belibi, B.D. Cowley, J.C. Pelling, J.J. Grantham, Cyclic AMP activates B-Raf and ERK in cyst epithelial cells from autosomal-dominant polycystic kidneys, Kidney Int 63(6) (2003) 1983-94.
[85] N. Minagawa, J. Nagata, K. Shibao, A.I. Masyuk, D.A. Gomes, M.A. Rodrigues, G. Lesage, Y. Akiba, J.D. Kaunitz, B.E. Ehrlich, N.F. Larusso, M.H. Nathanson, Cyclic AMP regulates bicarbonate secretion in cholangiocytes through release of ATP into bile, Gastroenterology 133(5) (2007) 1592-602.
[86] H. Amano, K. Ando, S. Minamida, I. Hayashi, M. Ogino, S. Yamashina, H. Yoshimura, M. Majima, Adenylate cyclase/protein kinase A signaling pathway enhances angiogenesis through induction of vascular endothelial growth factor in vivo, Jpn J Pharmacol 87(3) (2001) 181-8.
[87] E.J. Lee, S.A. Song, H.W. Mun, K.H. Yoo, S.Y. Choi, E.Y. Park, J.H. Park, Blockade of interleukin-8 receptor signalling inhibits cyst development in vitro, via

suppression of cell proliferation in autosomal polycystic kidney disease, Nephrology (Carlton) 19(8) (2014) 471-8.
[88] A.R. Sartori-Cintra, C.S. Mara, D.L. Argolo, I.B. Coimbra, Regulation of hypoxia-inducible factor-1alpha (HIF-1alpha) expression by interleukin-1beta (IL-1 beta), insulin-like growth factors I (IGF-I) and II (IGF-II) in human osteoarthritic chondrocytes, Clinics (Sao Paulo) 67(1) (2012) 35-40.
[89] P.H. Maxwell, P.J. Ratcliffe, Oxygen sensors and angiogenesis, Semin Cell Dev Biol 13(1) (2002) 29-37.
[90] G.L. Semenza, L.A. Shimoda, N.R. Prabhakar, Regulation of gene expression by HIF-1, Novartis Found Symp 272 (2006) 2-8; discussion 8-14, 33-6.
[91] C. Spirli, C.M. Morell, L. Locatelli, S. Okolicsanyi, C. Ferrero, A.K. Kim, L. Fabris, R. Fiorotto, M. Strazzabosco, Cyclic AMP/PKA-dependent paradoxical activation of Raf/MEK/ERK signaling in polycystin-2 defective mice treated with sorafenib, Hepatology 56(6) (2012) 2363-74.
[92] A. Zsembery, C. Spirli, A. Granato, N.F. LaRusso, L. Okolicsanyi, G. Crepaldi, M. Strazzabosco, Purinergic regulation of acid/base transport in human and rat biliary epithelial cell lines, Hepatology 28(4) (1998) 914-20.
[93] O. Devuyst, V.E. Torres, Osmoregulation, vasopressin, and cAMP signaling in autosomal dominant polycystic kidney disease, Curr Opin Nephrol Hypertens 22(4) (2013) 459-70.
[94] A. Nemer, A.N. Azab, G. Rimon, S. Lamprecht, D. Ben-Menahem, Different roles of cAMP/PKA and PKC signaling in regulating progesterone and PGE2 levels in immortalized rat granulosa cell cultures, Gen Comp Endocrinol 269 (2018) 88-95.
[95] G. Aguiari, M. Banzi, S. Gessi, Y. Cai, E. Zeggio, E. Manzati, R. Piva, E. Lambertini, L. Ferrari, D.J. Peters, F. Lanza, P.C. Harris, P.A. Borea, S. Somlo, L. Del Senno, Deficiency of polycystin-2 reduces Ca2+ channel activity and cell proliferation in ADPKD lymphoblastoid cells, FASEB J 18(7) (2004) 884-6.
[96] G.I. Anyatonwu, B.E. Ehrlich, Calcium signaling and polycystin-2, Biochem Biophys Res Commun 322(4) (2004) 1364-73.
[97] J.D. Fu, J. Li, D. Tweedie, H.M. Yu, L. Chen, R. Wang, D.R. Riordon, S.A. Brugh, S.Q. Wang, K.R. Boheler, H.T. Yang, Crucial role of the sarcoplasmic reticulum in the developmental regulation of Ca2+ transients and contraction in cardiomyocytes derived from embryonic stem cells, FASEB J 20(1) (2006) 181-3.

[98] S.N. Kip, L.W. Hunter, Q. Ren, P.C. Harris, S. Somlo, V.E. Torres, G.C. Sieck, Q. Qian, [Ca2+]i reduction increases cellular proliferation and apoptosis in vascular smooth muscle cells: relevance to the ADPKD phenotype, Circ Res 96(8) (2005) 873-80.
[99] C. Spirli, L. Locatelli, R. Fiorotto, C.M. Morell, L. Fabris, T. Pozzan, M. Strazzabosco, Altered store operated calcium entry increases cyclic 3',5'-adenosine monophosphate production and extracellular signal-regulated kinases 1 and 2 phosphorylation in polycystin-2-defective cholangiocytes, Hepatology 55(3) (2012) 856-68.
[100] J. Soboloff, M.A. Spassova, X.D. Tang, T. Hewavitharana, W. Xu, D.L. Gill, Orai1 and STIM reconstitute store-operated calcium channel function, J Biol Chem 281(30) (2006) 20661-5.
[101] G.S. Bird, S.Y. Hwang, J.T. Smyth, M. Fukushima, R.R. Boyles, J.W. Putney, Jr., STIM1 is a calcium sensor specialized for digital signaling, Curr Biol 19(20) (2009) 1724-9.
[102] L. Albarran, J.J. Lopez, N.B. Amor, F.E. Martin-Cano, A. Berna-Erro, T. Smani, G.M. Salido, J.A. Rosado, Dynamic interaction of SARAF with STIM1 and Orai1 to modulate store-operated calcium entry, Sci Rep 6 (2016) 24452.
[103] I. Grigoriev, S.M. Gouveia, B. van der Vaart, J. Demmers, J.T. Smyth, S. Honnappa, D. Splinter, M.O. Steinmetz, J.W. Putney, Jr., C.C. Hoogenraad, A. Akhmanova, STIM1 is a MT-plus-end-tracking protein involved in remodeling of the ER, Curr Biol 18(3) (2008) 177-82.
[104] R. Hooper, J. Soboloff, STIMATE reveals a STIM1 transitional state, Nat Cell Biol 17(10) (2015) 1232-4.
[105] M.A. Spassova, J. Soboloff, L.P. He, W. Xu, M.A. Dziadek, D.L. Gill, STIM1 has a plasma membrane role in the activation of store-operated Ca(2+) channels, Proc Natl Acad Sci U S A 103(11) (2006) 4040-5.
[106] Y. Wang, X. Deng, Y. Zhou, E. Hendron, S. Mancarella, M.F. Ritchie, X.D. Tang, Y. Baba, T. Kurosaki, Y. Mori, J. Soboloff, D.L. Gill, STIM protein coupling in the activation of Orai channels, Proc Natl Acad Sci U S A 106(18) (2009) 7391-6.
[107] J.W. Putney, Alternative forms of the store-operated calcium entry mediators, STIM1 and Orai1, Curr Top Membr 71 (2013) 109-23.
[108] D.M. Cooper, Store-operated Ca(2)(+)-entry and adenylyl cyclase, Cell Calcium 58(4) (2015) 368-75.

[109] K. Lefkimmiatis, M. Srikanthan, I. Maiellaro, M.P. Moyer, S. Curci, A.M. Hofer, Store-operated cyclic AMP signalling mediated by STIM1, Nat Cell Biol 11(4) (2009) 433-42.
[110] J.W. Putney, Jr., New molecular players in capacitative Ca2+ entry, J Cell Sci 120(Pt 12) (2007) 1959-65.
[111] M. Bonora, C. Giorgi, A. Bononi, S. Marchi, S. Patergnani, A. Rimessi, R. Rizzuto, P. Pinton, Subcellular calcium measurements in mammalian cells using jellyfish photoprotein aequorin-based probes, Nat Protoc 8(11) (2013) 2105-18.
[112] A.I. Masyuk, T.V. Masyuk, P.L. Splinter, B.Q. Huang, A.J. Stroope, N.F. LaRusso, Cholangiocyte cilia detect changes in luminal fluid flow and transmit them into intracellular Ca2+ and cAMP signaling, Gastroenterology 131(3) (2006) 911-20.
[113] A.C. Martin, D.M. Cooper, Layers of organization of cAMP microdomains in a simple cell, Biochem Soc Trans 34(Pt 4) (2006) 480-3.
[114] Y.H. Choi, A. Suzuki, S. Hajarnis, Z. Ma, H.C. Chapin, M.J. Caplan, M. Pontoglio, S. Somlo, P. Igarashi, Polycystin-2 and phosphodiesterase 4C are components of a ciliary A-kinase anchoring protein complex that is disrupted in cystic kidney diseases, Proc Natl Acad Sci U S A 108(26) (2011) 10679-84.
[115] K.N. Klotz, S. Kachler, Inhibitors of membranous adenylyl cyclases with affinity for adenosine receptors, Naunyn Schmiedebergs Arch Pharmacol 389(3) (2016) 349-52.
[116] T.C. Mou, N. Masada, D.M. Cooper, S.R. Sprang, Structural basis for inhibition of mammalian adenylyl cyclase by calcium, Biochemistry 48(15) (2009) 3387-97.
[117] R. Fiorotto, M. Amenduni, V. Mariotti, L. Fabris, C. Spirli, M. Strazzabosco, Liver diseases in the dish: iPSC and organoids as a new approach to modeling liver diseases, Biochim Biophys Acta Mol Basis Dis 1865(5) (2019) 920-928.
[118] M. Huch, H. Gehart, R. van Boxtel, K. Hamer, F. Blokzijl, M.M. Verstegen, E. Ellis, M. van Wenum, S.A. Fuchs, J. de Ligt, M. van de Wetering, N. Sasaki, S.J. Boers, H. Kemperman, J. de Jonge, J.N. Ijzermans, E.E. Nieuwenhuis, R. Hoekstra, S. Strom, R.R. Vries, L.J. van der Laan, E. Cuppen, H. Clevers, Long-term culture of genome-stable bipotent stem cells from adult human liver, Cell 160(1-2) (2015) 299-312.
[119] S.F. Vatner, M. Park, L. Yan, G.J. Lee, L. Lai, K. Iwatsubo, Y. Ishikawa, J. Pessin, D.E. Vatner, Adenylyl cyclase type 5 in cardiac disease, metabolism, and aging, Am J Physiol Heart Circ Physiol 305(1) (2013) H1-8.

[120] N. Defer, M. Best-Belpomme, J. Hanoune, Tissue specificity and physiological relevance of various isoforms of adenylyl cyclase, Am J Physiol Renal Physiol 279(3) (2000) F400-16.
[121] M.B. Jimenez-Castro, A. Casillas-Ramirez, M. Massip-Salcedo, M. Elias-Miro, A. Serafin, A. Rimola, J. Rodes, C. Peralta, Cyclic adenosine 3',5'-monophosphate in rat steatotic liver transplantation, Liver Transpl 17(9) (2011) 1099-110.
[122] M. Periasamy, A. Kalyanasundaram, SERCA pump isoforms: their role in calcium transport and disease, Muscle Nerve 35(4) (2007) 430-42.
[123] I.M. Manjarres, A. Rodriguez-Garcia, M.T. Alonso, J. Garcia-Sancho, The sarco/endoplasmic reticulum Ca(2+) ATPase (SERCA) is the third element in capacitative calcium entry, Cell Calcium 47(5) (2010) 412-8.
[124] S. Marchi, S. Patergnani, P. Pinton, The endoplasmic reticulum-mitochondria connection: one touch, multiple functions, Biochim Biophys Acta 1837(4) (2014) 461-9.
[125] V. Padovano, I.Y. Kuo, L.K. Stavola, H.R. Aerni, B.J. Flaherty, H.C. Chapin, M. Ma, S. Somlo, A. Boletta, B.E. Ehrlich, J. Rinehart, M.J. Caplan, The polycystins are modulated by cellular oxygen-sensing pathways and regulate mitochondrial function, Mol Biol Cell 28(2) (2017) 261-269.
[126] C. Podrini, I. Rowe, R. Pagliarini, A.S.H. Costa, M. Chiaravalli, I. Di Meo, H. Kim, G. Distefano, V. Tiranti, F. Qian, D. di Bernardo, C. Frezza, A. Boletta, Dissection of metabolic reprogramming in polycystic kidney disease reveals coordinated rewiring of bioenergetic pathways, Commun Biol 1 (2018) 194.
[127] L.D. Osellame, T.S. Blacker, M.R. Duchen, Cellular and molecular mechanisms of mitochondrial function, Best Pract Res Clin Endocrinol Metab 26(6) (2012) 711-23.
[128] C. Bergmann, Genetics of Autosomal Recessive Polycystic Kidney Disease and Its Differential Diagnoses, Front Pediatr 5 (2017) 221.
[129] C. Bergmann, ARPKD and early manifestations of ADPKD: the original polycystic kidney disease and phenocopies, Pediatr Nephrol 30(1) (2015) 15-30.
[130] R. Boddu, C. Yang, A.K. O'Connor, R.C. Hendrickson, B. Boone, X. Cui, M. Garcia-Gonzalez, P. Igarashi, L.F. Onuchic, G.G. Germino, L.M. Guay-Woodford, Intragenic motifs regulate the transcriptional complexity of Pkhd1/PKHD1, J Mol Med (Berl) 92(10) (2014) 1045-56.
[131] L.F. Menezes, Y. Cai, Y. Nagasawa, A.M. Silva, M.L. Watkins, A.M. Da Silva, S. Somlo, L.M. Guay-Woodford, G.G. Germino, L.F. Onuchic, Polyductin, the PKHD1

gene product, comprises isoforms expressed in plasma membrane, primary cilium, and cytoplasm, Kidney Int 66(4) (2004) 1345-55.
[132] L.F. Onuchic, L. Furu, Y. Nagasawa, X. Hou, T. Eggermann, Z. Ren, C. Bergmann, J. Senderek, E. Esquivel, R. Zeltner, S. Rudnik-Schoneborn, M. Mrug, W. Sweeney, E.D. Avner, K. Zerres, L.M. Guay-Woodford, S. Somlo, G.G. Germino, PKHD1, the polycystic kidney and hepatic disease 1 gene, encodes a novel large protein containing multiple immunoglobulin-like plexin-transcription-factor domains and parallel beta-helix 1 repeats, Am J Hum Genet 70(5) (2002) 1305-17.
[133] C. Bergmann, J. Senderek, B. Sedlacek, I. Pegiazoglou, P. Puglia, T. Eggermann, S. Rudnik-Schoneborn, L. Furu, L.F. Onuchic, M. De Baca, G.G. Germino, L. Guay-Woodford, S. Somlo, M. Moser, R. Buttner, K. Zerres, Spectrum of mutations in the gene for autosomal recessive polycystic kidney disease (ARPKD/PKHD1), J Am Soc Nephrol 14(1) (2003) 76-89.
[134] C.J. Ward, D. Yuan, T.V. Masyuk, X. Wang, R. Punyashthiti, S. Whelan, R. Bacallao, R. Torra, N.F. LaRusso, V.E. Torres, P.C. Harris, Cellular and subcellular localization of the ARPKD protein; fibrocystin is expressed on primary cilia, Hum Mol Genet 12(20) (2003) 2703-10.
[135] J.A. Follit, L. Li, Y. Vucica, G.J. Pazour, The cytoplasmic tail of fibrocystin contains a ciliary targeting sequence, J Cell Biol 188(1) (2010) 21-8.
[136] T. Hiesberger, E. Gourley, A. Erickson, P. Koulen, C.J. Ward, T.V. Masyuk, N.F. Larusso, P.C. Harris, P. Igarashi, Proteolytic cleavage and nuclear translocation of fibrocystin is regulated by intracellular Ca2+ and activation of protein kinase C, J Biol Chem 281(45) (2006) 34357-64.
[137] J.Y. Kaimori, Y. Nagasawa, L.F. Menezes, M.A. Garcia-Gonzalez, J. Deng, E. Imai, L.F. Onuchic, L.M. Guay-Woodford, G.G. Germino, Polyductin undergoes notch-like processing and regulated release from primary cilia, Hum Mol Genet 16(8) (2007) 942-56.
[138] H. Lu, M.C.R. Galeano, E. Ott, G. Kaeslin, P.J. Kausalya, C. Kramer, N. Ortiz-Bruchle, N. Hilger, V. Metzis, M. Hiersche, S.Y. Tay, R. Tunningley, S. Vij, A.D. Courtney, B. Whittle, E. Wuhl, U. Vester, B. Hartleben, S. Neuber, V. Frank, M.H. Little, D. Epting, P. Papathanasiou, A.C. Perkins, G.D. Wright, W. Hunziker, H.Y. Gee, E.A. Otto, K. Zerres, F. Hildebrandt, S. Roy, C. Wicking, C. Bergmann, Mutations in DZIP1L, which encodes a ciliary-transition-zone protein, cause autosomal recessive polycystic kidney disease, Nat Genet 49(7) (2017) 1025-1034.

[139] I.D. Davis, M. Ho, V. Hupertz, E.D. Avner, Survival of childhood polycystic kidney disease following renal transplantation: the impact of advanced hepatobiliary disease, Pediatr Transplant 7(5) (2003) 364-9.
[140] M. Strazzabosco, R. Fiorotto, M. Cadamuro, C. Spirli, V. Mariotti, E. Kaffe, R. Scirpo, L. Fabris, Pathophysiologic implications of innate immunity and autoinflammation in the biliary epithelium, Biochim Biophys Acta Mol Basis Dis 1864(4 Pt B) (2018) 1374-1379.
[141] A.R. Gallagher, E.L. Esquivel, T.S. Briere, X. Tian, M. Mitobe, L.F. Menezes, G.S. Markowitz, D. Jain, L.F. Onuchic, S. Somlo, Biliary and pancreatic dysgenesis in mice harboring a mutation in Pkhd1, Am J Pathol 172(2) (2008) 417-29.
[142] L. Locatelli, M. Cadamuro, C. Spirli, R. Fiorotto, S. Lecchi, C.M. Morell, Y. Popov, R. Scirpo, M. De Matteis, M. Amenduni, A. Pietrobattista, G. Torre, D. Schuppan, L. Fabris, M. Strazzabosco, Macrophage recruitment by fibrocystin-defective biliary epithelial cells promotes portal fibrosis in congenital hepatic fibrosis, Hepatology 63(3) (2016) 965-82.
[143] C. Spirli, L. Locatelli, C.M. Morell, R. Fiorotto, S.D. Morton, M. Cadamuro, L. Fabris, M. Strazzabosco, Protein kinase A-dependent pSer(675) -beta-catenin, a novel signaling defect in a mouse model of congenital hepatic fibrosis, Hepatology 58(5) (2013) 1713-23.
[144] L. Azzolin, F. Zanconato, S. Bresolin, M. Forcato, G. Basso, S. Bicciato, M. Cordenonsi, S. Piccolo, Role of TAZ as mediator of Wnt signaling, Cell 151(7) (2012) 1443-56.
[145] M.J. Perugorria, P. Olaizola, I. Labiano, A. Esparza-Baquer, M. Marzioni, J.J.G. Marin, L. Bujanda, J.M. Banales, Wnt-beta-catenin signalling in liver development, health and disease, Nat Rev Gastroenterol Hepatol 16(2) (2019) 121-136.
[146] M. Elbadawy, T. Usui, H. Yamawaki, K. Sasaki, Emerging Roles of C-Myc in Cancer Stem Cell-Related Signaling and Resistance to Cancer Chemotherapy: A Potential Therapeutic Target Against Colorectal Cancer, Int J Mol Sci 20(9) (2019).
[147] Y. Zhang, L. Xu, A. Li, X. Han, The roles of ZEB1 in tumorigenic progression and epigenetic modifications, Biomed Pharmacother 110 (2019) 400-408.
[148] D. Fang, D. Hawke, Y. Zheng, Y. Xia, J. Meisenhelder, H. Nika, G.B. Mills, R. Kobayashi, T. Hunter, Z. Lu, Phosphorylation of beta-catenin by AKT promotes beta-catenin transcriptional activity, J Biol Chem 282(15) (2007) 11221-9.

[149] M. Anson, A.M. Crain-Denoyelle, V. Baud, F. Chereau, A. Gougelet, B. Terris, S. Yamagoe, S. Colnot, M. Viguier, C. Perret, J.P. Couty, Oncogenic beta-catenin triggers an inflammatory response that determines the aggressiveness of hepatocellular carcinoma in mice, J Clin Invest 122(2) (2012) 586-99.
[150] R. Medzhitov, Origin and physiological roles of inflammation, Nature 454(7203) (2008) 428-35.
[151] F. Marra, F. Tacke, Roles for chemokines in liver disease, Gastroenterology 147(3) (2014) 577-594 e1.
[152] E. Hintermann, M. Bayer, J.M. Pfeilschifter, A.D. Luster, U. Christen, CXCL10 promotes liver fibrosis by prevention of NK cell mediated hepatic stellate cell inactivation, J Autoimmun 35(4) (2010) 424-35.
[153] X. Zhang, J. Shen, K. Man, E.S. Chu, T.O. Yau, J.C. Sung, M.Y. Go, J. Deng, L. Lu, V.W. Wong, J.J. Sung, G. Farrell, J. Yu, CXCL10 plays a key role as an inflammatory mediator and a non-invasive biomarker of non-alcoholic steatohepatitis, J Hepatol 61(6) (2014) 1365-75.
[154] K. Tomita, B.L. Freeman, S.F. Bronk, N.K. LeBrasseur, T.A. White, P. Hirsova, S.H. Ibrahim, CXCL10-Mediates Macrophage, but not Other Innate Immune Cells-Associated Inflammation in Murine Nonalcoholic Steatohepatitis, Sci Rep 6 (2016) 28786.
[155] T.A. Wynn, L. Barron, Macrophages: master regulators of inflammation and fibrosis, Semin Liver Dis 30(3) (2010) 245-57.
[156] C. Ju, F. Tacke, Hepatic macrophages in homeostasis and liver diseases: from pathogenesis to novel therapeutic strategies, Cell Mol Immunol 13(3) (2016) 316-27.
[157] C.X. Li, C.C. Ling, Y. Shao, A. Xu, X.C. Li, K.T. Ng, X.B. Liu, Y.Y. Ma, X. Qi, H. Liu, J. Liu, O.W. Yeung, X.X. Yang, Q.S. Liu, Y.F. Lam, Y. Zhai, C.M. Lo, K. Man, CXCL10/CXCR3 signaling mobilized-regulatory T cells promote liver tumor recurrence after transplantation, J Hepatol 65(5) (2016) 944-952.
[158] D.L. Clarke, R.L. Clifford, S. Jindarat, D. Proud, L. Pang, M. Belvisi, A.J. Knox, TNFalpha and IFNgamma synergistically enhance transcriptional activation of CXCL10 in human airway smooth muscle cells via STAT-1, NF-kappaB, and the transcriptional coactivator CREB-binding protein, J Biol Chem 285(38) (2010) 29101-10.

[159] A.R. Simon, H.G. Vikis, S. Stewart, B.L. Fanburg, B.H. Cochran, K.L. Guan, Regulation of STAT3 by direct binding to the Rac1 GTPase, Science 290(5489) (2000) 144-7.
[160] S. Pugazhenthi, Y. Zhang, R. Bouchard, G. Mahaffey, Induction of an inflammatory loop by interleukin-1beta and tumor necrosis factor-alpha involves NF-kB and STAT-1 in differentiated human neuroprogenitor cells, PLoS One 8(7) (2013) e69585.
[161] J.W. Oh, L.M. Schwiebert, E.N. Benveniste, Cytokine regulation of CC and CXC chemokine expression by human astrocytes, J Neurovirol 5(1) (1999) 82-94.
[162] S. Yeruva, G. Ramadori, D. Raddatz, NF-kappaB-dependent synergistic regulation of CXCL10 gene expression by IL-1beta and IFN-gamma in human intestinal epithelial cell lines, Int J Colorectal Dis 23(3) (2008) 305-17.
[163] Z. Yu, W. Zhang, B.C. Kone, Signal transducers and activators of transcription 3 (STAT3) inhibits transcription of the inducible nitric oxide synthase gene by interacting with nuclear factor kappaB, Biochem J 367(Pt 1) (2002) 97-105.
[164] M. Lamkanfi, V.M. Dixit, Mechanisms and functions of inflammasomes, Cell 157(5) (2014) 1013-22.
[165] F.L. van de Veerdonk, M.G. Netea, C.A. Dinarello, L.A. Joosten, Inflammasome activation and IL-1beta and IL-18 processing during infection, Trends Immunol 32(3) (2011) 110-6.
[166] E. Latz, T.S. Xiao, A. Stutz, Activation and regulation of the inflammasomes, Nat Rev Immunol 13(6) (2013) 397-411.
[167] H. Buss, A. Dorrie, M.L. Schmitz, E. Hoffmann, K. Resch, M. Kracht, Constitutive and interleukin-1-inducible phosphorylation of p65 NF-{kappa}B at serine 536 is mediated by multiple protein kinases including I{kappa}B kinase (IKK)-{alpha}, IKK{beta}, IKK{epsilon}, TRAF family member-associated (TANK)-binding kinase 1 (TBK1), and an unknown kinase and couples p65 to TATA-binding protein-associated factor II31-mediated interleukin-8 transcription, J Biol Chem 279(53) (2004) 55633-43.
[168] L.F. Chen, S.A. Williams, Y. Mu, H. Nakano, J.M. Duerr, L. Buckbinder, W.C. Greene, NF-kappaB RelA phosphorylation regulates RelA acetylation, Mol Cell Biol 25(18) (2005) 7966-75.
[169] J. Jang, J.H. Ha, S.I. Chung, Y. Yoon, Beta-catenin regulates NF-kappaB activity and inflammatory cytokine expression in bronchial epithelial cells treated with lipopolysaccharide, Int J Mol Med 34(2) (2014) 632-8.

[170] K. Yun, J.S. So, A. Jash, S.H. Im, Lymphoid enhancer binding factor 1 regulates transcription through gene looping, J Immunol 183(8) (2009) 5129-37.
[171] G. Solanas, M. Porta-de-la-Riva, C. Agusti, D. Casagolda, F. Sanchez-Aguilera, M.J. Larriba, F. Pons, S. Peiro, M. Escriva, A. Munoz, M. Dunach, A.G. de Herreros, J. Baulida, E-cadherin controls beta-catenin and NF-kappaB transcriptional activity in mesenchymal gene expression, J Cell Sci 121(Pt 13) (2008) 2224-34.
[172] J. Yang, X. Liao, M.K. Agarwal, L. Barnes, P.E. Auron, G.R. Stark, Unphosphorylated STAT3 accumulates in response to IL-6 and activates transcription by binding to NFkappaB, Genes Dev 21(11) (2007) 1396-408.
[173] K. Schroder, J. Tschopp, The inflammasomes, Cell 140(6) (2010) 821-32.
[174] C.A. Dinarello, Immunological and inflammatory functions of the interleukin-1 family, Annu Rev Immunol 27 (2009) 519-50.
[175] A.A. de Jesus, S.W. Canna, Y. Liu, R. Goldbach-Mansky, Molecular mechanisms in genetically defined autoinflammatory diseases: disorders of amplified danger signaling, Annu Rev Immunol 33 (2015) 823-74.
[176] J. Petrasek, S. Bala, T. Csak, D. Lippai, K. Kodys, V. Menashy, M. Barrieau, S.Y. Min, E.A. Kurt-Jones, G. Szabo, IL-1 receptor antagonist ameliorates inflammasome-dependent alcoholic steatohepatitis in mice, J Clin Invest 122(10) (2012) 3476-89.
[177] L. Fabris, R. Fiorotto, C. Spirli, M. Cadamuro, V. Mariotti, M.J. Perugorria, J.M. Banales, M. Strazzabosco, Pathobiology of inherited biliary diseases: a roadmap to understand acquired liver diseases, Nat Rev Gastroenterol Hepatol 16(8) (2019) 497-511.
[178] T.V. Masyuk, B.N. Radtke, A.J. Stroope, J.M. Banales, S.A. Gradilone, B. Huang, A.I. Masyuk, M.C. Hogan, V.E. Torres, N.F. Larusso, Pasireotide is more effective than octreotide in reducing hepatorenal cystogenesis in rodents with polycystic kidney and liver diseases, Hepatology 58(1) (2013) 409-21.
[179] T.V. Masyuk, A.I. Masyuk, V.E. Torres, P.C. Harris, N.F. Larusso, Octreotide inhibits hepatic cystogenesis in a rodent model of polycystic liver disease by reducing cholangiocyte adenosine 3',5'-cyclic monophosphate, Gastroenterology 132(3) (2007) 1104-16.
[180] C. Spirli, V. Mariotti, A. Villani, L. Fabris, R. Fiorotto, M. Strazzabosco, Adenylyl cyclase 5 links changes in calcium homeostasis to cAMP-dependent cyst growth in polycystic liver disease, J Hepatol 66(3) (2017) 571-580.

[181] P. Munoz-Garrido, J.J. Marin, M.J. Perugorria, A.D. Urribarri, O. Erice, E. Saez, M. Uriz, S. Sarvide, A. Portu, A.R. Concepcion, M.R. Romero, M.J. Monte, A. Santos-Laso, E. Hijona, R. Jimenez-Aguero, M. Marzioni, U. Beuers, T.V. Masyuk, N.F. LaRusso, J. Prieto, L. Bujanda, J.P. Drenth, J.M. Banales, Ursodeoxycholic acid inhibits hepatic cystogenesis in experimental models of polycystic liver disease, J Hepatol 63(4) (2015) 952-61.
[182] E. Kaffe, R. Fiorotto, F. Pellegrino, V. Mariotti, M. Amenduni, M. Cadamuro, L. Fabris, M. Strazzabosco, C. Spirli, beta-Catenin and interleukin-1beta-dependent chemokine (C-X-C motif) ligand 10 production drives progression of disease in a mouse model of congenital hepatic fibrosis, Hepatology 67(5) (2018) 1903-1919.
[183] Y.H. Chuang, Z.X. Lian, C.M. Cheng, R.Y. Lan, G.X. Yang, Y. Moritoki, B.L. Chiang, A.A. Ansari, K. Tsuneyama, R.L. Coppel, M.E. Gershwin, Increased levels of chemokine receptor CXCR3 and chemokines IP-10 and MIG in patients with primary biliary cirrhosis and their first degree relatives, J Autoimmun 25(2) (2005) 126-32.
[184] K.L. de Graaf, G. Lapeyre, F. Guilhot, W. Ferlin, S.M. Curbishley, M. Carbone, P. Richardson, S. Moreea, C.A. McCune, S.D. Ryder, R.W. Chapman, A. Floreani, D.E. Jones, C. de Min, D.H. Adams, P. Invernizzi, NI-0801, an anti-chemokine (C-X-C motif) ligand 10 antibody, in patients with primary biliary cholangitis and an incomplete response to ursodeoxycholic acid, Hepatol Commun 2(5) (2018) 492-503.
[185] M.E. Guicciardi, C.E. Trussoni, A. Krishnan, S.F. Bronk, M.J. Lorenzo Pisarello, S.P. O'Hara, P.L. Splinter, Y. Gao, P. Vig, A. Revzin, N.F. LaRusso, G.J. Gores, Macrophages contribute to the pathogenesis of sclerosing cholangitis in mice, J Hepatol 69(3) (2018) 676-686.
[186] T. Tang, M.H. Gao, N.C. Lai, A.L. Firth, T. Takahashi, T. Guo, J.X. Yuan, D.M. Roth, H.K. Hammond, Adenylyl cyclase type 6 deletion decreases left ventricular function via impaired calcium handling, Circulation 117(1) (2008) 61-9.
[187] T.C. Walser, S. Rifat, X. Ma, N. Kundu, C. Ward, O. Goloubeva, M.G. Johnson, J.C. Medina, T.L. Collins, A.M. Fulton, Antagonism of CXCR3 inhibits lung metastasis in a murine model of metastatic breast cancer, Cancer Res 66(15) (2006) 7701-7.